Aalto University
School of Electrical Engineering

Maria Hakonen

Towards the Control of an Upper-Limb Prosthesis Using Surface Electromyography

Master´s thesis submitted in partial fulfillment of the requirements for the degree of Master of Science in Technology in the Degree Programme in Bioinformation Technology.

Espoo, 13.8.2012

Supervisor: Professor Arto Visala

Aalto University School of Electrical Engineering	ABSTRACT OF THE MASTER'S THESIS
Author: Maria Hakonen	
Title: Towards the Control of an Upper-Limb Prosthesis Using Surface Electromyography	
Title in Finnish: Kohti yläraaja-proteesien ohjausta pintaelektromyografialla	
Degree Programme: Degree Programme in Bioinformation Technology	
Major subject: Bioautomation	Minor subject: Biotronics
Chair (code): AS-84	
Supervisor: Professor Arto Visala	Instructor: Professor Arto Visala

The loss of an upper limb is a life-altering accident which makes everyday life more difficult. A multifunctional prosthetic hand with an user-friendly control interface may significantly improve the life quality of amputees. However, many amputees do not use their prosthetic hand regularly because of its low functionality, and low controllability. This situation calls for the development of versatile prosthetic limbs that allow amputees to perform tasks that are necessary for activities of daily living.

The non-pattern based control scheme of the commercial state-of art prosthesis is rather poor and non-natural. Usually, a pair of muscles is used to control one degree of freedom. A promising alternative to the conventional control methods is the pattern-recognition-based control that identifies different intended hand postures of the prosthesis by utilizing the information of the surface electromyography (sEMG) signals. Therefore, the control of the prosthesis becomes natural and easy.

The objective of this thesis was to find the features that yield the highest classification accuracy in identifying 7 classes of hand postures in the context of Linear Discriminant Classifier. The sEMG signals were measured on the skin surface of the forearm of the 8 able-bodied subjects. The following features were investigated: 16 time-domain features, two time-serial-domain features, the Fast Fourier Transform (FFT), and the Discrete Wavelet Transform (DWT). The second objective of this thesis was to study the effect of the sampling rate to the classification accuracy. A preprocessing technique, Independent Component Analysis (ICA), was also shortly examined. The classification was based on the steady state signal. The signal processing, features, and classification were implemented with Matlab.

The results of this study suggest that DWT and FFT did not outperform the simple and computationally efficient time domain features in the classification accuracy. Thus, at least in noise free environment, the high classification accuracy (> 90 %) can be achieved with a small number of simple TD features. A more reliable control may be achieved if the features are selected individually of a subset of the effective features. Using the sampling rate of 400 Hz instead of commonly used 1 kHz may not only save the data processing time and the memory of the prosthesis controller but also slightly improve the classification accuracy. ICA was not found to improve the classification accuracy, which may be because the measurement channels were placed relatively far from each other.

Date: 13.8.2012	Language: English	Number of pages: 8+100

Keywords: sEMG, upper-limb prostheses, pattern-based control, hand posture classification

Aalto Yliopisto Sähkötekniikan Korkeakoulu	DIPLOMITYÖN TIIVISTELMÄ
Tekijä: Maria Hakonen	
Työn nimi: Kohti yläraaja-proteesien ohjausta pintaelektromyografialla	
Title: Towards the Control of an Upper-Limb Prosthesis Using Surface Electromyography	
Tutkinto-ohjelma: Bioinformaatioteknologia	
Pääaine: Bioautomatiikka	Sivuaine: Biotroniikka
Opetusyksikön (ent. professuuri) koodi: AS-84	
Työn valvoja: Arto Visala	Ohjaaja: Arto Visala

Yläraaja-amputaatio vaikuttaa suuresti päivittäiseen elämään. Helposti ohjattavalla toiminnallisilla proteeseilla amputoitujen henkilöiden elämänlaatua voitaisiin parantaa merkittävästi. Suurin osa amputoiduista henkilöistä ei kuitenkaan käytä proteesiaan säännöllisesti proteesin vähäisten toimintojen ja vaikean ohjattavuuden vuoksi. Olisikin tärkeää kehittää helposti ohjattava ja riittävästi toimintoja sisältävä proteesi, joka mahdollistaisi päivittäisessä elämässä välttämättömien tehtävien suorittamisen.

Markkinoilla olevat lihassähköiset yläraajaproteesit perustuvat yksinkertaiseen hahmontunnistusta hyödyntämättömään ohjaukseen, jossa lihasparilla ohjataan yleensä yhtä proteesin vapausastetta. Lupaava vaihtoehto perinteisille ohjausmenetelmille on hahmontunnistukseen pohjautuva ohjaus. Se tunnistaa käyttäjän käden asennot käsivarren iholta mitatun lihassähkösignaalin sisältämän informaation avulla mahdollistaen helpon ja luonnollisen ohjauksen.

Tämän diplomityön tavoitteena oli löytää piirteet, jolla seitsemän erilaista käden asentoa pystytään luokittelemaan mahdollisimman tarkasti lineaarisella diskriminantti luokittelijalla. Lihassähkösignaalit mitattiin kahdeksan ei-amputoidun koehenkilön käsivarresta ihon pinnalle kiinnitetyillä elektrodeilla. Työssä vertailtiin seuraavia piirteitä: 16 aika-alueen piirrettä, kaksi aikasarja-alueen piirrettä, nopea Fourier-muunnos (FFT), diskreetti Aalloke-muunnos (DWT). Työn toinen tavoite oli tutkia näytteenottotaajuuden vaikutusta luokittelutarkkuuteen. Myös esiprosessointia riippumattomien komponenttien analyysillä tutkittiin lyhyesti. Luokittelu tehtiin staattisen lihassupistuksen aikana mitatun signaalin perusteella. Signaalin prosessointi, piirteet ja luokittelu toteutettiin Matlabilla.

Tämän tutkimuksen tulokset osoittivat, etteivät diskreetti Aalloke-muunnos ja nopea Fourier-muunnos yllä laskennallisesti tehokkaampia aika-alueen piirteitä parempaan luokittelutarkkuuteen. Pienellä määrällä yksinkertaisia aika-alueen piirteitä voidaan saavuttaa hyvä luokittelutarkkuus (>90 %). Luokittelutarkkuutta voitaneen edelleen parantaa valitsemalla optimaaliset piirteet yksilöllisesti pienestä joukosta hyviksi havaittuja piirteitä. Käyttämällä 400 Hz:n näytteenottotaajuutta yleisesti käytetyn 1 kHz:n sijasta, voidaan sekä säästää prosessointiaikaa ja proteesin prosessorin muistia että myös parantaa hieman luokittelutarkkuutta. Esiprosessointi riippumattomien komponenttien analyysillä ei parantanut luokittelutarkkuutta, mikä johtunee siitä, että mittauskanavat olivat suhteellisen kaukana toisistaan.

Date: 13.8.2012	Language: Englanti	Number of pages: 8+100
Keywords: sEMG, upper-limb prostheses, pattern-based control, hand posture classification		

Preface

First of all I would like to thank Professor Arto Visala for providing me the opportunity to work on this interesting and challenging task, as well as the freedom and trust he gave to converge and focus my work over the course of the thesis.

I am very grateful to my colleagues Jouko Kalmari and Teemu Kemppainen who provided friendly support during my work by discussing the ideas related to the thesis work. Our discussions have resulted in an improved quality of the research. Jouko Kalmari also was a great help with some of the measurements for this thesis. Further I would like to thank my colleague Juha Backman for giving his last minute comments on the thesis, and the rest of the staff of the laboratory for a nice working environment.

Contents

Symbols and Abbreviations

C_x	Coveriance matrix
Σ_b	Intra-class scatter matrix
Σ_w	Inter-class scatter matrix
w^T	Transpose of an initial weight vector
A	Mixing matrix
$s(t)$	sEMG signal
w	Initial weight vector
W	Un-mixing matrix
$C(a, b; f(t), \psi(t))$	Continuous Wavelet Transform
$X(f)$	Fourier Transform
$X(m)$	Discrete Fourier Transform
$X(n, \omega)$	Discrete Short Time Fourier Transform
$X(\tau, \omega)$	Short Time Fourier Transform
σ	Standard derivation
$\psi(t)$	Wavelet Function

ACh	Acetylcholine
AR	Autoregressive Coefficients
bior	BiorSplines
CC	Cepstral Coefficients
CMS	Common Mode Sense
coif	Coiflets wavelet
cPCA	Classweise Principal Component Analysis
DASDV	Difference Absolute Standard Derivation
DAV	Differential Absolute Value
db	Daubechies wavelet
DFT	Discrete Fourier Transform
DOF	Degree Of Freedom
DRL	Driven Right Leg
DWT	Discrete Wavelet Transform
ECG	Electrocardiography
EEG	Electroencephalogram
EMG	Electromyography
FD	Frequency Domain
FFT	Fast Fourier Transform
FR	Frequency Ratio
FT	Fourier Transform
HIST	Histogram
ICA	Independent component analysis
iPCA	Independent Principal Component Analysis
LDA	Linear Discriminant Analysis
LOGDET	Log Detector
MAV	Mean Absolute Value
MAV1	Mean Absolute Value that uses the weighted window function
MAV2	Mean Absolute Value that uses the weighted window function
MAVS	Mean Absolute Value Slope
MEG	Magnetoencephalogram

MLP	Multilayer Perception
MNF	Mean Frequency
MNP	Mean Power
MUAP	Motor Unit Action Potential
MV	Majority Voting
MVC	Maximum Voluntary Contraction
MYOP	Myopulse Precentage
PCA	Principal Component Analysis
RMS	Root Mean Square
sEMG	Surface Electromyography
SENIAM	Surface EMG for Non-Invasive Assessment of Muscles
SFS	Sequential Forward Selection
SNR	Signal to Noise Ratio
SOBI	Second Order Blind Identification
SSI	Simple Square Integral
STFT	Short Time Fourier Transform
sym	Symlets wavelet
TD	Time Domain
TDSEP	Temporal Decorrelation Source Separation
TM3	3^{rd} Order Temporal Moment
TM4	4^{th} Order Temporal Moment
TM5	5^{th} Order Temporal Moment
TSCD	Time-Scale Domain
TSD	Time-Serial Domain
uPCA	Universal Principal Component Analysis
VAR	Variance
WAMP	Wilson Amolitude
WL	Waveform Length
WPT	Wavelet Packet Transform
WSS	Wide Sense Stationary
WT	Wavelet Transrorm
ZC	Zero Crossing

1 Introduction

1.1 The need for the upper limb prostheses

Little is known about the number of persons currently living with the loss of a limb. A deep analysis has been performed by NHI in United States in 1988 and 1996. At that time, approximately 133 735 people have undergone an amputation per year.[1] Most recent estimates of the number of amputations in United States are from the year 2005 [2]. According to these estimates, 1.6 million persons were living with the loss of the limb, and the number of amputations per year was 185 000. The number living with the loss of an upper limb, excluding finger amputations, was 41 000. According to Miscera et al. the amount of upper-limb amputations in European countries ranges from 50 to 270 per year, with about 1900 traumatic upper-limb amputees per year and a total of 94 000 upper-limb amputees in Europe [3]. In contrast with lower-limb amputations, which were usually due to vascular diseases, upper-limb amputations are mostly trauma-related (68% out of all). After accidents and injuries, certain diseases, such as tumors, vascular diseases, and infections are the most common reasons for upper limb amputations. [1] Table 1 shows numbers and causes of upper and lower limb amputations in United States in the year 2005.

The loss of an upper limb is a life-altering accident. After an amputation, even the simplest everyday tasks may become difficult, time-consuming, or fully impossible. A psychological adaption to a new situation is a long and difficult process. Thus, it is easy to see the great need for a low-cost and functional prosthetic arm for these people. However, a survey from 2002 revealed that 44% of all 70 amputees participated in the study do not use their prosthetic hand regularly due to its low functionality, poor cosmetic and unnatural appearance, lack of sensory feedback, and low controllability [4] . This situation calls for the development of versatile prosthetic limbs that will allow amputees to perform tasks that are necessary for activities of daily living.

Table 1: Estimated Prelevance by Type and Level of Limb Loss and Etiology (in thousands): Year 2005, United States. United States. (Totals may not equal sum because of rounding.) [2]

		Lower Limb		Upper Limb	
Etiology	Total	Major	Minor	Major	Minor
All etiologies	1568	623	404	41	500
Dysvascular disease: total	846	504	302	5	34
Dysvascular disease with comorbidity of diabetes	592	359	212	3	19
Trauma	704	106	101	34	464
Cancer	18	13	1	2	1

1.2 Myoelectric Information for Upper-Limb Prosthesis Control

Upper-limb prostheses can be controlled either by gross body movements (body-powered prostheses) or by using the information from myoelectric signals (myoelectric prostheses). A body-powered prosthesis captures the movements (usually of the shoulder, upper arm, or chest) by a harness system and uses them to pull a cable that is connected to a prosthesic hand or a hook. A myoelectric prosthesis utilizes the electrical action potential of the muscles of the residual limb that are emitted during muscular contractions. The emissions are picked up by electrodes and are amplified for use as control signals to the functional elements of the prosthesis. The electrodes can be either implantable electrodes (placed under the skin) or surface electrodes (places on the skin surface). [3] The myoelectric control using surface electrodes, i.e. surface electromyography (sEMG) seems to be the most used approach for the upper limb prostheses. For amputees lacking adequate dual EMG output or control, or for prostheses that require additional inputs to control more degrees of freedom the following control methods can be used: single-site electrode control schemes, servo control, linear potentiometers, linear transducers, force-sensing resistors, push-buttons, and harness switch control mechanisms.

sEMG has several advantages over other input types. Unlike body powered prostheses or mechanical switch control prostheses, myoelectrical prostheses do not need straps or other harnesses. In addition, body-powered prostheses are limited in utility, frustratingly slow to operate, awkward to maintain, and they can operate only one joint a time. The muscle activity required to provide control signals is relatively small and can resemble the effort required of an intact limb. When compared to implantable electrodes, the major advantage is noninvasiveness: the signal can be detected on the skin surface without any injury for the patient. sEMG is also relatively low cost method to control the prosthesis. [3]

However, myoelectric control has also limitations. The random nature of myoelectric signal and limits on prosthesis activation delay make fine control difficult. The other disadvantage is lack of robustness in the processing of the input to specify the output and the disparity of the means of manipulation from natural motor control and learning. [3, 5] In addition, noise can affect sEMG signals degrading the signal to noise ratio (SNR). Noise can be due to different factors such as inherent noise in electronics equipment, motion artifacts, inherent stability of signal (signal is affected by the firing rate of motor units which, in most conditions, fire in the frequency of 0 to 20 Hz) and crosstalk (the signal is detected over a muscle but generated by another muscle close to the first one).

Implantable electrodes may solve many problems related to surface electrodes and improve the MES quality: They are not affected by crosstalk and provide more stabile and independent control sites. In addition, the tissue filter effect is reduced because there is

no fat between the signal source and the electrode. However, it is somewhat unclear whether the local information of intramuscular recordings outweighs the loss of the more global information contained in the sEMG. Two present studies have compared the performance of needle and surface sEMG for prostheses control application. Farrel et al. found that it may be possible to improve the classification accuracy by acquiring the EMG intramuscularly. The improvement in classification accuracy was 9 % when Root mean square (RMS) was used as a feature but only 2.0 % when root mean square and autoregressive (AR) coefficients were used. [6] Hargrowe et al. compared six different feature set/classifier combinations and suggested that the benefits associated with intramuscular EMG do not outweigh the more global information contained in the sEMG recordings for myoelectric control. Although, sEMG has higher inter-channel correlation than the intramuscular EMG, the classification accuracy remained high for both cases in their study. [7] Fig. 1 shows the results achieved in the study by Hargrove et al.

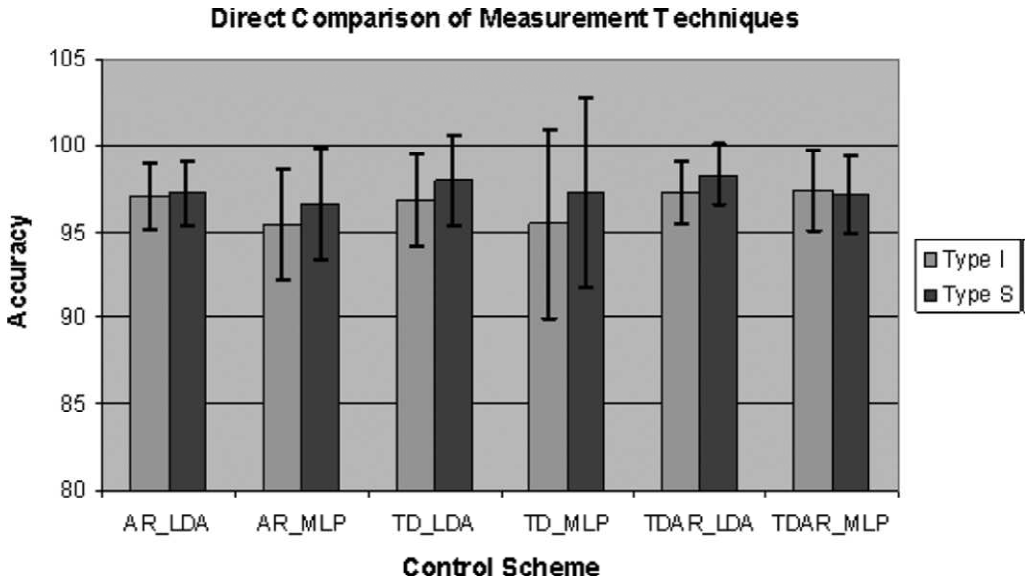

Fig. 1. The average classification accuracy and standard derivation for the six different cases. Type I refers to intramuscular recordings and type S refers to surface measurements. The classifiers used were Linear Discriminant Classifier (LDA) and a multilayer perception (MPL) artificial neural network classifier with 12 hidden layer nodes. The following features/ feature sets were used: the time domain statistics (TD), a sixth-order AR model plus the RMS signal value, and concatenated TD and sixth-order AR (TDAR). Features are described more detail in Chapter 3.6.2. [7]

1.3 Commercial Myoelectric Prosthesis

The concept of sEMG-based control of artificial devices was introduced several decades ago, in the 1940s. The first commercial arm was developed in 1960 by the Central Prosthetic Research Institute of the USSR. It had one degree of freedom and a control principle (opening and closing based on the strong contraction of antagonistic muscles, respectively) that is still state of art. [3] A multifunctional myoelectric hand was developed in Japan in 1969, and the first myoelectric elbow prosthesis was developed in the United States in 1970s. Beginning in the 1970s, the powered upper-limb myoelectric prostheses were clinically and routinely fitted to upper-limb amputees. [8] Before 1975, the common control scheme was based upon the identification of active muscle remnants in the stump of the amputee and the coding of two, at most three levels of activity of each remnant of prosthetic control. From the mid-seventies pattern-recognition-based methods began to be used. The pattern-recognition-based control allows an amputee to command a grasp posture of the prosthesis just by performing the corresponding action with the phantom limb. Thus, the pattern-based control is much more intuitive than non-pattern-based control where an amputee must learn to associate muscle remnants actions to unrelated postures of the prosthesis. In addition, non-pattern based control does not permit effective control of multiple joints, and the control may also become very difficult if the number of possible grasps shapes in the prosthesis is high. The significant breakthrough over the past years is connected to technological advances including development of new electrodes, hardware systems for sEMG signal acquisition, personal computers and embedded systems for off-line and on-line processing. [9]

To date, the most advanced upper-limb prostheses on the market are the i-limb ultra by Touch Bionics [10] and the Bebionic hand [11] by RLS Steeper. They are a real breakthrough with respect to the previous state-of –art, Otto Bock's SensorHand Speed, which is essentially an open-close mechanism. Each finger of the i-limb ultra moves independently and bends at the natural joints so that it can accurately adapt to fit around the shape of the object. The i-limb ultra also allows the user to create custom gestures. In addition, it is the only prosthetic hand that is able to gradually increase the strength of its grip on an object. However, the non-pattern-based control scheme employed in the bebionic hand and the i-limb ultra is still rather poor, using one or two electrodes to choose among a five predefined grasp shapes. [4] In addition of Touch Bionics and RLS Steeper, electronic prostheses and their components are sold by several companies, including Otto Bock, Liberating Technologies, TRS Inc, Centri, and Shanghai Kesheng Prostheses Co.

The commercial prostheses are still far from the state-of –art non-prosthetic mechanical hands, such as the Shadow Dexterous Hand by Shadow Robot Company Ltd with 20 degrees of freedom (DOFs) [12]. These hands cannot be used as prostheses, because their actuation and control system are too heavy and bulky. The power-weight ratio is a problem for the prosthetic hands, because the motor is placed on the base of the hand, which, in order to increase the motor torque, resulting in a heavier device. Two com-

mercial prosthetic hands, the i-limb ultra and SensorHand Speed, and a robotic hand The Shadow Dexterous Hand are shown in Fig. 2.

Fig. 2: a) Touch Bionics's i-limb ultra prosthetic hand; b) The Shadow Dexterous Hand; c) Otto Bock's SensorHand Speed prosthetic hand. [13]

Table 2 presents a comparison among some commercially available prosthestic hands a robotic hand, and human hand. The natural forearm consists of five fingers, palm, and wrist joint. Each finger has three joints and 4 DOF. The palm has many joints, but the motive freedom is integrated into one DOF. The wrist joint has 3 DOF. Thus, the ideal prosthetic hand should have 24 DOF. However, because of their physical restrictions, such as weight, size, and power, the DOFs of commercial prostheses to five. Sensor Hand Speed has Autograsp feature that enables the hand to sense a change in the center of gravity and re-adjusts its grip automatically [14]. In many prosthesis the control speed and grip force are determined by the level of the muscle signal. Usually, only the open-close –function can be controlled with myoelectric signals and wrist rotation is passive. In order to make the appearance closer to human arm, prosthesis is usually covered with an artificial skin. The prostheses are available with different size and skin colors.

Table 2: Comparison of human hand, a robotic hand, and some commercial prosthetic hands.

Prosthestic hand	DOFs	Weight of the hand (g)	Number of fingers	Opening Width (mm)	Opposable thumb	Maxi-mal Grip force (N)	Proportional Speed (mm/ sec)	Achievable Grasps	Manufacturer	References
Human hand	24	500	5	-	yes	150	-	Most common: power, index point, precision, lateral pinch (3)	-	[15]
Shadow Dexterous Hand (1)	20	4000	5	-	yes	40	1.4 for full open or close	Power, Precision, Lateral, Hook, Tripod, Fingerpoint, Counting (2)	The Shadow Robot Company Ltd	[16] [17]
Centri Myoelectric Hand	1	205-250	3	66-76	no	63-81	150	power	Centri	[18]
SensorHand Speed	1	350-500	3	100	no	100	15-300	Power	Otto Bock	[14] [17]
Proportional DMC Plus	1	440	2	100	no	90	15-130	Power	Otto Bock	[19]
i-limb ultra	11	450-615	5	135	yes	100	200	Allows user to create custom grasps	Touch Bionics	[20] [17]
Bebionic Hand	11	495-539	5	100	yes	75	1.9 s (power) 0.8 s (precision) 1.5-1.7 s (key)	Power, Lateral, Hook, Precision, Index point	RSL Steeper	[11] [17]

(1) A robotic hand, (2) No independent control of fingers 3-5 (3) It has been shown that nearly 80 % of the time the house maid used just six grasps and the machinist used nine [15].

1.4 Objective of the Thesis

This thesis examines the pattern-recognition-based control of myoelectric prosthesis. The EMG signals of the forearm muscles vary between different hand postures. The pattern-recognition-based control identifies different intended hand postures of the prosthesis by utilizing the information of the EMG signals. Thus, the pattern-recognition-based approach enables much more natural and easy control than the non-pattern-based control strategy used in commercial prosthesis. The aim of this thesis is to find the feature vector that yield the highest classification accuracy when the EMG signals, measured on the forearm of the subject during six hand postures and resting state, are classified with Linear Discriminant Analysis (LDA) classifier. The selection of appropriate features is very important because the feature set has a significant effect on the classification accuracy. LDA classifier is used in this study because it has shown to be the most suitable classifier for hand posture classification of sEMG signals.

The second goal was to investigate whether it is possible to use lower sampling rate than the commonly used 1000 Hz. Lower sampling rate is desired because it saves the data processing time and memory of the prosthesis controller. In addition, Independent Component analysis is examined as a preprocessing method because it has shown to be promising to eliminate crosstalk artifacts. The effect of a postprocessing method, Majority voting, is also demonstrated. The measurements are collected with surface electrodes on the right forearm of eight able-bodied subjects.

The thesis is organized as follows. Firstly, we introduce the anatomy and physiology of the muscles in the human forearm. The formation of the sEMG signal and the most common artifacts related to sEMG are also described. In addition, we examine electrode types and review previous studies about optimal electrode placement. Secondly, we study the preprocessing of the EMG signal by discussing an optimal cut-off frequency and an optimal sampling rate as well as two preprocessing algorithms, Independent Component Analysis and Classwise Principal Component Analysis. We present the two control methods used in myoelectric prostheses: a pattern-based method and a non-pattern-based method. However, because the focus of this study is on the pattern-based approach, the non-pattern-based control scheme is described only briefly. The pattern-based control is described step by step: segmentation, feature extraction, feature normalization, dimensionality reduction, classification, and postprocessing. Evaluating methods for classification accuracy are also discussed. Thirdly, we present the measurement system, electrode placement, and experimental setup used in this study. Data preprocessing and representation as well as feature selection are also described. Finally, the results are presented and discussed.

2 Application Area

2.1 Anatomy and Physiology of the Arm Muscles

The aim of this chapter is to give an overview of anatomy and physiology of the forearm muscles. The physiology of the muscle contraction is the basis of sEMG. The electrical model for the motor action potential, described in this chapter, reveals how the sEMG signals provide a quantitative, reliable, and objective means of accessing muscular information. The knowledge of anatomy of the human arm is important when optimal electrode placement is determined. Thus, the anatomy of the human forearm and function of each forearm muscle are introduced.

2.1.1 Action Potential

An action potential is a sequence of rapidly occurred events that reverse the membrane potential, and then eventually restore it to the resting state. When muscle fibers become innervated, the diffusion characteristics on the muscle fiber membrane are briefly modified, and sodium ions flow into muscle cell membranes resulting in depolarization. As a result of the inflow of positively charged sodium ions the membrane potential changes from -80 mV to +30 mV. At the peak of the action potential the inside of the cell is 30 mV more positive than the outside. After this, sodium channels close and potassium channels open. Some potassium ions leave a neuron, and a few negative charges begin to buildup along the inside surface of the membrane restoring immediately the ionic equilibrium through the repolarization process which lasts typically 2-3ms. [21] Following the repolarization there may be an after-hyperpolarization phase where the membrane potential temporarily becomes more negative than the resting state. Action potential is illustrated in Fig. 3.

A nerve action potential elicits a muscle action potential similar to the action potential in neurons. Muscle action potential begins from the motor end plates, and spreads across the muscle fibers in both directions at a propagation speed of 2-6 m/s. The action potential causes a release of calcium ions in the intracellular fluid, and produces a chemical response resulting in a shortening of the contractile elements of the muscle cells. [21]

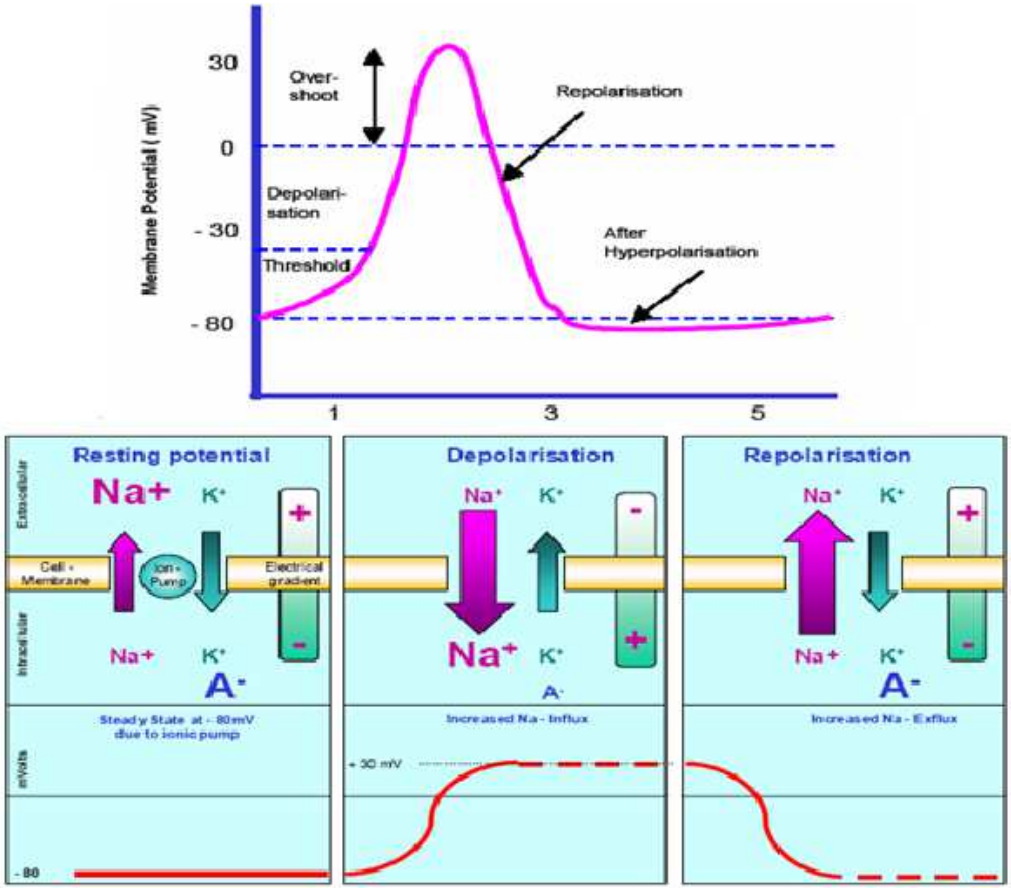

Fig. 3: a) General shape of an Action Potential. b) Three phases of action potential. [22]

2.1.2 Muscle Contraction

A skeletal muscle consists of individual muscle fibers each of which is a single cylindrical muscle cell. Fibers are bundled into fascicles and surrounded by three connective tissue layers that are extensions of the fascia. Muscle fibres consist of the myofibrils, the contractile elements, which contain overlapping thick and thin filaments. The filaments inside a myofibril are arranged in components called sarcomeres, which are basic functional units of a myofibril. Narrow, plate-shaped regions of dense protein material called Z-disks separate one sarcomere from the next. Organization of skeletal muscle and its connective tissue coverings is illustrated in Fig. 4. [21]

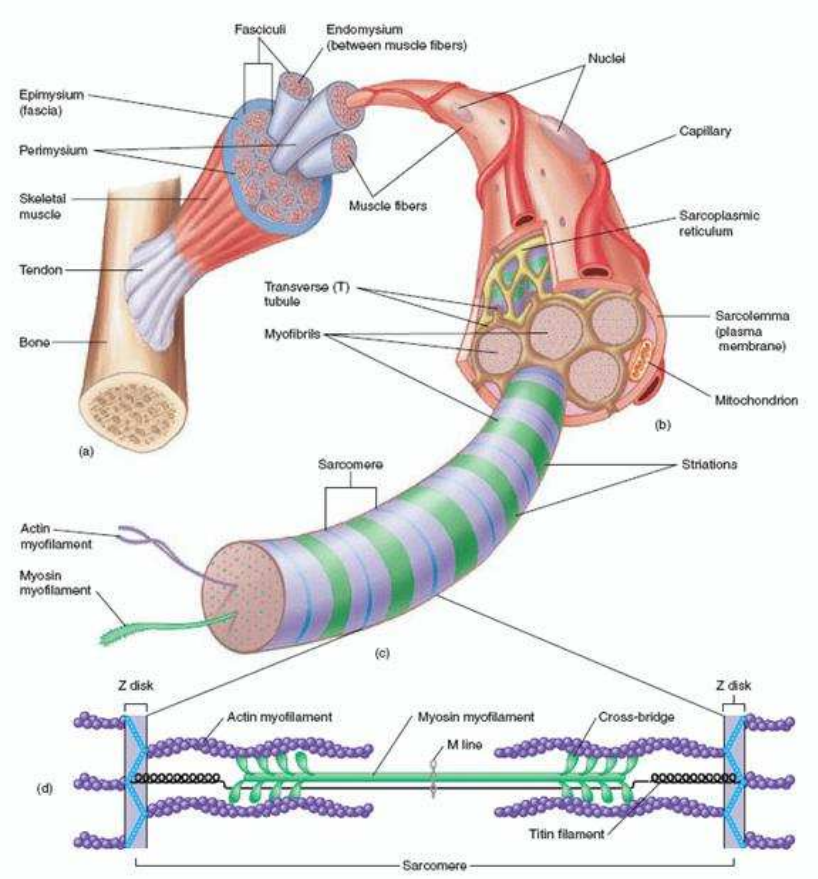

Fig. 4: Organization of skeletal muscle. [21]

Each skeletal muscle fibre is controlled by a neuron at a single neuromuscular junction midway along the length of the fibre. A motor neuron and the muscle fibers it innervates form a motor unit. Muscle contraction begins when a motoneuron cell is activated induced by the central nervous system or as a result of reflex. Secondly, impulses triggered by integrating center propagate along the axon of motor nerve to the motor endplates where neurotransmitters are released. Arrival of the nerve impulse at the synaptic end bulbs causes many synaptic vesicles to fuse with the motor neuron's plasma membrane, liberating a neurotransmitter Acetylcholine (ACh) into the synaptic cleft. The ACh diffuses across the synaptic cleft between the motor neuron and the motor end plate. Binding of ACh molecules to the receptors on the motor end plate opens ion channels in the ACh receptors allowing sodium ions (Na+) to flow across the membrane. As a result of the sudden inrush of sodium ions the inside of the muscle fiber become more positive which triggers a muscle action potential. A muscle action potential propagating along the sarcolemma causes Ca^{2+} channels to open and the Ca^{2+} ions to flow out of the sarcoplastic reticulum into the cytosol around the tick and thin filaments. An increase in Ca^{2+} concentration in the cytosol starts muscle contraction and a decrease stops it. The calcium ions combine with tropomyosin. As a result tropomyosin changes its shape and moves away from the myosin-binding sites on actin. Myosin heads bind to these free binding sites, and the concentration cycle begins. [21]

Four steps of the contraction cycle can be seen in Fig. 5. Muscle contraction occurs when myosin heads attach to and slide along the thin filaments at both ends of a sarcomere, progressively pulling the thin filaments toward the middle of the sarcomere (M-line). Thin filaments slide inward and meet at the center of the sarcomere. As a result, the Z discs come closer together, and the sarcomere and shortens, causing shortening of the whole muscle fiber, which in turn leads to shortening of the entire muscle. This can culminate in the whole muscle shortering by as much as 50 %. [21]

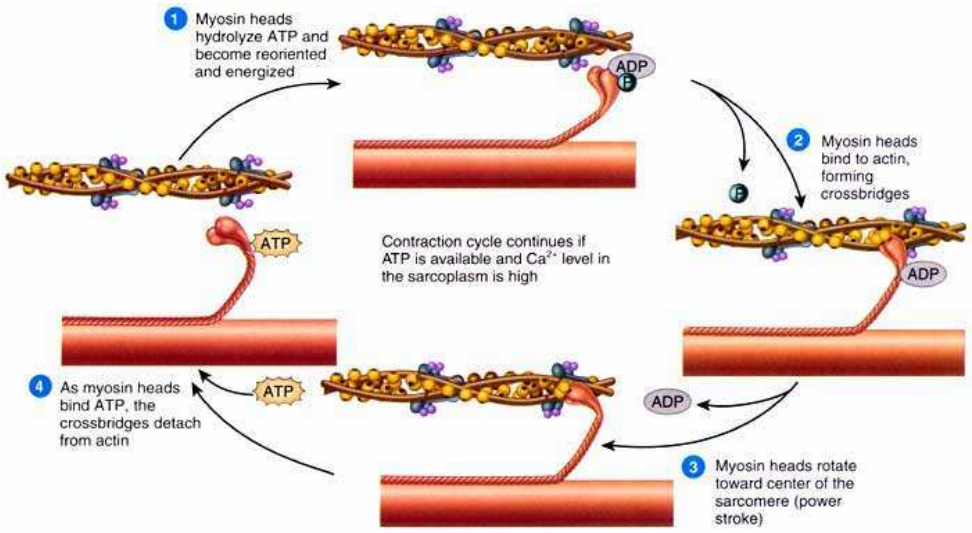

Fig. 5: Contraction cycle. [21]

2.1.3 Anatomy of Human Arm

The forearm muscles act on the elbow and wrist joints and on those of digits. These muscles can be divided into flexor-pronator and extensor-supinator groups. The anterior forearm muscles are divided into three muscular layers, a deep layer, intermediate layer and superficial layer, as can be seen from Fig. 6. A septum of deep fascia separates the deep layer of the flexor muscles from the superficial and intermediate layers. The muscles of the posterior of the forearm are divided into the superficial and deep groups. These muscle layers are shown in Fig 7. Table 3 describes the action of each arm muscle.

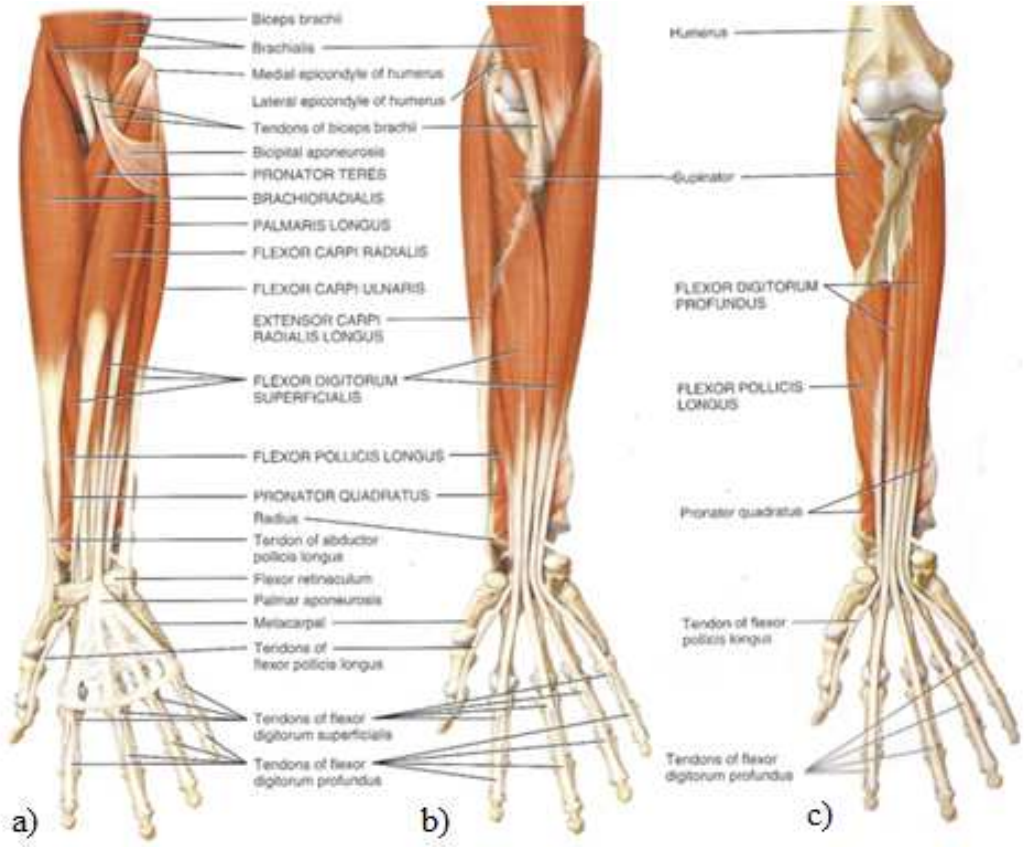

Fig. 6: The anterior compartment muscles of the forearm that move the wrist, hand, and fingers. a) Superficial view b) Intermediate view c) Deep view [21]

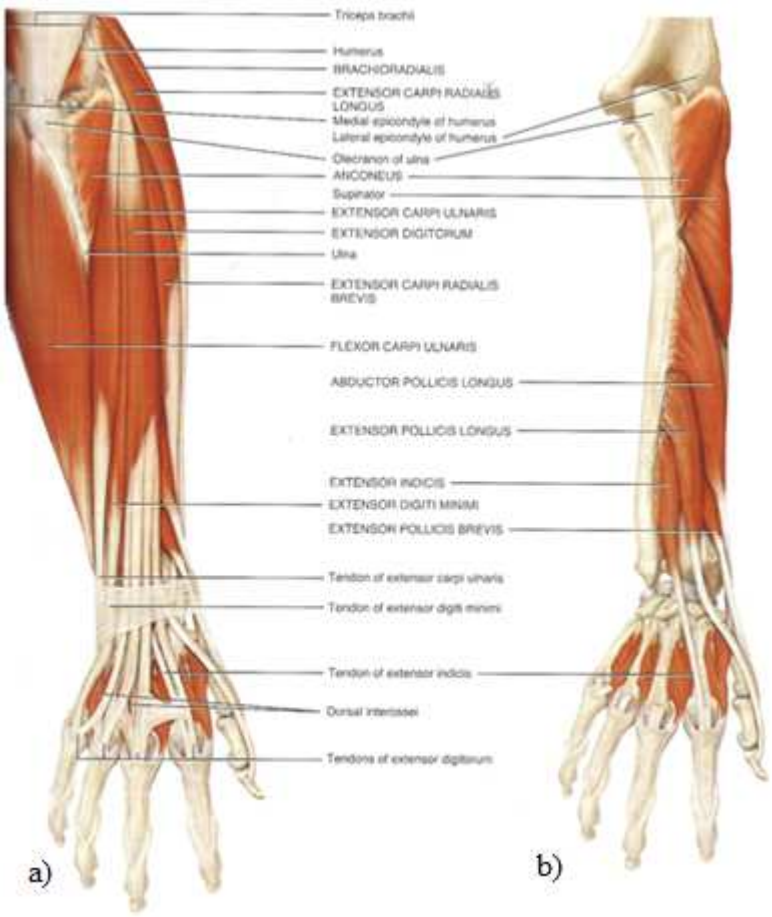

Fig. 7: The posterior compartment muscles of the forearm that move the wrist, hand, and fingers. a) Superficial view b) Deep view [21]

Most of the muscles that move the forearm and hand originate within the forearm. This is not the case with the biceps bachii and triceps brachii however, which insert from the arm. Contraction of the biceps brachii flexes the elbow and supinates the forearm and contraction of the triceps brachii extends the elbow. The brachialis and brachioradialis flex the elbow and are opposed by the anoconeus and the triceps brachii respectively. The flexor capri radialis flexes and abducts the wrist, whereas the flexor capri ulnaris flexes and adducts. The Palmaris longus aid the flexor capri radialis and flexor capri ulnaris in the flexion of the wrist. The extensor capri radialis produces extension and abduction of the wrist and the extensor capri ulnaris produces extension and abduction. The pronator teres and the supinator rotate the radius without either flexing or extending the elbow. They arise on both the humerus and forearm. The pronator quadratus arises on the ulna and assist the pronator teres in opposing the actions of the supinator or biceps brachii. [23]

Several superficial and deep muscles of the forearm move the digits in various ways. These so called extrinsic muscles stop before reaching the wrist and only their tendons cross over into the hand. The tendons pass through tendon sheaths that reduce friction and keep the tendons lubricated. This provides the hand and wrist with maximum mobility, while at the same time providing muscle forces far in excess of those which the

intrinsic muscles of the hand are able to generate. The extrinsic muscles produce powerful but crude movements of the hand and fingers. Weak but fine control of the hand is performed by the intrinsic muscles which originate on the carpal and metacarpal bones. No muscle originates on the phalanges, and only tendons extend across the distal joints of the fingers. [23]

Table 3:The actions of arm muscles

Muscle name	Function
Flexor capri radialis	Flexes and abducts hand (radial derivation) at wrist joint.
Palmaris longus	Weakly flexes hand at wrist joint.
Flexor capri ulnaris	Flexes and adducts hand at wrist joint.
Flexor digitorum superficialis	Flexes middle phalanx of each finger at proximal interphalangeal joint, proximal phalanx of each finger at metacarpophalangeal joint, and hand at wrist joint.
Flexor pollicis longus	Flexes distal phalanx of thumb at interphalangeal joint.
Flexor digitorum superficials	Flexes distal and middle phalanges of each finger at interphalangeal joints, proximal phalanx of each finger at metacarpophalangeal joint, and hand at wrist joint.
Extensor Capri Radialis longus	Extends and abducts hand at wrist joint.
Extensor Capri radialis brevis	Extends and abducts hand at wrist joint.
Extensor digitorum	Extends distal and middle phalanges of each finger at interphalangeal joints, proximal phalanx of each finger at metacarpophalangeal joint, and hand at wrist joint.
Extensor digiti minimi	Extends proximal phalanx of little finger at metacarpophalangeal joint and hand at wrist joint.
Extensor Capri ulnaris	Extends and adducts hand at wrist joint.
Abductor pollicis longus	Abducts and extends thumb at carpometacarpal joint and abducts hand at wrist joint.
Extensor pollicis brevis	Extends proximal phalanx of thumb at metacarpophalangeal joint, first metacarpal of thumb at carpometacarpal joint, and hand at wrist joint.
Extensor pollicis longus	Extends distal phalanx of thumb at interphalangeal joint, first metacarpal of thumb at carpometacarpal joint, and abducts hand at wrist joint.
Extensor indicis	Extends distal and middle phalanges of index finger at interphalangeal joints, proximal phalanx of index finger at metacarpophalangeal joint, and hand at wrist joint.
Pronator teres	Pronation of forearm, flexes elbow
Pronator Quadratus	Pronates the forearm

2.2 Surface Electromyography

This Chapter introduces the principles of sEMG, a noninvasive technique for detecting the electrical activity produced by electrically or neurologically activated skeletal muscle cells. The formation of sEMG-signal is firstly described. After that, the typical features and artifacts of the sEMG signal are examined.

2.2.1 Formation of sEMG signal

sEMG measures the actiopotential, described in the previous chapter. A depolarization-repolarization process is a monopolar action potential that travels across the surface of the muscle fiber. Electrodes in contact with this wave front present a bipolar signal to

the sEMG differential amplifiers because the electrodes are measuring the difference between two points along the direction of propagation of the wave front. Because these electrodes are not very selective, the sEMG signal is formed by a superposition of the motor unit action potential trains (MUAPT) from many muscle fibers. [8,7] Merlo et al. [24] modeled the sEMG signal *s(t)* as

(1)

where *j* indicates the specific motor unit, k_j is an amplitude factor, θ_{ij} are the occurrence times of the MUAPs of the motor unit, α_j is a scaling factor, and *n(t)* is additive noise. The formation of sEMG signals is illustrated in Fig. 8.

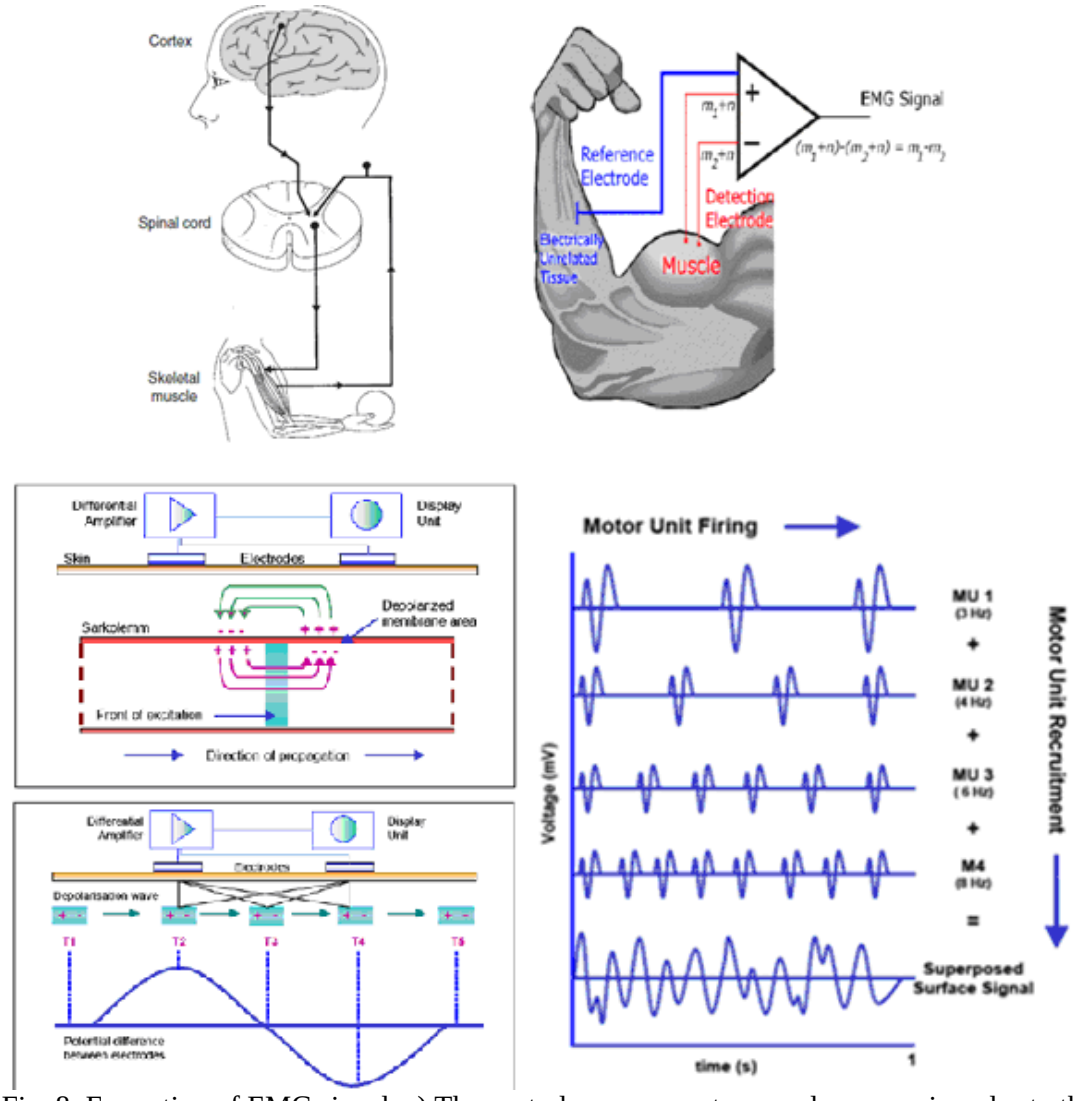

Fig. 8: Formation of EMG signal. a) The central nervous system sends a nerve impulse to the working muscle, causing it to contract. b) Electrodes at the surface of the skin measure the action potentials of several motor units. c) Usually, bipolar measurements (i.e. difference between two adjacent electrodes) are used to eliminate the noise. In addition, the signal is amplified. d) The final signal is superposition of many motor unit action potentials. [22]

The amplitude of the sEMG signal is about 10 mV (peak to peak). However, sEMG signal is strongly influenced by physiological, anatomical and biochemical factors. The strength of the EMG signal is depending on the size of the muscle that is measured and its position relative to the electrode. Thus with different electrode placements the EMG amplitude at maximum force production of underlying muscles may be very different. Because of a high number of overlapped MUAPs, and the irregular nature of motor unit discharge, the signal may be considered a complex and non-stationary stochastic signal. Because of the inherent physiology of the organ, sEMG signal is non-stationary, even during a constant voluntary contraction. However, during low-level (20-30% of the Maximum Voluntary Contraction, MVC) and short-time contractions (20-40 s), sEMG signal can be assumed to be wide-sense stationary (i.e. the mean of the process can be assumed to be a constant, the autocorrelation $rx(k,l)$ can be assumed to depend only on the difference $k-l$, and the variance of the process can be assumed to be finite [25]. Higher level contractions (50-80% MVC) can be assumed locally stationary for a period of 500-1500 ms. Thus, sEMG can be assumed to be stationary in real-time applications. The level and duration of contraction, muscle states (constant or dynamic), muscle fatigue, and sweat from skin determine the characteristics of the signal. Especially, sEMG signals at higher contraction levels are usually assumed to be a zero-mean Gaussian processes. At low-level contractions signals can be assumed zero-mean Laplacian processes. [26] Clancy et al. found that a myoelectric signal model for a constant-force, constant-posture, non-fatiguing contractions falls between Gaussian and Laplacian models, but on average Gaussian model fits better. [27]

Fig. 9 illustrates the effect of the grasping force to the signal amplitude. The subject increased the grasping force in four steps. This can be clearly seen from the signal: The amplitude increases in four steps from very small to high. As it is apparent from Fig. 9, the amplitude of EMG signal is correlated with the force generated by the muscle. However, estimating this force in general is challenging because of the difficulties in activating a single muscle in isolation, isolating the signal generated by a muscle from the signals of its neighbors (muscle crosstalk), and other associated problems.

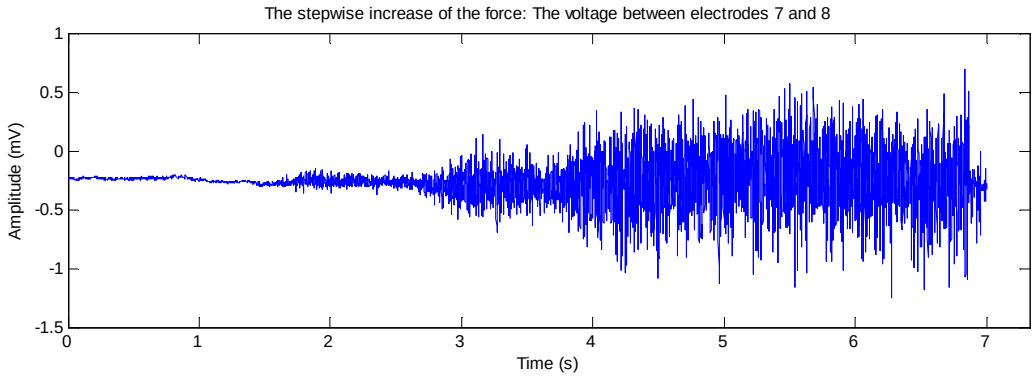

Fig. 9: Effect of the muscle contraction force to the sEMG signal amplitude.

2.2.2 The Raw EMG Signal

An unfiltered and unprocessed EMG signal is called a raw EMG signal. In Fig. 10 a raw recording was done for three static contractions of the biceps brachii muscle. When the muscle is relaxed, an EMG baseline can be seen. The healthy relaxed muscle shows no significant EMG activity. Raw EMG spikes are of random shapes and thus one raw recording burst cannot be precisely reproduced in exact shape. This is because the actual set of recruited motor units constantly changes within the matrix and diameter of available motor units. [22]

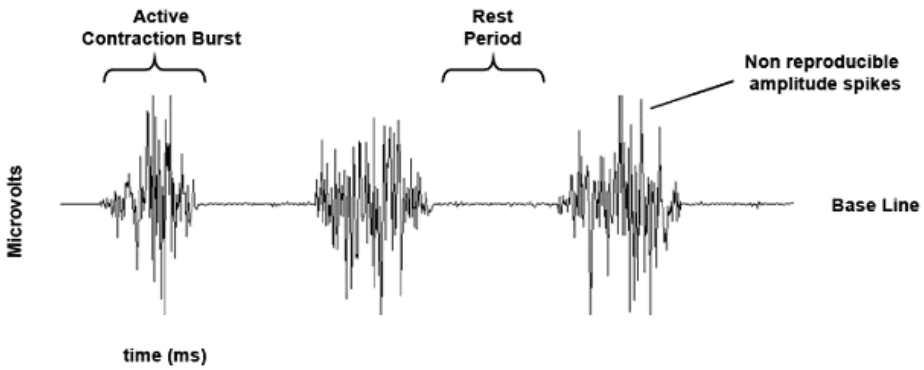

Fig. 10: The raw EMG recording of three static contractions of the biceps brachii muscle.[22]

2.2.3 Surface EMG Artifacts

An artifact is unwanted information contained within a signal. An EMG signal is very tiny and thus sensitive to artifacts. The most common sEMG artifact is the line interference of 50/60 Hz noise. It originates from the power line and is transmitted by the electrical devices placed near the EMG data acquisition device. An example of line interference is shown in Fig. 11. [22]

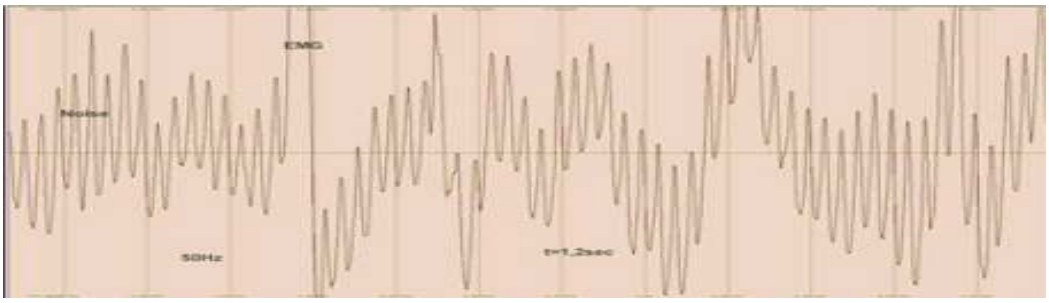

Fig. 11:50 Hz noise in the signal.

Another very common type of artifact is a movement artifact. Movement artifacts occur when patient moves and the electrode slips around on the surface of the skin. Any change of distance between signal origin and detection site will alter the EMG reading. Movement artifacts are inherent problems of all dynamic movement studies and can also be caused by external pressure. They can be avoided by affixing leads to the subject

with tape or wraps. Electrodes should also be prevented from being struck. The use of strong high-pass filter in post-processing may eliminate this type of artifacts. [22] Fig. 12 shows a movement artifact when the electrode is moving with respect to the skin.

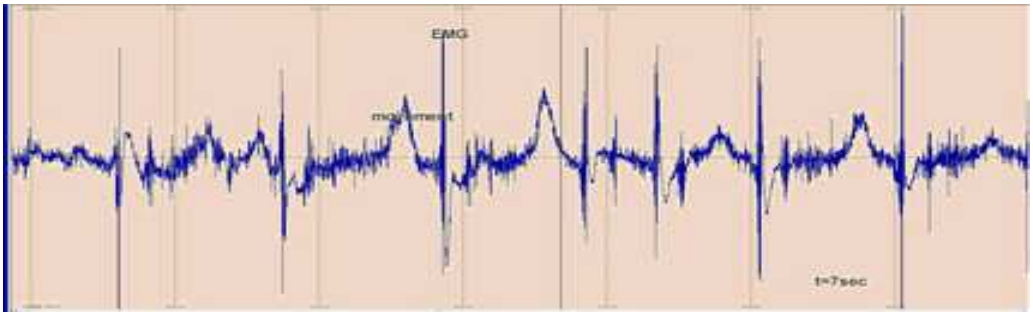

Fig. 12: Artifact when the electrode is moving with respect to the skin.

When the muscle is moving, the body will show some movements as well. As a result the cable may move in the space between the electrode and the input of the amplifier causing movement artifacts shown in Fig. 13. [28]

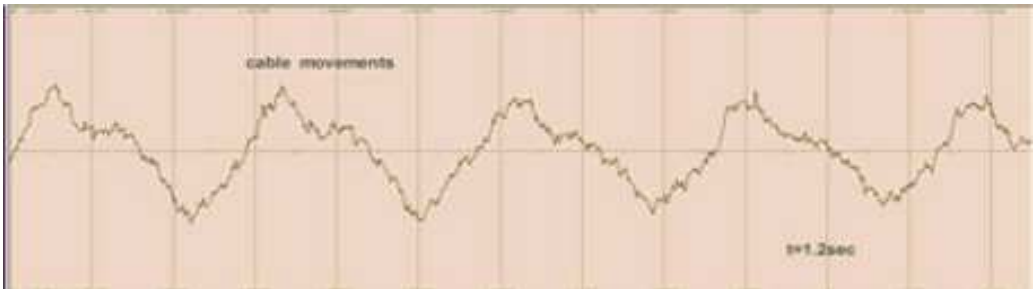

Fig. 13: Movement artifact when the cable is moving.

The difference in the impedance between the skin and the electrodes may cause DC offset artifacts. It adds an offset to the raw signal which is normally centered on zero. Usually proper skin preparation and firm placement of electrodes on the skin prevent the problem. [22]

Electrocardiography (ECG) artifact occurs when recording near the heart. ECG has higher voltages than EMG. ECG artifacts are difficult to remove from the EMG signal but they can be avoided by placing the electrodes so that they are not aligned with the axis of the heart activity.[22] Electrodes should also be placed as far away from the heart as possible and on the same side of the body. Proper electrode and cable fixation and very good skin preparation can solve these problems.[29] ECG artifact can be seen in Fig. 14.

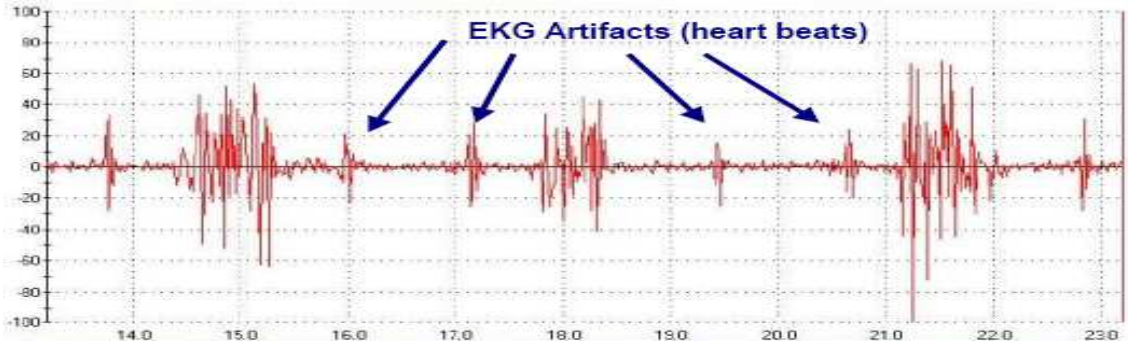

Fig. 14: EMG raw recording with ECG spikes. [29]

Muscle crosstalk is due to EMG signals coming from other muscles than the ones being monitored. Crosstalk can be reduced by placing electrodes at the middle of the muscle belly as well as choosing the appropriate inter-electrode distance (around 2 cm). [22] Also a preprocessing by independent component analysis or classwise principal component analysis may reduce crosstalk artifacts [30, 31].

2.3 Electrodes

A good acquisition of sEMG signal by electrodes is prerequisite for good signal processing. This chapter introduces different electrode types used to measure sEMG signal as well as the optimal electrode placement on the surface of the skin. Secondly, the effect of electrode structure and configuration to the signal is described. Thirdly, we review some recent studies that have been done to optimize the electrode placement to identify different hand postures.

2.3.1 Electrode Types

sEMG electrode can be defined either as a sensor of the electrical activity of a muscle or as a transducer of the ionic current, flowing in the tissue, into the electronic current, flowing in the metal wires. Two types of sEMG electrodes exist: floating electrodes and dry electrodes. Floating or wet electrodes have a layer of conductive gel as a chemical interface between the skin and the metallic part of the electrode. Dry electrodes are in direct contact with the skin, and they can be made of noble metals, carbon, sintered silver or silver chloride. Another classification is based on electro-chemical behavior. On this basis, it is possible to distinguish between polarizable and non-polarizable electrodes. In polarizable electrodes no actual charge crosses the electrode-electrolyte interface (e.g. Platinum electrode), but non-polarizable electrodes allow current freely pass across the interface (e.g Ag/AgCl electrode). Non-polarizable electrodes are, however, not suitable to record sEMG because of the risk of motion artifacts. [32] Electrodes are often accomplished by miniature pre-amplifiers to differentiate small signals of interest. [3]

2.3.2 The effect of Electrode Placement on the EMG-signal

The importance of electrode structure and configuration lies in their effect on classification accuracy, and prosthesis production cost. The number of electrodes also affect the processing time of the data. Thus, a configuration that yields high classification accuracy with few electrodes would be a very useful in prosthetic control. [33] The electrode configuration describes the area and shape of the electrode detection surfaces which determine the number of active motor units that are detected by virtue of the number of muscle fibers in the vicinity. In addition, the electrode configuration includes the distance between electrode detection surfaces which influences the bandwidth of the differential electrode configuration. The location of the electrode with respect to the motor points in the muscle and myotendonous junction determines the amplitude and frequency characteristics of the detected signal. The location of the electrode on the surface of the muscle with respect to the lateral edge of the muscle determines the possible amount of crosstalk that may be detected by the electrode. The orientation of the detection surfaces with respect to the muscle fibers affects the value of the measured conduction velocity of the action potentials and the amplitude and frequency content of the signal. Fig. 15 displays the influence of the electrode location on the amplitude and frequency spectrum of the signal. [34]

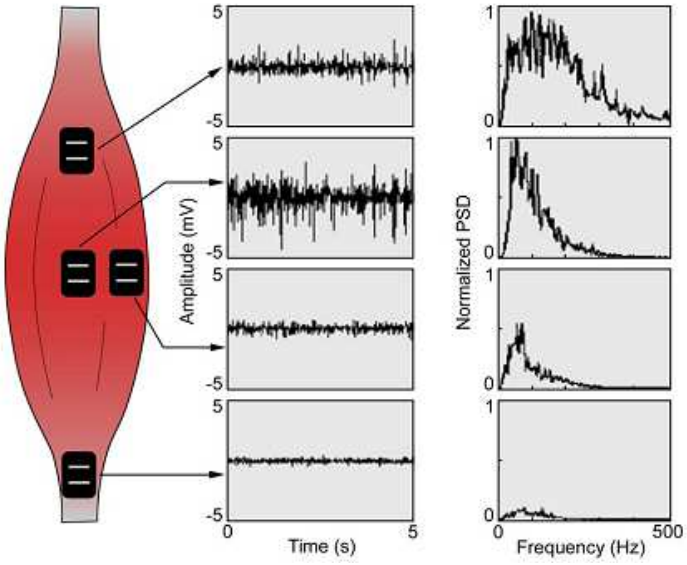

Fig. 15: The amplitude and frequency spectrum of the EMG signal is affected by the location of the electrode with respect to the innervation zone (top electrode), the myotendonous junction (bottom electrode) and the lateral edge of the muscle (middle right electrode). The preferred location, where the EMG signal with the greatest amplitude is detected, is in the midline of the belly of the muscle between the nearest innervation zone and the myotendonous junction. [34]

Two alternative configurations commonly used to acquire sEMG signals are a monopolar configuration and a bipolar configuration. In the monopolar configuration an electrode is placed over the skin along the muscle, and the sEMG signal is recorded with respect to a reference electrode located to away on a neutral part of the skin. In the

bipolar configuration the signal recorded at two sites, the two signals are subtracted and the difference is amplified, as illustrated in Fig 8. Therefore, the signals that are common to both recording sites will cancel each other and only the signals that are different at the two sites will have a differentiate. Common signals originate from far away from the detection sites, whereas signals in the vicinity of the recording site will be different. As a result, relatively distant power lines noise signals will be removed and relatively local EMG signals will be amplified. The other advantage of the bipolar measurements is that because they have no single reference site, amplification can occur at the recording site, before noise becomes introduced into the system. [3]

2.3.3 Studies for Optimizing Electrode Placement for Electromyographic Control

Despite of the importance of the electrode configuration to the quality of the EMG recordings, only few researchers have studied an optimal electrode placement for EMG control of prosthesis. This is because EMG is generally limited to on/off control. While it has been shown that EMG can be used to identify different hand postures, or to control single fingers, the issue has been the number and location of electrode sites on forearm.

Walbarn et al. have shown that electrode sites can be optimized in order to provide maximum accuracy control actuation. They created a silicon mould of a human hand with an array of electrodes embedded within it and recorded data from each electrode site. The sites that provide the greatest difference in signal strength from resting to activation were identified. Several points in the extensor compartment of the forearm were found to be useful in recognizing hand postures, while several points in the flexor compartment of the forearm were found to be useful in differentiating between hand postures. Some of their results are shown in Fig. 16. The figures show an unrolled coordinates of the electrodes in the silicon armband. Positive θ refers to the flexor muscles (under the forearm), and negative θ refers to the extensor muscles (on top of the forearm). [35]

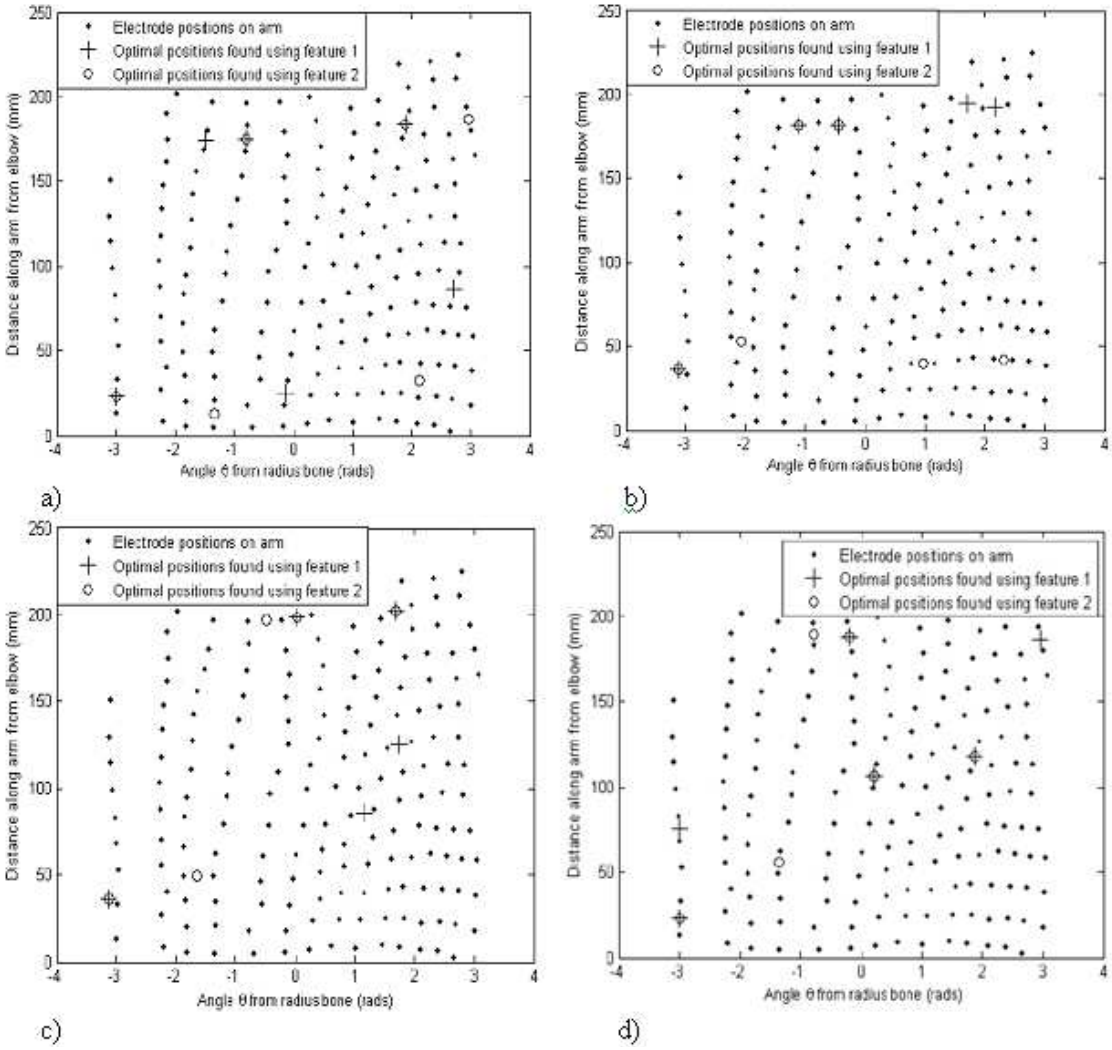

Fig. 16: a) Optimal electrode positions found using longitudinal derivates for discriminating between cylinder grasp and relaxing. b) Optimal electrode positions found using radial derivates for discriminating between cylinder grasp and relaxing. c) Optimal electrode positions found using radial derivates for discriminating between pinch grasp and relaxing. d) Optimal electrode positions found using longitudinal derivates for discriminating between pinch grasp and relaxing. [35]

Walbarn et al. have also extended their study to identify the optimal sites for grasp control, between different grasp types. They collected and processed data from 128 sites on a human forearm while two different grasps (a pinch grasp and a cylindrical grasp) were performed. Two feature extraction methods were used to gain different representations of the data: integral of absolute value (IAV) and differential absolute value (DAV). The regions around the wrist seemed to be best for using circumferential derivates (circles and squares), while regions around the elbow seemed to be best for using longitudinal derivates. [36]

As the thumb is responsible for a majority of the grasp forming, it is likely that optimal electrode places would be found in the wrist region, the only place where the thumb muscles are close to the surface of the skin. The signals from that area would be expected to show large changes when a grasp type is changed. This can be seen in the cir-

cumferential data. However, for longitudinal derivates the majority of the useful sites are found closer to the elbow. These derivates would be expected to represent action potentials running the length of the muscle fiber. This could represent a region where rotator muscles run or it is possible that there are subject specific characteristics with the subjects.[36] Fig.17 shows the regions which would be best for using circumferential derivates (circles and squares) and the regions suggested to be best for using longitudinal derivates (triangles left and right.)

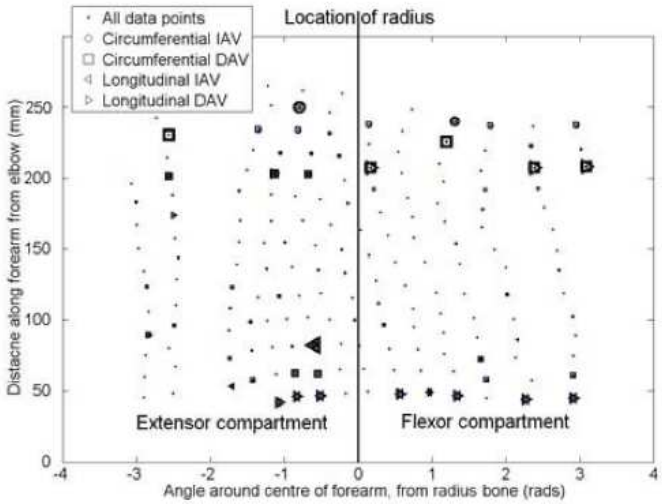

Fig. 17: The regions which would be best for using circumferential derivates and the regions which would be best for using longitudinal derivates. [36]

Andrews et al. investigated the effect of the number and location of electrodes on finger movement classification during a typing task [33, 37]. They found that optimal classification systems [37] and the best-performing electrode arrangement for each array size may be subject-dependent. They also suggested that for many subjects an array size of three electrodes can provide comparable classification performance to array sizes of up to eight electrodes. The effect of an array size on classification accuracy can be seen in Fig. 18. Dashed lines represent individual subjects and the solid line shows the average over all subjects. [33]

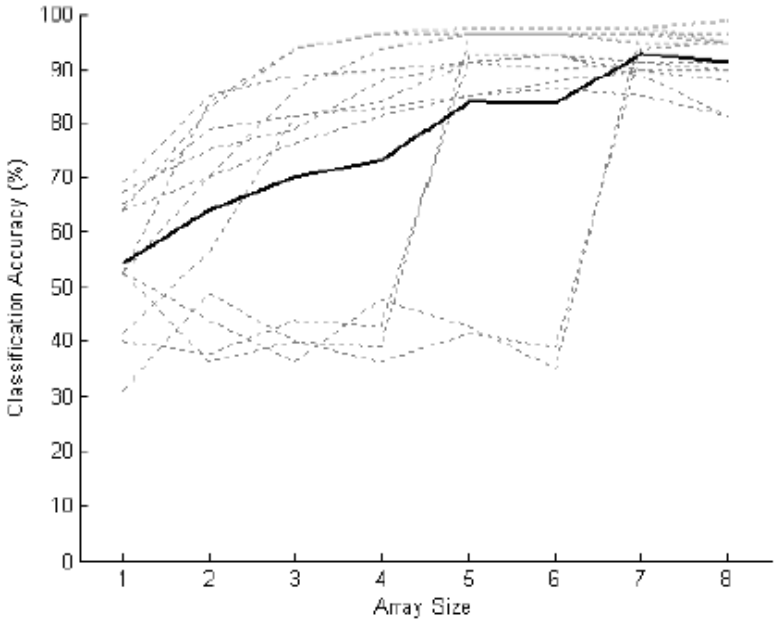

Fig. 18: The effect of array size on classification accuracy: individual subjects (dashed lines), average over all subjects (solid line). [33]

Andrews et al. found also some trends associated with the electrode positions. Fig. 18 shows the electrode placement on the posterior (top) surface and anterior (bottom) surface of the forearm. In array sizes of six or fewer electrodes, positions 1 and 7 were most commonly selected while locations 4, 5 and 8 were least commonly selected. Electrodes at positions 7 and 8 would be expected to receive similar signals because both of them are placed approximately over the flexor digitorum profundus, a muscle that is responsible for finger movement. The difference in their performance may be due to the proximity of position 8 to the ulna, so that position 7 yielded a stronger signal and was therefore often favored over position 8. Positions 4 and 5 were located farther from the finger movement muscles than many of the other electrode positions. The good performance of position 1 may be due to its proximity to the extensor digitorum communis muscle and its proximity to fewer muscles tan positions 2 and 3 that are unrelated to finger movement (for example supinator and extensor Capri radialis longus), which would have affected signal-to-noise ratio. [33]

Hargrove et al. determined the optimal electrode placement locations for their study where they compared the surface and intramuscular myoelectric signal classification. They found that surface electrodes placed over the extensor/supinator, flexor Capri ulnaris, and flexor digitorum subliminus are essential in providing good classification accuracy. These locations are shown in Fig. 19. There was some variation in the manner the surface electrode was applied between subjects because of the need to insert around the intramuscular fine-wire electrodes and the differences in the physical dimensions of the subjects forearm. Therefore, more judicious surface electrode placement strategy may result in more precise optimal channel locations. However, it can be seen that general regions may provide better discrimination information for the 10 hand posture investigated. [7]

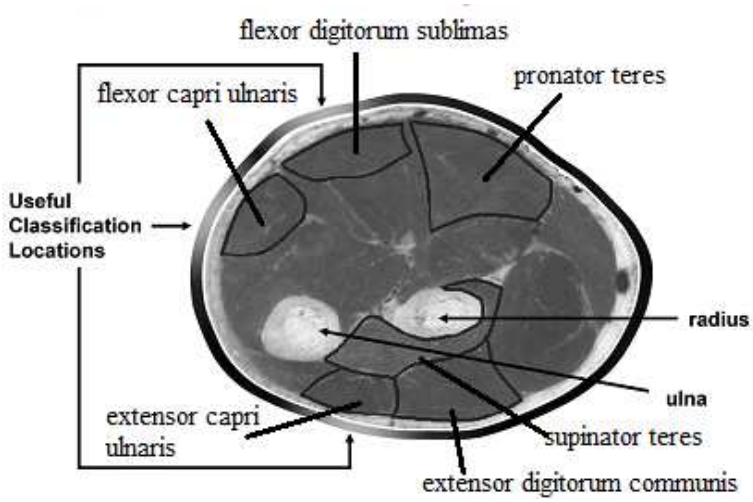

Figure 19: A cross section of the upper forearm. The light regions of the ring surrounding the forearm indicate electrode placement areas which were most useful for classification. [7]

Previous studies have placed the electrodes either with reference to particular muscles [6, 13, 38, 39] or equidistantly over an area of interest [6, 40]. The number of electrodes vary between 1 [41] to 35 [42]. However, the effect of electrode configuration on classification accuracy cannot be clearly deduced through comparison of these studies because of differences in the study details.

3 Methods

3.1 Pre-processing

The goal of pre-processing is to maximize the quality of the acquired signals in terms of SNR and minimize possible distortion. Usually, this is done by using amplifiers. In addition, classification accuracy can be improved by using preprocessing algorithms whose aim is to suppress undesired distortions or enhances important features for further processing. This chapter introduces the typical filters and two algorithms, Independent Component Analysis (ICA) and Classwise Principal Component Analysis (cPCA), which have been used to preprocess the data in hand gesture classification.

3.2 Filters

The interferences and noise are eliminated from the sEMG signals by band-pass filtering the signal. A low-pass filter attenuates the unwanted high-frequency components. The cut-off frequency of the low-pass filter is usually determined by the requirement of Nyqvist sampling theory. [43] According to Nyqvist rule, the cut-off frequency should be equal or less than sampling frequency. Otherwise, less than two samples are acquired per cycle of the signal which results a phenomenon called aliasing. Aliasing means the presence of unwanted components in the reconstructed signal. These components were not present when the original signal was sampled. In addition, some of the frequencies in the original signal may be lost in the reconstructed signal. Aliasing results because signal frequencies can overlap due to the too low sampling frequency.

High-pass cut-off frequency is determined according to the need to eliminate slow variations in the signal caused by the motion artifacts. The cut-off frequencies, used in previous studies, range between 5-20 Hz. The lower frequency components of sEMG spectrum mainly contain the information of firing rates of active motor units. These components may not make a significant contribution to the hand movement classification. [43] The typical frequency range of cable motion artifacts is 1-50 Hz, and the power density of electrode motion artifacts is up to 20 Hz. In addition, ambient electromagnetic fields exist in the vicinity of AC 120 V (or 230 V) power lines and electric equipment. The frequency of these fields is the frequency of the AC power supply (50 Hz in Europe) and its harmonics. [44] Therefore, a high-pass filter with higher cut-off frequency than commonly used 2-50 Hz is needed to effectively attenuate the motion artifacts and alternating current power interferences. Although, properly choosing the frequency band for the band-pass filter may significantly increase the control accuracy and stability of a myoelectric prosthesis, only one study [43] has considered this issue. In the study it was found that the low-frequency components in the sEMG recordings may provide limited information for the classification of hand movements. The frequency band components of 20-100 Hz only slightly improved the classification accuracy for able bodied subjects (0.25%) and transradial amputees (1.6%). For shoulder disarticulation amputees, the

accuracy did not benefit from the information below 25 Hz. The study suggests a high-pass cut-off frequency of 60 Hz an optimal for sEMG classification.

3.3 Sampling Frequency

The dominant energy (about 95%) of sEMG signal is accounted for by harmonics up to 400-500 Hz, and most of the components with the frequencies over 500 Hz are noise. According to the Nyqvist rule, the sampling frequency should be equal to twice the highest frequency of interest contained within the signal. Therefore, the sampling rate of 1000 Hz is commonly used in sEMG studies. The same sampling frequency is usually used also in most studies of sEMG pattern recognition for prosthetic control. However, these studies have not considered if a lower sampling rate still preserves sufficient neural control information for accurate classification of movements. Although, the signal sampled with higher frequency may contain more high-frequency information, the high sampling rate also adds more processing and computational complexity to the controller of a prostheses. Therefore, it would be desirable to use a low sampling frequency without compromising much of classification accuracy. Only one previous study has investigated the effects of sampling rate on the performance of sEMG pattern recognition in identifying hand postures. The study shows that, at least by using the feature subset of mean absolute value, number of zero crossings, waveform length and number of slope sign changes, lower than 1 kHz sampling rate is possible for accurate classification of 11 hand postures. Compared to a 1 kHz sampling rate, a sampling rate of 500 Hz decreased the classification accuracy only 0.8 % in able-bodied subjects and 2.2 % in amputees, but saved 50 % storing memory and halved data processing time.[43] However, more investigations are needed to determine an optimal sampling rate for sEMG pattern recognition.

3.4 Independent Component Analysis

Independent component analysis (ICA) is a powerful statistical method applied to the field of biomedical signal processing. ICA estimates the set of independent signals from the mixture of the given signals by estimating un-mixing matrix. It has been successfully used for source extraction to isolate brain activity related to specific brain functions and artifact removal from Electroencephalogram (EEG) and Magnetoencephalogram (MEG) data. [45]

As mentioned in Chapter 2.2.3 crosstalk may be a problem in sEMG-recordings. Especially, when the muscle activity and therefore also signal strength is small, the impact of crosstalk is very high. ICA can be used as a preprocessing technique for hand gesture identification in order to reduce the crosstalk effect. It assumes that observed signals are n linear mixtures $x_1,\ldots x_n$ of n independent components expressed as

$$x = As, \tag{2}$$

where x is the vector whose elements are the measured signals $x_1,\ldots x_n$, s is the vector with original sources $s_1,\ldots s_n$, and A is the mixing matrix. The goal of ICA is transform the vector of measurements into a signal space where the signals are statistically independent. To separate the measured signals from the original signals, ICA will search the un-mixing matrix W by which observations can be linearly translated to form Independent output components [45]

$$s(t) = Wx(t) = WAs(t). \tag{3}$$

Thus, ICA describes how the observed signals are generated by a process of mixing components s. Both s and A are unknown and we must estimate them using observations x under as general assumptions as possible. In ICA it is assumed that the components are statistically independent and have non Gaussian distributions. In addition, the mixing matrix is assumed to be square. [45]

Before applying the ICA algorithm on the data x, the data x is centered by subtracting its mean vector so as to make x a zero-mean variable. Another useful preprocessing method is to whiten the observed data. After centering the data is linearly transformed so that it becomes white, i.e. its components are uncorrelated and their variances equal unity. Additionally, the success of ICA may depend on performing some application-dependent preprocessing steps, such as band-pass filtering. [45]

Many ICA algorithms have been developed, such as, second order blind identification (SOBI), Temporal Decorrelation Source Separation (TDSEP), FastICA, and information maximization algorithm (Infomax). Ganesh et al. [46] compared the performance of different ICA algorithms for isometric hand gesture identification using four channel sEMG. TDSEP yielded the best performance for an analysis window of 1 s duration. However, 1s analysis window cannot be used in myoelectric control because it exceeds the optimal controller delay of 50-400 ms. Al-Timemy et al. [31] found that FastICA preprocessing technique increased the classification accuracy for different window length from 88 % to 93 %. FastICA is used also in this study because it is relatively simple, has very fast convergence, and no step-size parameters are required to be chosen. In addition, the sEMG data has showed to be super Gaussian [31] which matches the FastICA assumption about the non-gaussianity.

The basic form of the FastICA algorithm for one unit is as follows:

1. Choose an initial weight vector w.
2. $w^+ = E\{xg(wTw)\} - E\{g'(wTx)\}$
3. Let $w = w^+/|w^+|$
4. If not converged, go back to 2.

FactICA for several units run the one-unit FastICA algorithm using several units with weight vectors $w_1 \dots, w_n$. The outputs $w_1^T x, \dots, w_n^T x$ are decorrelated after the every iteration to prevent different vectors from converging to the same maxima. [45]

3.5 Classwise Principal Component Analysis

Principal Component Analysis (PCA), or sometimes also termed as universal PCA (uPCA) or global PCA [47], is a linear transformation that linearly decorrelates multivariate data and projects it onto a new coordinate system such that the greatest variance of the data lies on the first coordinate while the least variance of the data lies on the last coordinate. However, PCA and the other global dimensionality reduction techniques are suboptimal for classification purposes because they utilize the statistical properties of common data distribution, while ignoring class-conditional statistics. [48] Additionally, some of the methods are computationally expensive when applied to large-scale biomedical data analysis.

Das and Nenadic introduced a computationally efficient, locally adaptive feature extraction and classification method Classwise PCA (cPCA), also referred as Individual PCA (iPCA)[47] that is suitable for statistical data under small sample size conditions. While PCA approximates data by using a single low-dimensional subspace, cPCA generates *c* subspaces for *c*-class problem and represents the data points from class ω_i in its local subspace S_i Thus, each class has a separate projection matrix, which approximate some nonlinear low-dimensional data manifold. Because cPCA effectively tunes the data prior to classification, it has improved classification accuracies for some pattern recognition problems. [48]

Fig. 20 illustrates the principle of cPCA on a two-class example. Two-dimensional data is confined to a one-dimensional manifold, and thus the class-specific one-dimensional subspaces, S_1 and S_2, can be seen as a piecewise linear approximation of the data manifold. Both classes and an unlabelled test data *x* are projected to S_1 and S_2. The membership of *x* is determined by performing statistical tests within each subspace, and the final decision is taken from the subspace that provides the strongest decision evidence. [48]

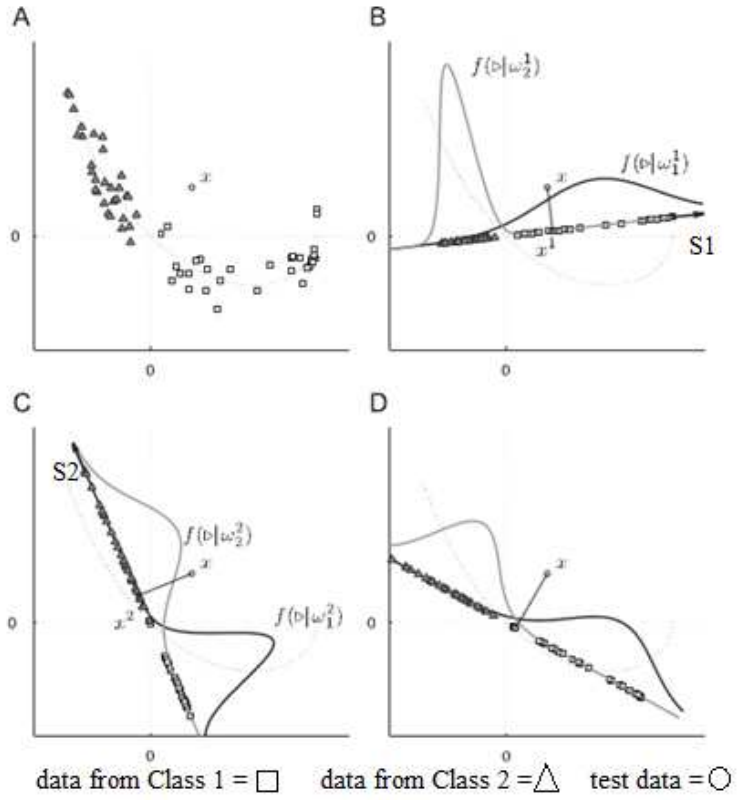

Fig. 20: A) Data from two classes, ω_1 and ω_2, are confine to a 1D manifold. B) Projection of the data to the 1D principal component subspace S_1 of class ω_1. $f(\cdot|\omega_1^1)$ and $f(\cdot|\omega_2^1)$ are Gaussian fits of classes ω_1 and ω_2, respectively, and x^1 is the projection of the test data. C) Projection of class ω_2 to the principal component subspace S2, with Gaussian fits $f(\cdot|\omega_1^1)$ and $f(\cdot|\omega_2^1)$, and the projection, x^2, of the test data. D) Projection of the data to the global principal component subspace. [48]

For c-class problem, cPCA generates c subspaces $\{S_1, S_2,\ldots, S_c\}$. Presumably, data belonging to a class random variable ω_i, (i=1,2,3,…,c) will be on average best represented in its corresponding principal component subspace S_i, although this does not necessarily hold for classification and further tests are required. Information from the other subspaces may also be needed to correctly classify the data from ω_i. [48]

The first step of cPCA is to calculate the between-class scatter matrix

$$\sum\nolimits_b = \sum_{i=1}^{C} P(\omega_i)(\mu_i - \mu)(\mu_i - \mu)^T \in R^{n\times n}, \tag{4}$$

where $P(\omega_i)$ is the class probability, μ_i is the sample mean of class ω_i, is the sample mean, defined by

$$\mu = \sum_{i=1}^{C} P(\omega_i)\mu_i \in R^{n\times 1}, \tag{5}$$

and *n* is the dimension of the data vector. It follows from equations 4 and 5 that the number of linearly independent columns of $\sum_b$ is at most *c-1*, and therefore $d \leq c-1$. [48]

The next step is to calculate the principal component subspaces S_i. The $m_i^{'}$ principal eigenvectors of the class covariance $\sum_b$ are taken as the columns of the matrix $W_i^{CPCA} \in R^{n \times m_i^{'}}$, which forms the basis of S_i. Usually, $m_i^{'}$ is selected such that $m_i^{'} + d \leq n$. Therefore, the small sample size problem and curse of dimensionality are no longer concerns when data is projected to a basis defined by matrix E_i that is computed concatenating matrixes W_i^{CPCA} and W_b. However, calculating W_b is optional and if it is omitted, the definition of E_i reduces to $E_i = W_i^{CPCA}$. Matrix W_b is calculated such that its columns form an orthonormal basis for the range of $\sum_b$, defined as { $R(\sum_b) = \xi \in R^n : \xi = \sum_b \eta, \forall \eta \in R^n$ }. Including the matrix W_b in the algorithm is useful if discriminatory information lies in the class means and not in the class covariances. [48]

Finally, we need to compute the feature extraction matrix which is defined as $F_i = E_i T_i^{DEF}$, where $T_i^{DEF} \in R^{(m_i^{'}+d) \times m_i}$ is a feature extraction matrix of the chosen linear discriminant feature extraction (DFE) technique, and m_i is the final size of the feature space. Calculating T_i^{DEF} is optional and if it is omitted, the feature extraction matrix is simply $F_i = E_i$. In any case, the algorithm finally gives c feature extraction matrixes, whose columns provide bases for c subspaces. [48]

Hargrowe et al. have used a cPCA as a preprocessing step for pattern-recognition based prosthetic system. The raw sEMG data are rotated by class specific PCA matrixes to spatially decorrelate the data before features are extracted. This “tunes” the data so that a classifier can discriminate the test motions better. Because cPCA algorithm increases the number of inputs by a factor of C where C is the total number of classes, it is very likely that some of the output channels contain some redundant information and therefore the number of linearly combined channels can be reduced. Hargrove et al. used iterative sequential backward selection (SBS) algorithm to reduce the dimensionality. They showed that by using cPCA, the analysis window length can be cut from 256 ms to 128 ms without affecting the classification accuracy. [49] In the other study Hargrowe et al. found that when cPCA is used, classification errors reduced significantly for both intact-limbed and amputee subjects. Fig. 21 displays the effect of cPCA and uPCA to the classification error in for amputees on a subject-by-subject basis. All other control systems showed similar trends: cPCA yields the smallest classification error. uPCA was not expected to improve the classification accuracy because it orders the components by the amount of variance each component explained and not by a discrim-

inatory power. However, it was somewhat surprising that the accuracies were even lower when uPCA is used. [47]

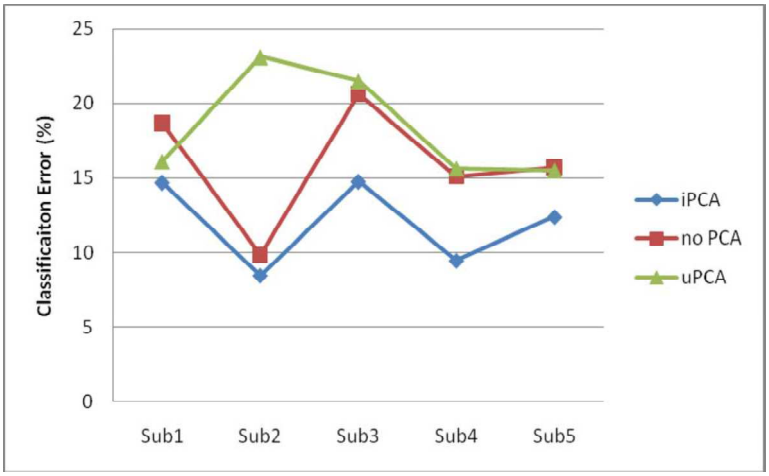

Fig. 21:The classification error for the six-channel, seven-class problem for amputees on a subject by subject basi. Preprocessing with iPCA/cPCA outperforms other preprocessing methods.It is interesting that uPCA yields lower classification accuracy than no PCA preprocessing.[47]

3.6 Pattern Recognition-based Myoelectric Control

Myoelectric control systems can be divided into two groups: pattern recognition- and non-pattern recognition-based systems. Fig. 22 shows the schematic diagram of the structures of the two systems. [3] In the following subsections both of these methods are described. However, because pattern-recognition-based classifier is used in this study, non-pattern-based methods are described only briefly.

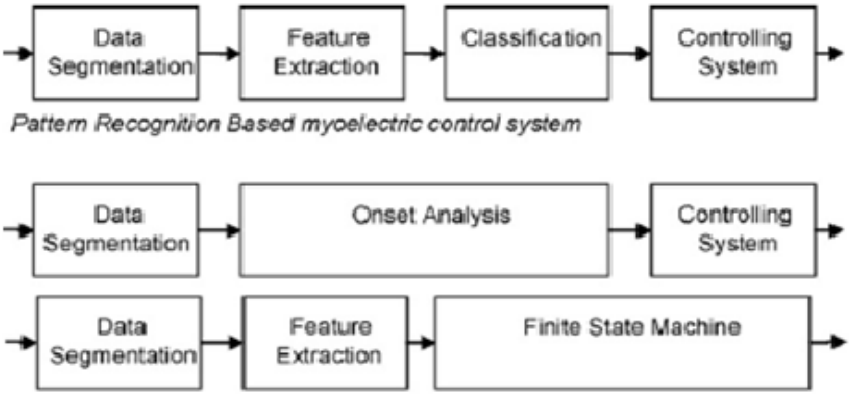

Fig. 22: Pattern and nonpattern based myoelectric control methods.[26]

A control approach using pattern recognition of EMG signals yields a significant improvement in control over the conventional non-pattern recognition based myoelectric control strategy. It is grounded on the assumption that the patterns of EMG signals in the forearm contain information about many desired movements of the hand and wrist,

and this information can be used to identify a variety of different intended movements of the prosthesis. Even though the sEMG signals are stochastic, repeatable EMG patterns can be observed from different muscle contractions. This can also be seen in amputees, even though they may not have fully functioning muscles. In the pattern recognition based myoelectric control features, extracted from different time segments of the acquired sEMG signal, are used as input to a classifier for the recognition of muscle activation or for the prediction of different hand motions. Once a pattern has been classified, a command is sent to a prosthesis controller to implement the movement. This approach is also intuitive, as the intended movement matches the prosthesis function. [11, 2] Next sections describe each stage of pattern-recognition-based control: data segmentation, feature extraction, feature normalization, and classification.

3.6.1 Segmentation

A segment is a time section used to analysis and feature extraction of sEMG data. Three issues that need to be considered before segmentation are windowing technique, segment length and state of data. These issues are discussed in this chapter.

3.6.1.1 Windowing Technique

Data windowing technique deals with the continuous classifier that is able to classify continuous stream of steady-state data instead of acting on a series of disjoint recordings. The benefit of the continuous classification is that an amputee does not need to elicit a contraction from rest. The continuous classifier can deal either with adjacent or overlapped windows. In the former case custom length adjacent segments are used for analysis and feature extraction. Because of high-speed processors, the processing time is usually less than the duration of time segment, as can be seen in Fig. 23a. As a consequence, there remains a certain amount of time that the processor is idle. In the overlapping windowing technique, the idle time is used for acquiring more data to be processed. As Fig. 23b illustrates, each segment slides over the one before. The overlapped window approach produces a more constant controller delay and decreases the maximum delay.[50]

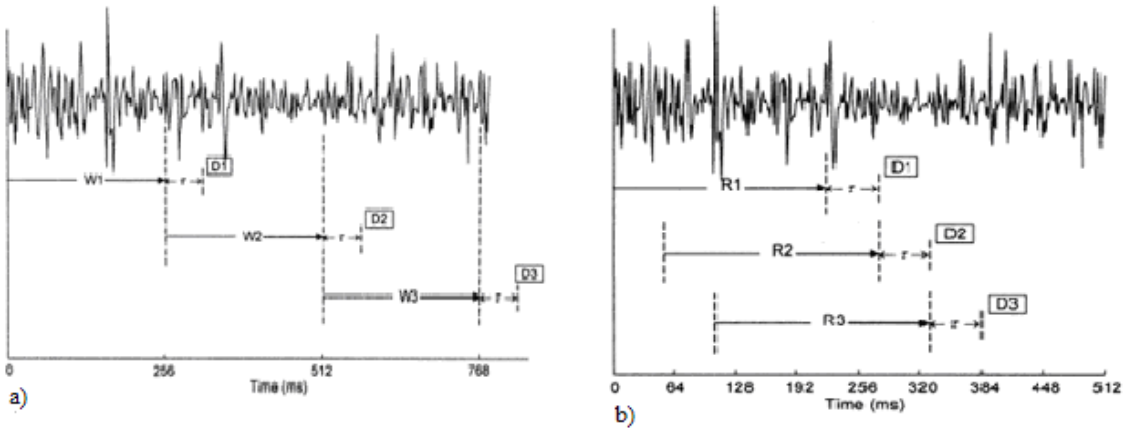

Fig. 23: Adjacent windowing technique. For each analysis window (W1, W2, and W3) a classification decision (D1, D2, and D3) is made t seconds later, where t is the processing time required of the classifier. b) Overlapped windowing technique that maximally utilizes computing capacity and produces a decision stream that is as dense as possible. [51, 52]

3.6.1.2 Segment Length and Real Time Constraint

Performing feature extraction and pattern recognition on larger data windows increases the classification accuracy, but the drawback is that more time is required to collect and process the larger data set. Thus, trade-off has to be done between real-time constrains and classification performance. Previous studies have used variety of analysis window attributes for their prosthesis controllers but most of them have little regard for the overall delay. If a particular classifier may increase classification accuracy, this increase in accuracy must be done in a reasonable amount of time. For example, in the study of Peleg et al. the time between the onset of the contraction and the classification decision is 1.4 seconds, which would be quite frustrating for the user. The estimates of optimal delay, which does not make the prosthesis feel sluggish and unresponsiveness to the user, range between 50 to 400 ms [53]. The large range indicates that it is not quite clear what the optimal length for the delay would be, and the optimal delay may also be depending on the individual anatomy and physiology. It should also be noted that the minimum interval between distinct contractions is approximately 200 ms which suggests that, theoretically, a segment of equal or more than 200 ms contains enough information to estimate motion states of hand [54].

In the case of commonly used windowing strategies, the delay can vary substantially. Researches in virtual environment has shown that performance tends to degrade as the variability of the delay increases, and thus difference in delay between the best and the worst case should be small. Farrel presented equations to estimate worst-, average- and best-case delays as well as delay ranges in the context of different segmentation strategies [55]. These equations are presented in Table 4. As can be seen from the equations, the delay is not only the function of window length but also a function of the processing time, the amount of window overlap, and the number of majority votes used. Majority voting (MV) is a postprocessing technique that aims to increase the overall classifica-

tion accuracy by analyzing the current class decision along with the *n-1* previous class decisions. The class that occurs most frequently is selected as the controller output. MV is described more detail in Chapter 3.6.6

Table 4: The equations for worst-case, average, and best-case delays with delay ranges. [55]

Classifier Type	Worst-Case Delay	Average Delay	Best-Case Delay	Difference Between Best & Worst Cases
No Overlap, No Majority Voting	$D = \frac{3}{2}T_a + \tau$	$D = T_a + \tau$	$D = \frac{1}{2}T_a + \tau$	T_a
No Overlap, with Majority Voting	$D = \left(\frac{n}{2} + 1\right)T_a + \tau$	$D = \left(\frac{n+1}{2}\right)T_a + \tau$	$D = \left(\frac{n}{2}\right)T_a + \tau$	T_a
Overlap, No Majority Voting	$D = \frac{1}{2}T_a + T_{new} + \tau$	$D = \frac{1}{2}T_a + \frac{1}{2}T_{new} + \tau$	$D = \frac{1}{2}T_a + \tau$	T_{new}
Overlap, With Majority Voting	$D = \frac{1}{2}T_a + \left(\frac{n+1}{2}\right)T_{new} + \tau$	$D = \frac{1}{2}T_a + \left(\frac{n}{2}\right)T_{new} + \tau$	$D = \frac{1}{2}T_a + \left(\frac{n-1}{2}\right)T_{new} + \tau$	T_{new}

Note: Equations to estimate worst-case, average, and best-case controller delay as well as difference between best- and worst-case controller delays. General rule of thumb is that T_{new} is approximately an order of magnitude less than T_a, meaning that users should experience more consistent delay with overlapped windows. D = maximum delay between users intended movement and controller producing correct output class, n = number of majority votes, T_a = analysis window length, τ = processing time, T_{new} = amount of window overlap.

The window shift T_{new} is related to processing time τ which is determined by the analysis window length T_a, processor, memory, type of features, algorithms used to extract features and perform pattern recognition, and number of EMG channels. Thus, the only parameters under the designer's direct control for a given feature set are the window length and number of majority votes. It has been indicated that no remarkable difference exist in classification accuracy whether it is used a large window with small number of votes or a small window with a large number of votes. [55]

3.6.1.3 State of Data

A sEMG signal consists of two states: a transient state and a steady state. The transient state emanate from burst of fibers, as a muscle goes from rest to voluntary contraction level. In the steady state a muscle is constantly under contraction. Previous studies have shown that the features extracted during the steady state data can be classified more accurately than the features extracted during transient state. In addition, steady state data allows faster system response because the degradation of classification accuracy is not as profound when the window length is decreased. The main weakness in using transient state is that contractions should initialize from rest, thus reducing the ability to quickly switch from one state or hand task to another. [11,13]

3.6.2 Feature Extraction

A raw myoelectric sEMG-signal is not a suitable input for a classifier because of the large number of inputs, randomness of the signal and large dimension of the input vector. Especially, when the signal is used to control a prosthesis, the length of the input vector have to be reduced as much as possible because controllers of the prosthesis must

meet very strict real time constrains, and the classifiers they implement perform much faster when handling small input vectors. For this reasons raw signals have to be mapped into smaller dimension vectors, feature vectors. A feature of the EMG signal is a measurable characteristic of the signal that can be observed or described qualitatively, such as being fast or slow, large or small, spiky or smooth. Features can be grouped into four categories:

1. time domain (TD)
2. time serial domain (TSD)
3. frequency (spectral) domain (FD)
4. time-scale (time-frequency) domain (TSCD)

Feature selection is a very important step because the effect of the feature set on the classification accuracy is even greater than the effect of the type of the classifier. An optimal feature set can be determined using wider variety of methods than the other system elements. Three properties determine the quality of EMG feature space: maximum class separability, robustness and complexity. A high quality feature space results in clusters with maximum class separability or a minimum overlap thus minimizing the misclassification rate. Robustness means that the feature space preserves the cluster separability in noisy environment as much as possible. The computational complexity of the feature set should be low such that the related procedure can be implemented with reasonable hardware and in real-time. This task is easier if the window size is small. Another advantage of the small window size is that it improves the stationary of the signal. The following chapters introduce some features commonly used to classify sEMG signals. Comparative studies of features and feature subsets are also revived.

3.6.2.1 Time Domain Features

TD features are the most popular in myoelectric classification because of their accessibility and computational simplicity. The major advantage of TD features is that they do not need a mathematical transformation, thus being quickly to calculate. TD features based on time-amplitude representation of the signal, and can indicate measures like signal energy, force, and duration. [5, 26] A disadvantage of TD features is that they are sensitive to interference that is acquired during the recording. TD features assume the signal to be stationary, and therefore variation in this group may be largely obtained if EMG signal is recorded from dynamic movements. However, features in this group are widely used to classify steady state signals due to their classification performance in low noise environments and their low computational complexity.[56]

Integrated EMG (IEMG) is a sum of the absolute values of the sEMG signal amplitude, which can be expressed as

$$IEMG = \sum_{i=1}^{N} |x_i|. \quad (6)$$

IEMG is generally used as an onset detection index in sEMG non-pattern recognition and in clinical applications. It is related to the sEMG signal sequence firing point. [56]

Mean absolute value (MAV) is an estimate of the mean absolute value of the signal x_i in a segment *i* of *N* samples length. It is given by:

$$MAV = \frac{1}{N}\sum_{i=1}^{N}|x_i|. \quad (7)$$

MAV is one of the most commonly used in EMG analysis. [56]

Modified mean absolute value 1 (MAV1) is an extension of MAV that uses the weighted window function w_i to improve the robustness of MAV. [56] It is shown as

$$MAV1 = \frac{1}{N}\sum_{i=1}^{N} w_i |\, x_i \,|, \quad (8)$$

$$\text{where } w_i = \begin{cases} 1, & if\ 0.25N \le i \le 0.75N \\ 0.5, & otherwise \end{cases}.$$

Modified mean absolute value 2 (MAV2) is similar to MAV1. [56] However, the smooth window is improved in this method using continuous weighting window function w_i. MAV2 is expressed as

$$MAV2 = \frac{1}{N}\sum_{i=1}^{N} w_i |\, x_i \,|, \quad (9)$$

$$\text{where } w_i = \begin{cases} 1, if\ 0.25N \le i \le 0.75N \\ \frac{4i}{N}, elseif\ i \le 0.25N \\ \frac{4(i-N)}{N}, otherwise \end{cases}$$

Mean absolute value slope (MAVS) represents the difference in mean absolute value between adjacent segments *k* and *k+1*:

$$MAVS_k = MAV_{k+1} - MAV_k,\ k = 1, \dots, K-1, \quad (10)$$

where *K* is the number of segments covering the sEMG signal. [56]

Simple Square Integral (SSI) captures the energy of the EMG signal as a feature. [56] SSI is usually defined as an energy index. It is summation of square values of the EMG signal amplitude, which is claculated as

$$SSI = \sum_{i=1}^{N} x_i^2. \quad (11)$$

Variance of the EMG is another measure of its power. Generally, it is defined as an average of square values of the derivation of that variable. However, mean value of EMG is close to zero. In consequence, variance of EMG is defined as

$$VAR = \frac{1}{N-1}\sum_{i=1}^{N} x_i^2 \tag{12}$$

Absolute value of the 3rd, 4th, and 5th temporal moment were firstly used in control of a prosthetic arm by Saridis and Gootee in 1982 [57]. The definition of their equations can be respectively expressed as

$$TM3 = \left|\frac{1}{N}\sum_{i=1}^{N} x_i^3\right|, \tag{13}$$

$$TM4 = \frac{1}{N}\sum_{i=1}^{N} x_i^5, \tag{14}$$

$$TM5 = \left|\frac{1}{N}\sum_{i=1}^{N} x_i^5\right|. \tag{15}$$

The absolute value is taken to greatly reduce the within class separation for the odd moment case. The first moment and the second moment are similar to the MAV and VAR features, respectively. [57,56]

Root Mean Square (RMS) is modeled as amplitude modulated Gaussian random process whose RMS is related to the constant force and non-fatigue contraction. [56] RMS is commonly used feature an analysis of EMG signal. It is mathematically defined as

$$RMS = \sqrt{\frac{1}{N}\sum_{i=1}^{N} x_i^2}. \tag{16}$$

Clancy et al. have compared the MAV and the RMS [27, 27]. They suggested that when a signal is modeled as a Gaussian process, as is the case in high level contraction, RMS fits better. MAV fits well when signal is modeled as a Laplacian process i.e. during low level contractions. However, Clancy et al. found that a model for a constant force and constant posture, non-fatiguing contraction is between Gaussian and Laplacian. Therefore, MAV may give at least as justified estimate for the amplitude as RMS, and there is little reason to argue between them.

v-Order is a non-linear detector that implicitly estimates muscle contraction force m_i. It is defined from a functional mathematical model of the EMG signal generation, given by

$$x_i = (\gamma m_i^{\alpha}) n_i, \tag{17}$$

where γ and α are constants, and n_i is n_i denotes class of the ergodic Gaussian processes. Theoretical value for α is 0.5, but the experimental results have showed that it is ranged between 1 and 1.75. v-feature is mathematically defined as

$$V = \left(\frac{1}{N}\sum_{i=1}^{N} x_i^v\right)^{\frac{1}{v}}. \quad (18)$$

The best value for *v* has been reported to be 2, which leads to the definition of the EMG v-Order feature as the same as RMS feature. [56, 58]

Log-Derector (LOGDET) is another estimate for the muscle contraction force. However, definition of the nonlinear detector is changed to be based on logarithm and log detector feature, which can be expressed as

$$LOGDET = e^{\frac{1}{N}\sum_{i=1}^{N} log(|x_i|)}. \quad (19)$$

Waveform length (WL) is the cumulative length of the waveform over the time segment. It represents a combined measure of amplitude, frequency, and duration in a single parameter. WL appreciates the waveform complexity in each window. [56] WL is defined as the sum of absolute voltage differences between each pair of adjacent samples within the classification window, and can be expressed mathematically as

$$WL = \sum_{i=1}^{N-1}|x_{i+1} - x_i|. \quad (12)$$

Average amplitude change (AAC) is similar to WL with the exception that wavelength is averaged. It is formulated as

$$AAC = \frac{1}{N}\sum_{i=1}^{N-1}|x_{i+1} - x_i| \quad (21)$$

Difference absolute standard derivation value (DASDV) is a standard derivation value of the wavelength, defined as [59]

$$DASDV = \sqrt{\frac{1}{N-1}\sum_{i=1}^{N-1}(x_{i+1} - x_i)^2} \quad (22)$$

Zero crossing (ZC) is a measure of frequency information of the EMG signal that is defined in time domain. It is the number of times the waveform crosses zero. A threshold must be included in order to reduce the noise induced zero crossings, and it is typically selected between the range of 50-100 μV. Thus, a pair of consecutive samples constitutes a zero-crossing only if their absolute difference exceeds both a noise threshold and their absolute sum. Mathematically ZC is expressed as

$$ZC = \sum_{i=1}^{N-1} \text{sgn}(x_i \times x_{i+1}) \cap |x_i - x_{i+1}| \geq threshold, \quad (23)$$

with $sgn(x) = \begin{cases} 1, & if\ x \geq threshold \\ 0, & otherwise \end{cases}$. [60, 61]

Myopulse Percentage Rate (MYOP) is an average value of myopulse output. It is defined as one when the absolute value of the EMG signal exceeds a threshold value, and as zero otherwise. The typical value of the threshold is between 50 μV and 100 mV. The MYOP is the average value of the myopulse output. [56] Mathematically, it is defined as

$$MYOP = \frac{1}{N}\sum_{i=1}^{N}[f\ (x_i)] \tag{24}$$

Wilson amplitude (WAMP) is the number of times that the difference between two consecutive amplitudes is a time segment exceeds a threshold of 50 μV–100 mV. Mathematically, is can be formulated as

$$WAMP = \sum_{t=1}^{N-1}[f(|x_n - x_{n+1}|)], \tag{25}$$

$$\text{where} \qquad f(x) = \begin{cases} 1, & if\ x \geq threshold \\ 0, & otherwise \end{cases}.$$

WAMP is commonly used in classification of hand motions. It measures the frequency information of the sEMG signal same as ZC. It is also an indicator of firing of motor unit action potentials and thus it is related to the muscle contraction force.[2, 56, 61]

Slope sign change (SSC) is another method to represent the frequency domain properties of sEMG signal. It is related to ZC, MYOP, and WAMP. It is the number of times the signal that slope of the sEMG signal changes sign. The number of changes between positive and negative slope among three sequential segments are performed with threshold function for avoiding background noise. SSC can be given by

$$SSC = \sum_{t=2}^{N-1}[f(|(x_i - x_{i-1}) \times (x_i - x_{i+1})|], \tag{26}$$

$$\text{where} \qquad f(x) = \begin{cases} 1, & if\ x \geq threshold \\ 0, & otherwise \end{cases}.$$

Similarly as for ZC, WAMP, and MYOP, the threshold value for SSC is also selected within the range of 50 μV and 100 mV. It is depending on the setting gain value of the instrument and on level of background noises. [56]

Histogram (HIST) is determines the number of signal samples in different equally spaced amplitude levels in a time segment, and is an extension of ZC and WAMP, both of which compare a single threshold to the EMG signal. Previous studies have set the

number of levels to 9 because the performance has been shown to improve significantly as the number of levels was increased to 9. [2, 56, 61]

3.6.2.2 Time Serial Domain

Autoregressive coefficients (AR) is the simplest time-series model. It estimates signal samples by linear combination of their *P* earlier samples and is given by

$$AR = \sum_{p=1}^{P} a_p \, x_{i-p} + w_i \, . \tag{27}$$

In classification of the EMG signal, coefficients of the AR model have been used as a features. EMG spectrum changes with muscle contraction level, resulting in changes in AR coefficients. The larger the autoregressive model the greater computation time is needed to determine the AR coefficients. Thus, the model should be kept as small as possible without sacrificing classification accuracy. Depending on the survey best results have been achieved with 3rd[6], 4th[62] or 6th [63] order model.

The Cepstrum of a signal is the inverse Fourier Transform of the logarithm of the magnitude of the power spectrum of the signal. They can be derived from AR coefficients as follows:

$$CC = -a_p - \sum_{i=1}^{p-1}(1 - \frac{1}{p}) a_p c_{p-1} \tag{28}$$

where c_p is the *p*th order coefficients of the Cepstral analysis (CC) and $1 \leq l \leq P$. From the provided definition, CC can be considered as a time domain feature because it does not need a Fourier transform in process. The most important characteristic of CC is the deconvolution of a signal into two main parts so that each can be extracted by imposing a lifter in the cepstrum domain. [56, 61]

3.6.2.3 Frequency Domain Features

Frequency or spectral domain features are usually used to study muscle fatigue, and infer changes in MU recruitment, but they are not vary common in hand movement classification. Different statistical properties were applied to the Power spectral density (PSD) which is the Furrier transform of the autocorrelation function of the EMG signal. It can be estimated using Preiodogram or parametric methods, i.e., the AR model. A signal spectrum is influenced by the firing rate of a recruited MU in the low-frequency range (below 40 Hz, and the morphology of the action potential travelling along a muscle fiber in a high frequency range (above 40 Hz). It is non-stationary and directly depends on the contraction force, muscle fatigue, and inter-electrode distance. Phinyomark et al. investigated in their study eleven frequency domain features, and

showed that they are not suitable for hand movement classification.[26, 56] However, let's examine briefly some most common frequency domain features.

Mean Frequency (MF) is an average frequency defined as a sum of product of the sEMG power spectrum and the frequency divided by total sum of the spectrum density. Mathematically, it can be expressed as

$$MNF = \sum_{j=1}^{M} f_j P_j \,/\, \sum_{j=1}^{\infty} P_j, \tag{29}$$

where f_j denotes the frequency of the spectrum at frequency bin *j*, P_j the EMG power spectrum at the frequency bin *j*, and *M* the length of the frequency bin. [56]

Median power (MNP) is an average power of the EMG power spectrum. It can be calculated as [56]

$$MNP = \sum_{j=1}^{M} P_j / M \tag{30}$$

Frequency ratio (FR) was proposed in order to distinguish between contraction and relaxation of the muscle using ratio between the low frequency components and the high frequency components of the sEMG signal. It can be expressed as

$$FR = \sum_{j=LLC}^{ULC} P_j \Big/ \sum_{j=LHC}^{UHC} P_j \tag{31}$$

where ULC and LLC are upper- and lower-cutoff frequency of the low frequency band and UHC and LHC are upper- and lower-cutoff frequency of the high-frequency band, respectively. [56] The threshold for dividing between low frequencies and high frequencies can be determined either through the experiments [64] or by using the value of MF feature [65].

3.6.2.4 Time-scale (time-frequency) Domain Features

Fourier transform, Wavelet transform and Wavelet Packet transform are included in the category of time-scale domain features. Fourier Transform (FT) is used to transform an expression of a continuous time domain function into a continuous frequency-domain function. It decomposes a signal to complex exponential functions of different frequencies. FT is defined as

$$X(f) = \int_{-\infty}^{\infty} x(t) e^{-j2\pi f t} dt, \tag{32}$$

where *t* stands for time and *f* stands for frequency. According to Euler's rule, a complex exponential can be broken down into real and imaginary sinusoidal components as follows:

$$e^{-j2\pi ft} = \cos(2\pi ft) + isin(2\pi ft), \quad (33)$$

As can be seen from the equations 32 and 33, the signal is multiplied with the sinusoidal term of frequency *f*. If the signal has a high amplitude component of the same frequency *f*, then that component and the sinusoidal term coincide, and the product of them is relatively high value. Moreover, if the signal does not have a frequency component of *f* or if the amplitude component of *f* is low, the product will give zero or relatively small value respectively. When the integral in 32 is calculated for every value of *f*, we get complex valued scalars, the Fourier coefficients, which summarize the similarity between the two signals. However, the limitation of FT is that it only tells whether a certain frequency component exists or not in the signal, but gives no information where in time the frequency component exists. Thus, FT is not suitable if the signal has time varying frequency, i.e. the signal is non-stationary. [66]

To compute the FT with a microprocessor or digital signal processing based system we need a discrete-time to discrete-frequency transformation. This can be done by using the Discrete Fourier Transform (DFT), a discrete version of FFT. It is defined as

$$X(m) = \sum_{n=0}^{N-1} x(n)e^{-j2\pi nm/N}. \quad (34)$$

The disadvantage of DFT is that is it very inefficient: The number of complex multiplications and additions required to implement Eq. 34 is proportional to N^2. For every $X(m)$ that is calculated, we need to use all $x(0), \ldots, x(N-1)$ and there are N $X(m)$'s to calculate. Therefore, a faster version of DFT, so called Fast Fourier Transform (FFT) has been implemented. It reduces the number of multiplication and addition operations to $O(N\ log_2\ N)$. FFT can be implemented in number of different ways, but the most important FFT is the Cooley-Turkey algorithm. It breaks down a DFT of composite size $n = n_1 n_2$ into smaller DFTs of sizes n_1 and n_2, and can be combined arbitrary with any other FFT algorithm. A radix-2 decimation-in –time (DIT) algorithm is the simplest and most common Cooley-Turkey algorithm. It divides a DFT of size *N* into two DFTs of the even-indexed inputs x^{2m} (x_0,x_2,…,x_{N-2}) and of the odd-indexed inputs x^{2m-1} (x_1,x_3,…,x_{N-1}), both of size N/2. The two results are then combined to produce the DFT of the whole sequence. When this idea is performed recursively, the overall runtime can be reduced to O ($N\ log\ N$). The algorithm assumes N to be a power of two.[66, 67]

To capture also time varying information of the data, a revised version of FT, Short Time FT (STFT) has been developed. It divides the non-stationary signal into small

segments, where the signal is assumed to be stationary. STFT is defined as the FT of the signal multiplied by a window function that is nonzero for only a short period of time

$$X(\tau, \omega) = \int_{-\infty}^{\infty} x(t) w(t - \tau) e^{-j\omega t} dt, \tag{35}$$

where $x(t)$ is the signal and $w(t)$ is the window function. The width of the window function must be equal to the segment of the signal where its stationary is valid. The FT of the signal is taken as the window is slid along the time axis. Because the transform is a function of both time and frequency, the result is a two-dimensional representation of the signal.

The discretized version of the STFT of a signal $x(m)$ is

$$X(n, \omega) = \sum_{-\infty}^{\infty} x(m) w(n - m) e^{-j\omega n}, \tag{36}$$

where m is the discrete time variable and ω is continuous frequency. The discrete STFT divides the data into frames which usually overlap. Each of the frames is Fourier transformed and the complex result is added to a matrix, which records magnitude and phase for each point in time and frequency.

The problem with STFT is that according to Heisenberg Uncertainty Principle it is not possible to know the exact time-frequency representation of the signal. STFT does not tell what spectral components exist at what instances of times, but only the time intervals in which certain band of frequencies exist. When choosing a window length, tradeoff must be done between time and frequency resolution. Narrow window results in good time resolution and poor frequency resolution; wide window results in good frequency resolution and poor time resolution. In addition, wide windows may violate the condition of stationary.

Continuous Wavelet Transform (CWT) was developed as an alternative approach to the STFT to overcome the resolution problem. Multiresolution analysis makes it possible to analyze a signal at different frequencies with different resolutions. The constant resolution time-frequency plane of STFT and multiresolution time-frequency plane of CWT are schematically displayed in Fig. 24. In CWT the signal is multiplied with a function that is similar to the window function in STFT, and the transform is computed for each segment of the time-domain signal. However, the window function of the CWT can be chosen with more freedom, without the need of using sine-forms. In CWT the width of the window is changed as the transform is computed for every single spectral component. The definition of CWT is as follows:

$$C\big(a, b; f(t), \psi(t)\big) = \int_{-\infty}^{\infty} f(t) \frac{1}{\sqrt{a}} \psi^* \left(\frac{t-b}{a}\right) dt, \tag{37}$$

where b is translation, a denotes scale, and ψ is the transforming function, so called mother wavelet. For the CWT several kinds of mother wavelets are developed. The term wavelet i.e. a small wave describes the characteristics of window function: Smallness refers to the limited duration of the window function and wave describes the condition that function is oscillatory. Wavelets have an average value of zero and nonzero norm. All the wavelet functions used in the transformation are derived from the mother wavelet trough translation (shifting) and scaling (compression). Scaling is a mathematical operator that either dilates or compresses a signal. If the scale $s > 1$, it compresses the target function and if $s < 1$, scaling dilates the function. However, because in CWT the scaling term is in the denominator, opposite statements hold, i.e., scales $s > 1$ dilate and scales $s < 1$ compress the signal. [68, 69]

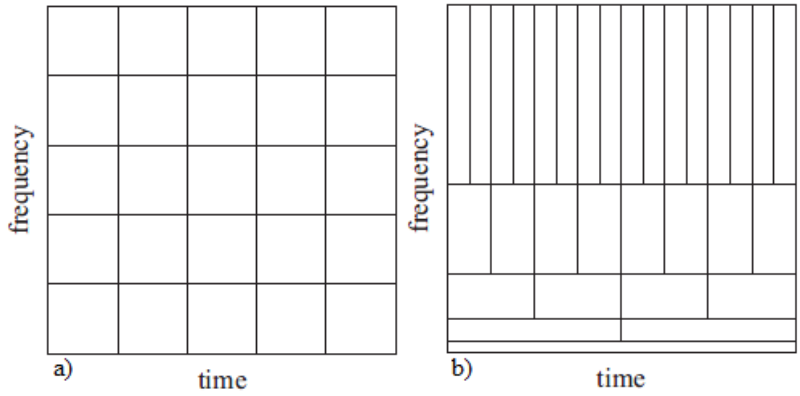

Fig. 24: a) Constant resolution time-frequency plane of STFT. b)Multiresolution time-frequency plane of WT.[68]

The computation of CWT may consume a significant amount of time and resources, depending on the resolution required. The Discrete Wavelet transform (DWT) yield a fast computation of WT. It is easy to implement as well as reduces the computation time and resources required. DWT computes a time-scale representation of the digital signal by using digital filtering techniques. DWT of a signal is calculated by passing it through a series of lowpass and highpass filters. At each decomposition level, the half band filters produce signals spanning only half the frequency band. The high-scale, low frequency components of the signal are called approximation coefficients, and the low scale, high frequency components detail coefficients. As a result of filtering, uncertainty in frequency is reduced by half and thus the frequency resolution is doubled. If the original signal has a highest frequency of ω, it requires, according to the Nyqvist rule, a sampling frequency of 2 ω. The filtering reduces the highest frequency of the signal to the half of the original allowing us to subsample the signal at a frequency of ω radians. This subsampling by 2 halves the time resolution as the entire signal is represented by only half of the number of samples. Therefore, while the half band lowpass filtering removes half of the frequencies and thus halves the resolution, the subsampling by 2 doubles the scale. The time resolution becomes good at high frequencies, while the frequency resolution becomes good at low frequencies. The filtering and subsampling process is continued until the desired level is reached. The maximum number of levels is

depending on the length of the signal. The DWT of the signal is obtained by concatenating all the coefficients starting from the last level of decomposition. [68, 69]

A wavelet packet transform (WPT) is a generalization of DWT where the signal is passed through more filters than in DWT. In DWT, a signal is split into an approximation and detail coefficients. The approximation coefficients are then further split into a second-level approximation and detail coefficients, and the process is repeated. For an n-level decomposition, the signal can be decomposed or encoded in n+1 possible ways. In WPT analysis, both detail coefficients and also approximation coefficients can be split, yielding over $2^{(2n-1)}$ possible ways to encode the signal.[69] DWT and WPT decomposition over 3 levels are shown in Fig. 25.

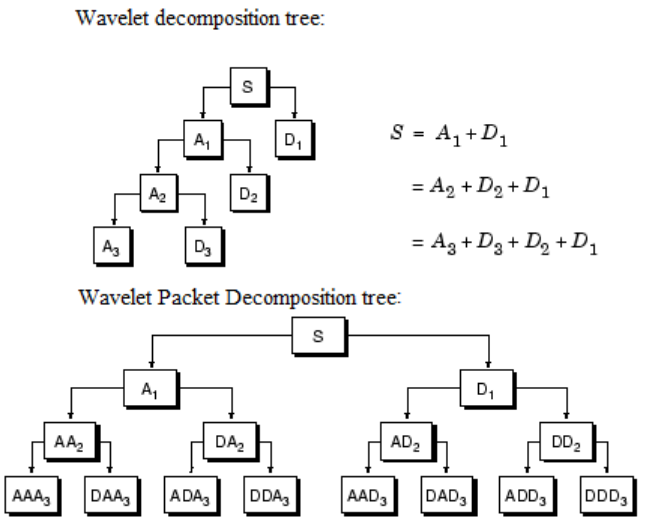

Fig 25: Decomposition tree over 3 levels for DWT and WPT. [67]

3.6.2.5 Comparison of Features

Many studies have evaluated and compared EMG features which are used to control prostheses. However, usually the performance of features has been evaluated independently, and only few combinations of TD features have been tested. Boostani and Moradi compared 19 features from ten amputees. Their results illustrate that energy of WPC, energy of wavelet coefficients and cepstrum coefficients of EMG signals present the best results from the classification and noise tolerance view points respectively. [61] However, the drawback of wavelet transform and especially of wavelet packet transform is computational complexity. Oskoei et al. compared the relative performance of various single features and feature sets. They found that so called Hudgin's feature set or TD feature set (i.e., MAV, WL, ZC and SSC), first introduced by Hudgins et al. in 1993, is superior to other features because of its relatively high rate of accuracy, stability against changes in segment length, low discrepancy over several sessions, and computational simplicity. WL outperforms single features because of its high rate of accuracy and stability to changes in segmentation method. [54] Du et al. yielded good results

by using feature set of IEMG, VAR, WL, ZC, SSC, and WAMP [70]. Englehart et al. showed that the feature set of AR and RMS significantly outperforms Hudgins's TD feature set in context of a Gaussian mixture model classifier. [71] Phinyomark et al. compared the classification performance of several individual time and frequency domain features as well as the performance of Hudgins's and Du's feature sets in context of the LDA classifier. They found that frequency domain features may not be suitable [60] Tkach et al. discovered that selecting appropriate feature combination can overcome the impact of electrode location shift, variation in muscle contraction effort, and muscle fatigue on EMG pattern classification to a certain extent. However, simple selection of these features cannot fully solve the problem. Stabilizing electrode contact locations and developing effective classifier training strategies are also needed to circumvent these undesired disturbances and minimize their effect on EMG pattern classification. [58]

As mentioned in Chapter 2.2.1, we can assume sEMG signal as a WSS process during short time intervals when a subject performs static contraction. Consequently, the STFT, DWT, and WPT coefficients calculated of the steady state signal do not have any temporal information of time-frequency plane. Additionally, all of these transformations are computationally expensive and impose time delay. TD features are simply to compute allowing fast response that is crucial in real time applications. They have also yield equally high classification accuracy as STFT, DWT, and WPT. However, DWT coefficients are commonly used in hand posture classification because they are more tolerant to noise. Chu et al. also argued WPT coefficients to be superior to TD features because the wavelet functions resemble the MUAPs that constitute the gross sEMG signal [72]. Karlsson et al. [73] investigated DWT and WPT for myoelectric signal analysis during static and dynamic contractions. Wavelet shrinkage method has shown to be a very useful method in signal analysis during static contractions, because of its de-noising characteristics. Wavelet shrinkage in WPT and FFT significantly reduced the mean squared error of spectral estimates. However, few studies have investigated DWT in the context of steady state sEMG signal, and therefore it remains still somewhat unclear whether DWT coefficients outperform simply TD features.

3.6.3 Feature Normalization

If the values of features lie within different dynamic ranges, features with large values may have more influence in the cost function than features with small ones, although this does not necessarily reflect their perspective significance in the design of the classifier. Thus, features are usually normalized to represent their values within similar ranges. Normalization methods may be linear or nonlinear. A commonly used linear normalization technique is normalization via the respective estimates of the mean and variance. This method results normalized features with zero mean and unit variance. For N data of the kth feature, normalization may be done as follows:

$$\bar{x}_k = \frac{1}{N}\sum_{i=1}^{N} x_{ik} \qquad , k=1,2,\ldots,l \tag{38}$$

$$\sigma_k^2 = \frac{1}{N-1}\sum_{i=1}^{N}(x_{ik} - \bar{x}_k)^2 \tag{39}$$

$$\hat{x}_{ik} = \frac{x_{ik} - \bar{x}_k}{\sigma_k} \tag{40}$$

The alternating method for normalization is min-max normalization method that can be shown as

$$normfeat_i = \frac{feat_i - \min_i}{\max_i - \min_i} \tag{41}$$

where *feat* and *normfeat* are original and normalized feature, respectively. The *normfeat* is range between 1 and 0. The min and max are the maximum and minimum value of every features in each dimension *i*. Also other linear techniques exists and they use proper scaling to limit the feature values in the range of [0,1] or [-1,1]. [56]

Nonlinear methods transform the data within specified intervals with nonlinear functions, such as logarithmic or sigmoid functions. Popular softmax scaling consists of the following steps:

$$y = \frac{x_{ik} - \bar{x}_k}{r\sigma_k}, \qquad \hat{x}_{ik} = \frac{1}{1+\exp(-y)} \tag{42}$$

As a squashing function, this limits the data between the interval [0,1]. This is approximately a linear function with respect to x_{ik} if *y* has small values. The standard derivation and the factor *r* defined by the user determine the range of values of x_{ik} that corresponds to the linear section. Values away from the mean squash exponentially. [74]

3.6.4 Dimensionality Reduction

The feature extraction methods transform the initial input space in a more adequate one, but not necessary in a smaller dimension. The dimensionality reduction is needed to retain the most important information for class discrimination and discard what is irrelevant information [75]. This is important especially in the case of STFT, CWT, DWT, and WPT, because they yield a high-dimensional feature vector, that generally causes an increase in the learning parameters of a classifier. Additionally, the classification performance resulting using all the coefficients of the time-domain and time-scale transformations is very poor due to both high computation cost and poor classification accu-

racy. Dimensionality reduction also improves the generalization of the classifier, reduce its complexity, and help to avoid overfitting.

Dimensionality reduction methods can be divided in feature projection and feature selection methods. In addition to these methods, the dimensionality of the time-domain and time-scale transformations can be reduced by calculating TD features of the transformed signal [76]. Feature projection methods reduce the dimension by linear or nonlinear projection of a feature vector onto lower dimensional feature vector. These methods include PCA, LDA, and ICA. [65, 77] Feature selection methods select a subset of original features. Usually the number of possible combinations of the features is unfeasible, and therefore a search procedure needs to be used.[65] Several search strategies have been developed, and they are divided into exponential, sequential and randomized algorithms. Exponential algorithms evaluate a number of subsets that grows exponentially with the dimensionality of the search space. This group of search algorithms includes for example Exhaustive Search, Branch and Bound, and Beam Search. Sequential algorithms add or remove features sequentially. They have a tendency to become trapped in a local minimum. Exemplars from this group are Sequential Forward Selection and Sequential Backward selection. Randomized algorithms incorporate randomness into the search procedure avoiding trapping in local minima. Genetic Algorithms is the most common method in this group. In this thesis Sequential Forward selection is used to select candidate subsets. It is described more detail in Chapter 4.8. In addition of search strategy, we need also an objective function that evaluates the candidate subsets. Objective functions are divided in filters and wrappers. Filters evaluate based on their information content, such as interclass distance or statistical dependence. Wrappers use a classifier to evaluate subsets by their predictive accuracy or cross-validation. In this study the classification accuracy of the LDA classifier is used as an evaluation criterion. [78]

3.6.5 EMG Pattern Classification

In order to recognition of desired motion patterns extracted features need to be classified. Both the nature of myoelectric signal and external factors such as changes in electrode position, fatigue, and sweat cause changes in signal over time. The changes may cause a large variation in a particular feature, and thus a classifier should be able to cope with such varying patterns optimally, as well as prevent over fitting. In addition, a suitable classifier has to meet real-time contractions and it has to be adequate efficient to in classifying novel patterns. [26]

EMG pattern classification has been investigated for neural control of upper-limb prostheses for decades and several possible classification algorithms exist. Examples of these classification methods are Neural Networks [79], Linear Discriminant Analysis, Bayes classifier [11], Fuzzy logic [80], Neuro-Fuzzy systems [28], Support Vector Machines [24], Hidden Markov Models and Gaussian Mixture Models [11]. However, it

has been demonstrated that a simple LDA classifier has equally high classification accuracy as more complex classifiers [7, 54, 81]. The results from a comparative study are presented in Fig. 26. Because the LDA classifier is also much simpler to implement as well as much faster to train, it have been selected to use it in this study. The following Chapter introduces the principles of the LDA classifier.

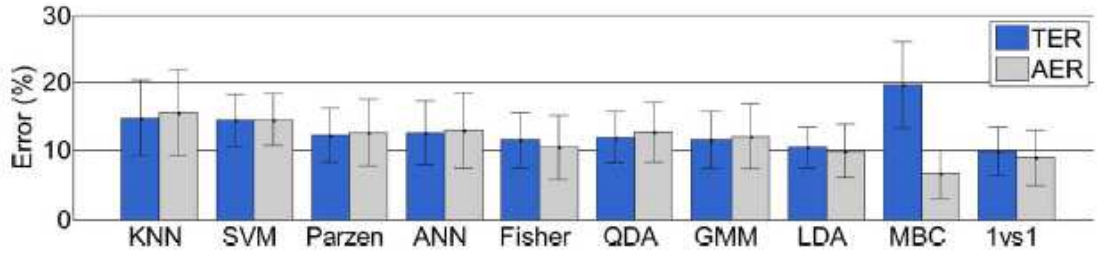

Fig. 26:Comparison of common classification techniques using conventional classification error. Results illustrate the average over seven hand postures collected from five transradial amputee. The error bars show the standard derivation across the subjects. [81]

3.6.5.1 Two Class Linear Discriminant Analysis

Linear Discriminant Analysis (LDA) is a commonly used method for data classification and dimensionality reduction, introduced first for two classes by Fisher in 1936. LDA transforms the multivariate observations *x* to univariate observations *y* such that the *y*'s derived from the two classes were separated as much as possible. [82]

Suppose that we have a set of m p-dimensional samples $x_1, x_2, ..., x_m$ (where $x_i = (x_{i1}, ..., x_{ip})$) from two classes c_1 and c_2. To maximize separability of the projections of the classes, we want projected means far from each other. However, as it can be seen in Fig. 27, the difference of the projected means $|u_1\text{-}u_2|$ is not a good measure of separability because it does not take into account the variance of the classes. Fisher's solution was to normalize the difference by scatter of both Class 1 and scatter of Class 2. For the two classes, the scatter matrices are defined as

$$S_i = \sum_{x \in c_i} (x - \bar{x}_i)(x - \bar{x}_i)' \tag{43}$$

where $\bar{x}_i = \frac{1}{m_i} \sum_{x \in c_i} x$ and m_i denotes the number of samples in c_i. Thus, the total intra-class scatter matrix is given by

$$\sum_w = S_1 + S_2 = \sum_i \sum_{x \in c_i} (x - \bar{x}_i)(x - \bar{x}_i)' \tag{44}$$

The inter-class scatter matrix is calculated with the equation

$$\sum_b = (\bar{x}_1 - \bar{x}_2)(\bar{x}_1 - \bar{x}_2)'. \tag{45}$$

Scatter measures the same thing as variance, spread around the mean. Scatter is just on different scale than variance. To ensure a good separability of classes, the scatters of the classes should be as small as possible, i.e. samples of Class 1 and Class 2 cluster around the projected means u_1 and u_2, respectively. Fisher's criterion suggested the linear transformation ϕ that maximizes the ratio of the determinant of the between-class scatter matrix of the projected samples to the within-class scatter matrix of the projected samples.

Thus, LDA projects all the data points into a new, normally lower dimensional, space, which maximizes the between-class separability while minimizing their within-class variability. If $\sum_w$ is non-singular, equation x can be solved as a conventional eigenvalue problem and ϕ is given by the eigenvectors of matrix $\sum_w^{-1}\sum_b$. [82]

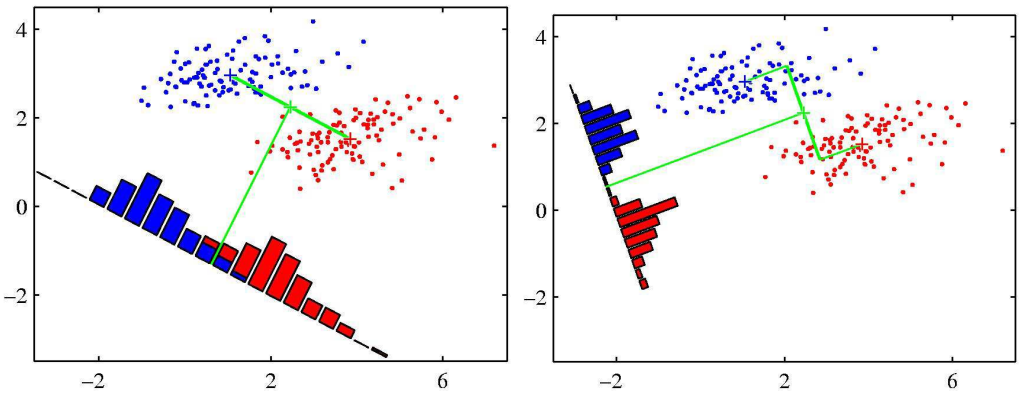

Fig. 27:The classes are not well separated if only the difference of the means of projections of classes 1 and 2 is used as a measure of separation. The problem with the difference of the projected means |u1-u2| is that it does not consider the variance of classes. If we normalize |u1-u2| by a factor which is proportional to variance, the classes are much better separated, even though their projected means are less far apart.

3.6.5.2 Multi-class Linear Discriminant Analysis

The multi-class LDA is an extension of Fisher Linear discriminant that is used if the number of classes is more than two. The principle of the multi-class LDA is similar to two-class case: the projection is from high dimensional space to lower dimensional space and the ratio of intra-class scatter to the inter-class scatter is minimized. The difference between these two methods is that in multiclass case, the maximization should be done among several competing classes.

If we have n classes, the intra-class scatter matrix is calculated similar to Eq. 44:

$$\sum_w = \sum_{i=1}^{n} \sum_{x \in c_i} (x - \bar{x}_i)(x - \bar{x}_i)'. \quad (46)$$

The inter-class scatter matrix in inter-class case is slightly different

$$\sum_b = \sum_{i=1}^{n} m_i(\bar{x}_i - \bar{x})(\bar{x}_i - \bar{x})' \quad (47)$$

where m_i represents the number the number of training samples for each class, x_i is the mean for each class and *x* is total mean vector calculated as

To maximize the between-class measure while minimizing the within-class measure, we should still maximize the equation x. It can be shown that the transformation can be obtained by solving the generalized eigenvalue problem:

$$\sum_b \phi = \lambda \sum_w \phi \quad (48)$$

When the transformation ϕ is known, the samples are classified in the transformed space based on some distance metric, such as Euclidean distance $d(x, y) = \sqrt{\sum_i (x_i - y_i)^2}$. The new instance c is classified to $\arg\min d(z\phi, \overline{x_k \phi})$, where x_k is the centroid of *k*th class. The running time of LDA consists of evaluating the inner and between covariance matrixes, eigenvalue decomposition, and selecting discriminanting features. The computational complexity of evaluating the covariance matrixes is mp^2, where m is the number of instances and *p* is the number of features. [82]

3.6.6 Majority Voting (MV)

Majority voting (MV) is a postprocessing technique that analyzes the current class decision along with the *n-1* (n is the number of majority votes) previous class decisions, and selects the class that occurs most frequently in those *n* decisions as the controller output. MV increases the overall classification accuracy by averaging out errors. It also allows using very short analysis windows without compromising the classification accuracy. As a result, much less storage space is needed for the necessary computations. The number of votes used in MV is determined by the acceptable delay T_d and the processing time τ as follows

$$m \leq \frac{T_d}{\tau} \quad (48)$$

Table 4 in Chapter 3.6.1.2 shows the equations for the controller delay when MV is used.[51, 55]

3.7 Non-pattern Based Control

Proportional control, threshold control, and finite state machines are approaches included in the category of conventional or a non-pattern control. [83] Exemplars of the non-pattern based approach are illustrated in Fig 28. Proportional control is usually used in conjunction with either pattern recognition-based, or non-pattern recognition based methods. The combination increases the accuracy of positioning and force control. The prosthesis may for example have two modes: proportional mode and on/off mode. In the on/off mode the speed of the prosthetic is constant where as in the proportional mode the level of contraction of a muscle controls the speed or force of a prosthesis limb. [26]

In threshold control the amplitude range generated from a relaxed muscle state to the full contraction is divided into two or three segments that have an associated amplitude threshold. Each segment corresponds to a specific movement of the prosthetic. To perform a specific movement function, the user must produce a constant contraction to keep the EMG amplitude in the range of the associated segment. In practice, the user can control with acceptable accuracy only two functions per control muscle. [5]

In Finite state machine based control, finite number of states, transition between them, and commands are used to describe the control. The states usually represent predefined motion commands and transition roles are associated with the signal features. Fig. 28 c) illustrates the simple hand opening/closing state machine. H is the part of the sensing vector related to hand opening/closing. Negative values of H close the hand and positive open it. The absolute value of the signal determines the force applied in Squeeze state. States with a dashed border are exited automatically when no signal is received.[84] For higher level amputees, who have limited number of muscles available after amputation, it may be difficult to control multiple DOFs using this control method. For instance, a transhumeral amputee only has parts of biceps and triceps which can serve as EMG signal sites to control the prosthesic movements. If all the three joint DOFs of elbow, wrist, and hand are required, the user must trigger a mode switch such as making a co-contraction of the agonist/antagonist muscle pair to select which of the joist is desired to be actuated.

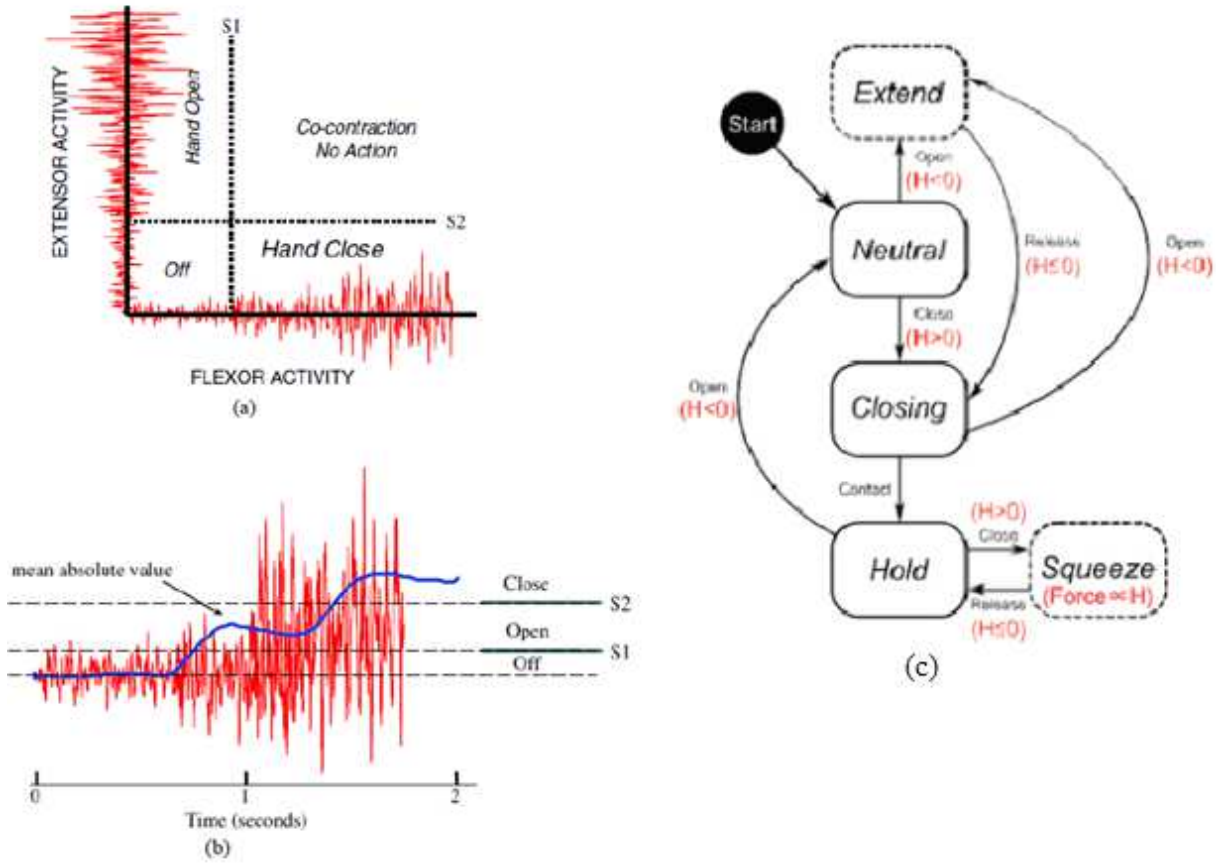

Fig. 28: a) Two channel amplitude coded myoelectric control; b) One channel amplitude coded myoelectric control; c) Hand opening/closing state machine.[84,modified]

Most of the commercial prosthetic hands use non-pattern-based control methods. For example, the Otto Bock two-state system incorporated this technique to assign each prosthetic limb function to a separate control muscle. Usually, a pair of muscles is used to control one DOF, one signal from flexor muscle and one from an extensor muscle. Each of two movements in a joint DOF is assigned to a separate control muscle, for example hand opening to biceps and hand closing to triceps. When the EMG amplitude from the control muscle exceeds the predefined threshold, the associated prosthetic movement is selected and performed. The number of functions that can be controlled by non-pattern recognition-based controllers is limited in comparison to pattern recognition based controllers. This is because the function per muscle is limited to two. The structure of nonpattern based control methods is simple, and they are mostly employed in ON/OFF control.

3.8 Classification Performance Evaluation

Resubstitution method uses the same data first for testing and then for training. This method provides an optimistic estimate of the true error probability. The amount of bias of the resubstitution estimate is a function of the ratio of the set size and the dimension of the feature space. The variance is inverse proportional to the data size. [85]

Because of overfitting the resubstitution method is not recommended. Instead, the most common methods for accuracy estimation is cross-validation. Cross-validation methods remove some of the data before training, and use the removed data to test the performance of the learned model as an unseen data. The simplest version of cross-validation is the hold out method that separates the data into training set and testing set. The classifier is trained using training set only. The classification accuracy of the classifier is tested by using the data in the testing set. The major drawback of this method is that the size of both training and testing data is reduced. Sometimes a random subsampling is used and the hold out method is performed a few times. The accuracy of each repetition is used to calculate the mean accuracy and its standard derivation. However, in the random subsampling method the data of the training and test set are not independent from each other which may influence the estimation of the accuracy. [85]

K-Fold cross-validation divides the dataset in K folds. K-1 folds are used for training and the remaining one for testing. The advantage of this method is that all the exemplars in the dataset are eventually used for both training and testing. [85]

Leave-one-out cross-validation is a special case of K-fold cross-validation. It performs N experiments for a dataset with N exemplars. For each experiment N-1 examples is used for training and the remaining example for testing. Thus, training is achieved using all samples, and at the same time independence between training and testing sets is maintained. The major drawback of this method is its high computational complexity. [85]

The benefit of using a large number of folds is that the bias of the true error rate estimator will be small. However, the variance of the true error rate estimator will be large. The other disadvantage is that more computation time is needed. With a small number of folds the number of experiments and, thus, also computation time is reduced. The variance of the estimator will be small but the bias will be large. In practice, the choice of the number of folds depends on the size of the dataset. For large datasets, even 3-fold cross-validation will be quite accurate, but for very sparse datasets, we may have to use leave-one-out in order to train on as many exemplars as possible. Some indications exist that a ten-fold cross-validation is sufficiently appropriate, and it has also been a common choice for model selection. [85]

4 Implementation

In this Chapter the hardware used in the EMG-measurements is firstly described. Secondly, the hand postures, investigated in this study, are presented. After that, we show the electrode placement and describe the experiment setup. Data preprocessing and feature selection are also described. Signal processing, features, and all tests in this study are implemented with Matlab.

4.1 SEMG Measurement System

EMG-measurements were made with BioSemi biopotential measurement system ActiveTwo. The hardware includes AD-box, battery-box, USB2 Receiver, and Laptop, as can be seen in Fig. 29. The AD-box can digitize up to 256 sensor-signals with 24 bit resolution. Each AD-box channel consist of a low noise DC coupled post-amplifier, with a first order anti-aliasing filter, followed by a Delta-Sigma modulator with an over-sampling rate of 64, and decimination filter with a steep fifth order sinc response and high resolution 24-bit output. The digital outputs of all the AD converters are digitally multiplexed and sent to the PC via single optical fiber. The power supply of AD-box and electrodes is the battery-box. The receiver converts the optical data from the AD-box to an USB2 output. The electrodes were flat-type active electrodes (11 mm width, 17 mm length, 4.5 mm height) with individual leads. The electrodes are sintered with Ag-AgCl to gain low noise minimal offset potentials and better DC-stability. They were attached to the skin with electrode paste and paper tape is used to hold the electrodes in place. The Common Mode Sense (CMS) and Driven Right Leg (DRL) electrodes drive the average potential of the patient as close as possible to the AD-box reference potential. The used software was BioSemi acquisition software ActiView. It is an acquisition program designed to display all ActiveTwo channels on screen and save all the data to disk in .BDF format (BioSemi Data Format). [86,87] In this study, the sampling rate was set at 2048 Hz.

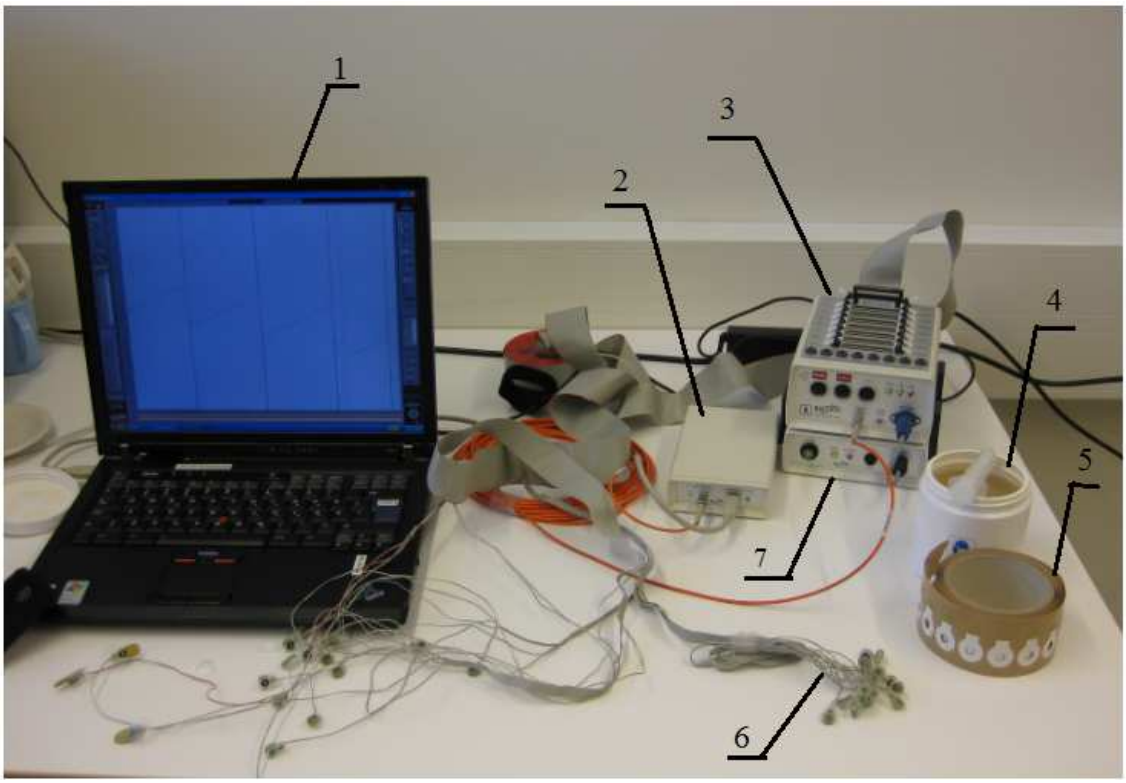

Fig. 29: Measurement system: 1. PC/laptop, 2. USB2 Receiver, 3. AD box, 4. electrode gel, 5. adhesive disks, 6. electrodes, 7. battery box

4.2 Subject Information

The data were collected from the right forearm of eight able-bodied subjects between the ages of 26-71. Five of the subjects were male and three were female. Subject 4 was left-handed. The detail information of each subject is presented in Table 5.

Table 5: Subject Information

subject	1	2	3	4	5	6	7	8
gender	male	male	female	female	male	male	female	male
age	27	26	52	29	27	29	58	71
Weight/kg	63	71	76	65	88	71	69	90
Height/cm	182	170	164	167	180	178	163	181
right-/ left handed	right	right	right	left	right	right	right	right

4.3 Selecting the Hand Postures

Although, the natural human hand is able to perform several hand postures, usually only the most common grasps are considered for the prostheses. This study investigates the six hand postures shown in Fig. 30 as a subset of the possible hand postures the human hand can make. The hand postures were selected because they are common in everyday life and they were also investigated in many prior studies.

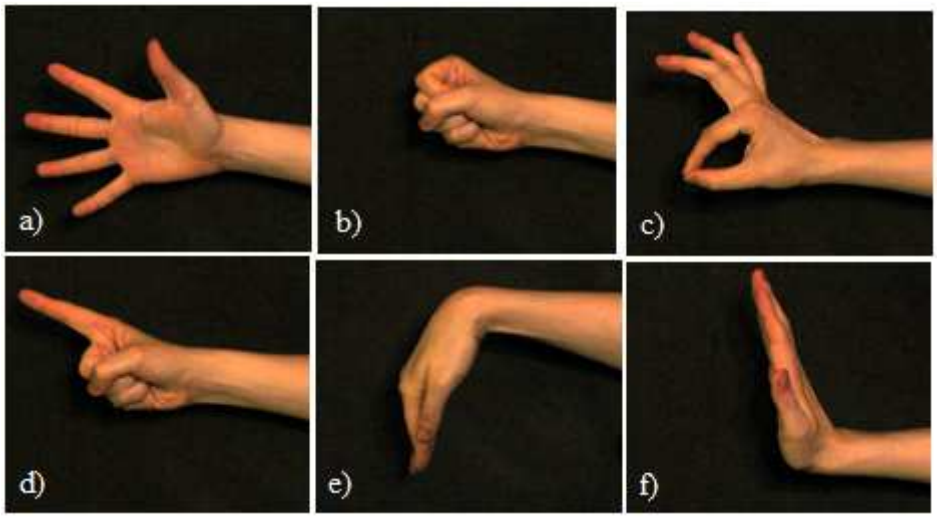

Fig. 30: Six daily-life upper-limb motions investigated in this study: a) hand open, b) hand close, c) precision grip, d) index point, e) wrist flexion, f) wrist extension

4.4 Selecting the Electrode Positions

The average positions of the electrodes were selected according to the anatomical chart of the muscles in the human forearm. In addition, the results of previous studies are also considered. The precise electrode positions were determined individually for each subject by viewing the signals online, and selecting the place that seemed to give the best signal. Data was recorded with 9 channels. Because we used bipolar measurements, two electrodes form a channel. Bipolar recordings were estimated by from unipolar recordings by taking spatial derivates, i.e. the rate of change of surface potential recordings with respect to their location on the forearm. The channel positions and specific muscles were:

The posterior compartment of the forearm:

1. Extensor pollicis brevis: CH1
2. Extensor digitorum: CH2
3. Extensor indicis: CH3
4. Flexor capri ulnaris: CH4

The anterior compartment of the forearm:

5. Brachioradialis: CH5
6. Flexor capri radialis: CH6
7. Flexor digitorum superficialis: CH7
8. Flexor pollicis longus: CH8

Fig. 31 shows the approximate location of the channels on the target muscles in the forearm.

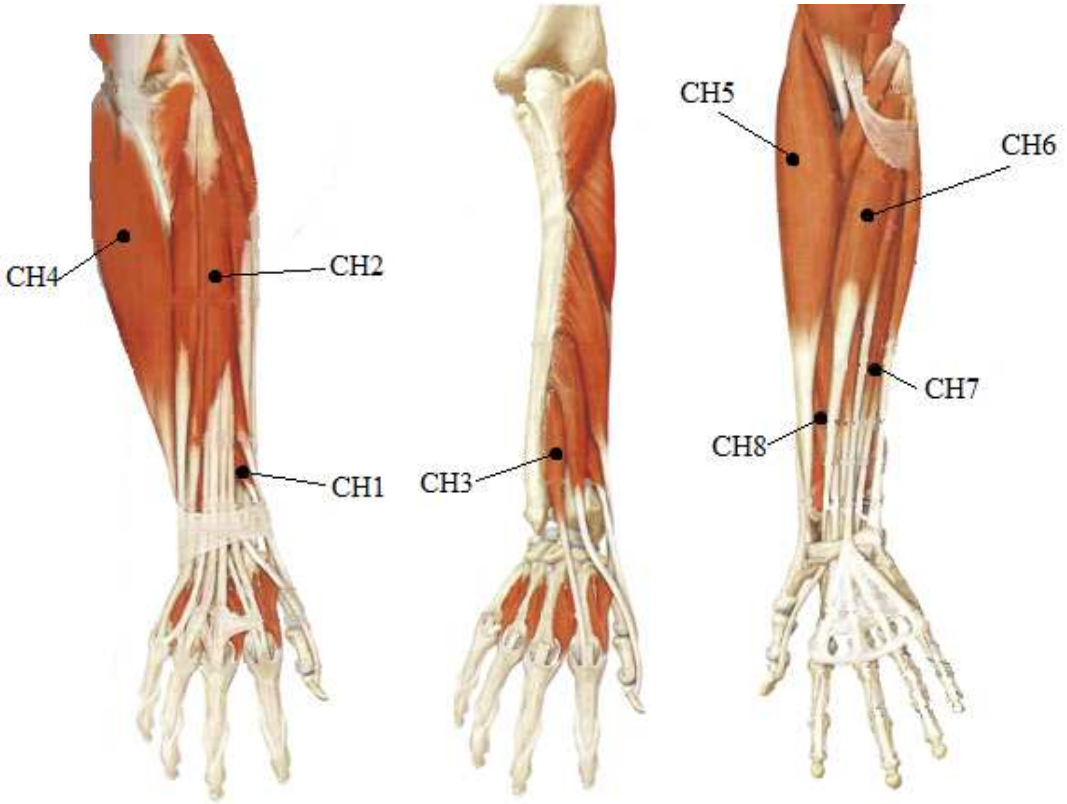

Fig. 31:Placement of electrodes on the forearm. [21, modified]

The CMS electrode is best located approximately in the center of the electrodes. In practice, the exact location is, however, not very critical and the best method to find the suitable place is by trying where to get the best signal. The DRL electrode can be located anywhere on the body. [86] In this study, CMS and DRL electrodes were placed on the biceps brachii.

4.5 Measurements

To prevent the baseline shifts the skin of the subject was cleaned with alcohol. After firstly theoretically estimating the optimal electrode sites, the exact locations were selected experimentally by placing the electrode in the area of interest, and examining where to get the best signal. The standard recommendations for electrode placement as

established by the Surface EMG for Non-Invasive Assessment of Muscles (SENIAM) specified that the size of the electrodes should not exceed 10 mm when placed in the direction of the target muscles and that the inter-electrode distance should not go beyond 20 mm. [88] In this study, the distance between the electrodes was approximately 1.5 cm. In order to get the greatest amplitude, the electrodes were tried to position so that the imaginary line connecting two electrodes is in parallel with the muscle group and the electrodepair is in the midline of the belly of the muscle between the nearest innervation zone and the myotendonous junction. After applying the electrodes, we waited a few minutes so that the chemical reactions in the electrode-gel-skin interface reach a stabile equilibrium and the baseline drift and noise have settled. During the measurement, the arm was resting on the support as can be seen in Fig. 32. This reduces movement artifacts because the electrodes are not pressed by the table.

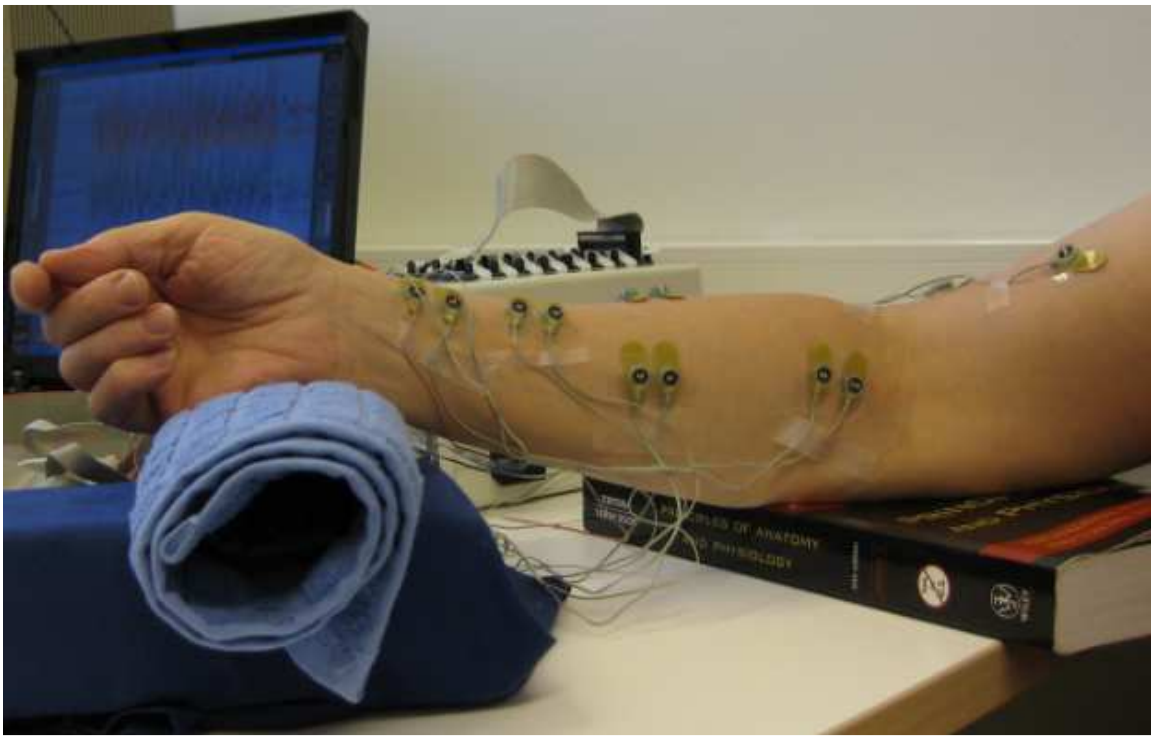

Fig. 32: The forearm was resting on the support during the measurement.

During the experiment the volunteers performed the six upper limb postures presented in Chapter 4.3. Additionally, the resting state was investigated. Totally 35 hand postures, including resting states, were performed. The first seven hand postures were used as a testing set and the rest of the data is used as a training set. The subjects maintained each posture for approximately five seconds, and the dynamic states between grasps were short (less than 1 second).

When the classification accuracy is evaluated, both the predicted class and the actual class need to be known. To determine the actual classes, the tests were recorded using a video camera. After starting the EMG measurement, we generated an impulse to the trigger channel by pressing a button, and at the same time the led turns on. Thus, we can see on the video the exact time instant when the impulse is generated on the trigger

channel. When we know a sampling rate of the equipment, we can calculate the time instants of the transient states and steady states accuracy out to milliseconds.

4.6 Data Preprocessing

The first step of the preprocessing is an estimation of the bipolar measurements from the 16 unipolar recordings. This is done with Matlab by taking the spatial derivatives of every sensing electrode pair. Secondly, we need to determine the time instants when the grasps start and end from the video recordings. When we know the time instants and sapling rate, we can calculate the state and class of the sample intervals as follows:

$$number\ of\ samples\ per\ interval = \frac{stop-start}{sampling\ rate} \tag{49}$$

where *start* and *stop* refers to the time instants when hand postures/dynamic states start and stop, respectively.

Secondly, the signal is subsampled. The sampling rate of the measurement system was set to 2048 Hz. However, the frequency range of EMG is 0-1000 Hz, and the dominant energy is concentrated in the frequencies of 20-500 Hz. Most of the remaining signal power is contributed by electrode and equipment noise. As mentioned in Chapter 3.3, little attention has been paid to the effect of sampling rate to the classification accuracy. In this thesis, we investigated the effect of different sampling frequencies to the classification accuracy when individual TD features were used. To avoid the aliasing, the signals higher than half the sample rate were filtered out.

The end of the dynamic period is evaluated by adding a delay to the time instant when a movement stops. The time instants when the movements start and stop are determined by watching the videos recorded during the test. The delay is calculated by using the equations presented in Table 4. The data is assumed to be correctly classified if the class changes within the dynamic period and do not return to the previous class after once changed to the next class. If the data is classified to some other class than the class before or after dynamic period, misclassification is assumed to be occurring. Total accuracy describes the classification accuracy of the data during both steady and dynamic states.

The classification accuracies were calculated by 10-fold cross-validation. Because the classification is based on the steady state data, the dynamic states between grasps need to be removed before 10-fold cross-validation. The data need also to be balanced so that it includes an equal number of records per class. Additionally, the classification accuracies have been evaluated by using the data that contains both steady and transient states. In this case, a holdout method is used and the data is divided into two set: a training set and a test set. Transients are removed from the training data, and an equal number of

records per class are selected in it. An estimate for classification accuracy is calculated as follows

$$Classification\ accuracy = \frac{number\ of\ correctly\ classified\ samples}{Total\ number\ of\ testing\ samples} \times 100(\%) \quad (50)$$

In addition of the total classification error, the error estimates were also calculated separately for the steady and the transient state. The sample is assumed to be correctly classified during the dynamic state if it is not classified to the class before the dynamic state after once classified to the class after dynamic state. If the sample is classified to some other class than the class before or after the dynamic state, it is, of course, assumed to be misclassified. The end of the dynamic period is evaluated by adding a delay to the time instant when a movement stops. The time instants when the movements start and stop are determined by watching the videos recorded during the test. The delay is calculated by using the equations presented in Table 4. When average classification accuracies were calculated over all subjects, the error bounds were obtained using the standard derivation as follows:

$$\sigma = \left(\frac{1}{n-1}\sum_{i=1}^{n}(x_i - \bar{x})^2\right)^{\frac{1}{2}} \quad (51)$$

4.7 Data Representation

Features are extracted from overlapped segments. The EMG features in the matrix form can be expressed as

$$feature\ matrix = \begin{bmatrix} f_{11} & \cdots & f_{1j} \\ \vdots & \ddots & \vdots \\ f_{i1} & \cdots & f_{ij} \end{bmatrix}. \quad (52)$$

Features of each 8 channels are represented as (8× 1)-dimensional vectors f_{ij}. In the feature matrix, j represents the window number ($1 \leq j \leq J$, J=L/N, N is the length of the window size function and L is the whole data set length) and i feature number ($1 \leq i \leq I$, I is the number of features). Each column in the feature matrix represents a feature vector that is to be classified. The length of the feature vectors (i.e. the number of rows in the feature matrix) is depending on the type and number of features. For example, if we have two features, MAV and RMS, the length of the feature vector is 16 (eight channels and two features per channel). If AR(6) coefficients is used as a feature, the total length of the feature vector will be 48 (eight channels and seven AR coefficients per channel). Feature matrix was normalized by Eq. 41.

4.8 Feature Selection

Most of the previous studies have compared only few combinations of TD features, or if the larger number of TD features have been compared, the performance of them has been evaluated independently with statistical methods. However, the feature vector consisting of the best M features evaluated separately rarely gives an optimal solution since it does not account for the feature dependence, as illustrates in Fig. 33. In addition, the classification accuracy achieved with the feature vector is depending on the classifier. If we want to find an optimal feature set for the classifier, the best way would be to compare classification accuracies instead of using statistical methods.

One of the objectives of this thesis is to find the optimal feature set among 16 TD features and two TSD features in context of an LDA classifier. The more detailed description of the features is given in Chapter 3.6.2. An ideal method to find the optimal feature subsets would be to form all combinations of the features, classify them with an LDA classifier, and compare the classification accuracies. However, the number of the all possible combinations of the 16 features is 65 536 ($2^{16} - 1$). Calculating all these combinations is extremely time consuming, and therefore it is needed to use a local optimization technique that involves examining only a subset of all possible combinations. However, it should be noted that the local optimization algorithms do no guarantee the selection of the globally best subset.

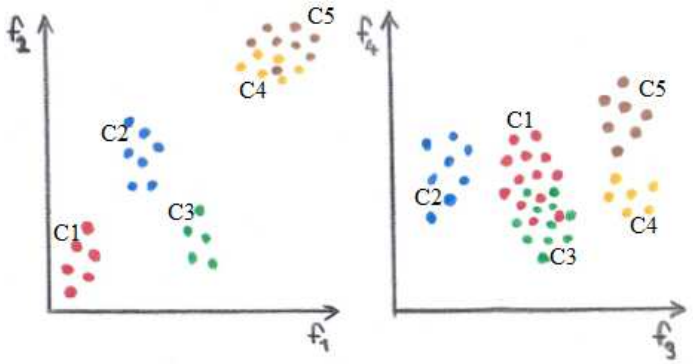

Fig. 33: 4D problem with 5 classes. If evaluated separately, f1 is the best feature (separates C1,C2, C3 and {C4,C5}), x2 and x3 are equivalent (separate classes in three groups) and f4 is the worst feature (separates only C4 from C5). Thus, if we choose features according to the individual scores, we would pick f1 and either f2 or f3, leaving classes C4 and C5 non-separable. However, the optimal feature subset would be the combination of f1 and f4, because f4 provides the only information that f1 needs: discrimination between classes C1 and C2.

In this study a Sequential Forward Selection (SFS) algorithm have been used to find an optimal feature set. It starts with zero features, and sequentially adds the feature that yields the best performance when combined with the features already selected. This cycle repeats until no improvement is obtained from extending the current subset. [89] The SFS algorithm is selected to use in this study because it is relatively simple to implement and performs well when the optimal subset is small. In addition, it turned out

that several alternative feature sets yield approximately equal high classification accuracy, and therefore more advanced algorithms, such as Genetic Algorithms, will not give any benefit.

5 Results and Discussion

This Chapter introduces and analyses the results achieved in this study. Firstly, the determination of the values for free parameters is described. Secondly, the classification accuracies achieved with different sampling rates are presented. We also examine the effect of ICA to the classification accuracy. After that different feature vectors are compared. Postprocessing with MV is also demonstrated. In addition, we present estimates for time delays. Finally, we discuss some problems related to the control of myoelectric prostheses.

Example of the sEMG signal acquired from the forearm of Subject 2 during six different hand postures is shown in Fig. 34. Rest periods are at the beginning and end of the recording. The hand postures are made in the following order: hand open, hand close, precision grip, index point, wrist flexion, and wrist extension. Dynamic states are marked with red. The amplitude of rest periods is small in all signals. Combinations of the amplitudes of the signals are different in each motion. This foundation suggests that the amplitude related features may yield the high classification accuracy.

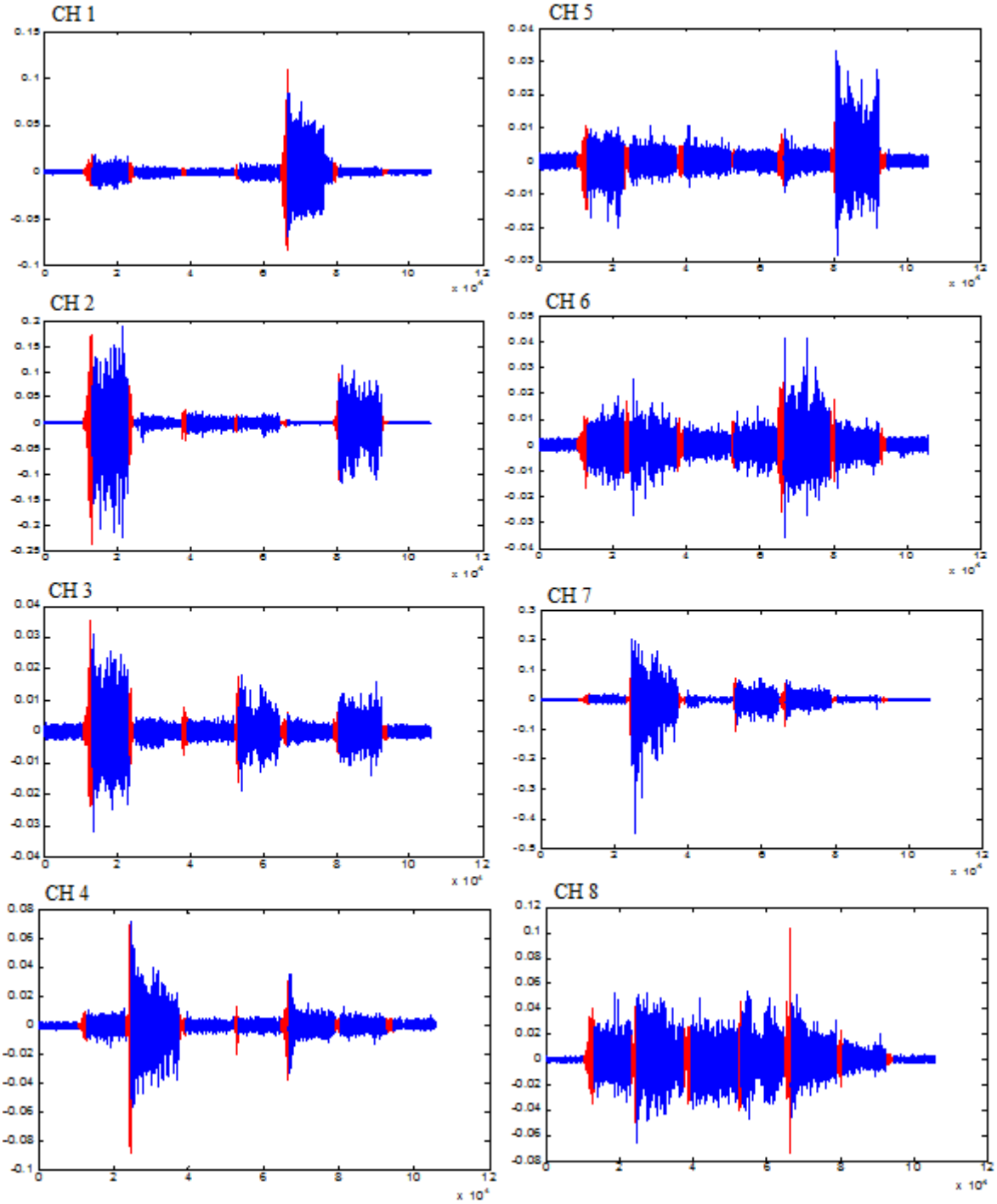

Fig. 34: Eight-channel sEMG signals acquired from the forearm of Subject 2 measured during he was performing six grasps in the following order: hand open, hand close, precision grip, index point, wrist flexion, and wrist extension. At the beginning and end of each signal is rest period. Dynamic states between grasps are marked with red.

5.1 Determination of Values for Free Parameters

Before comparing the performance of the features, we need to determine the values for the free parameters. The free parameters for features were determined separately for each frequency and for each subject. Fig. 35 demonstrates the significant effect of the ZC threshold value and the AR order to the classification accuracy. As described in Chapter 3.6.2.3, previous studies have suggested 3, 4 or 6 to be optimal values for AR order. In this study, the classification accuracy was rather poor for AR order 3, but increased significantly when the order is increased to 4. No significant increase in classification accuracy was observed with the order numbers over six, and therefore the AR(6) model is selected to use in this study. Appendix 1 includes the figures illustrating the effect of the threshold values of WAMP and MYOP as well as the effect the order of CC has to the classification accuracy. The values in Fig. 35 and in Appendix 1 are an average values calculated of the data from the eight subjects, but is should be noted that the optimal values also differ between subjects. However, for AR order and CC order the variation between subjects was not significant.

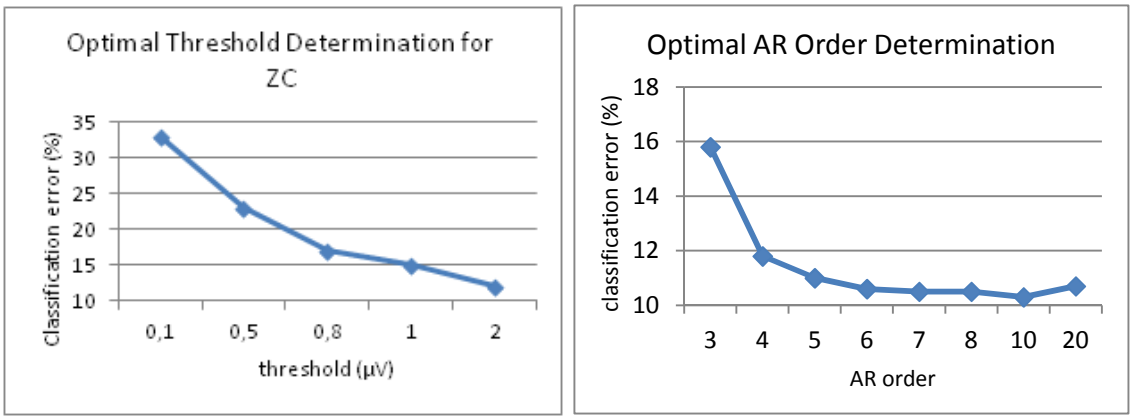

Fig. 35: The effect of the ZC threshold value and the AR order to the classification accuracy

5.2 Optimal Sampling Frequency

Most of the sEMG signal power lies in the frequency band below 500 Hz. This is demonstrated in Fig. 36 that shows the power spectra of the sEMG signal acquired from Subject 1 when he was holding his hand open. The same observation was made of the power spectra of the other hand movements for all subjects. The power spectra of the other hand movements for Subject 1 can be found in Appendix 2. However, it is unclear whether all these frequencies contain important information for movement classification. As discussed in Chapter 3.3, Li et al. found that the frequency components above 250 Hz may be rejected without compromising too much the classification accuracy, and therefore a sampling rate of 500 Hz, or even 400 Hz may be used instead of commonly used 1000 Hz [43, 90].

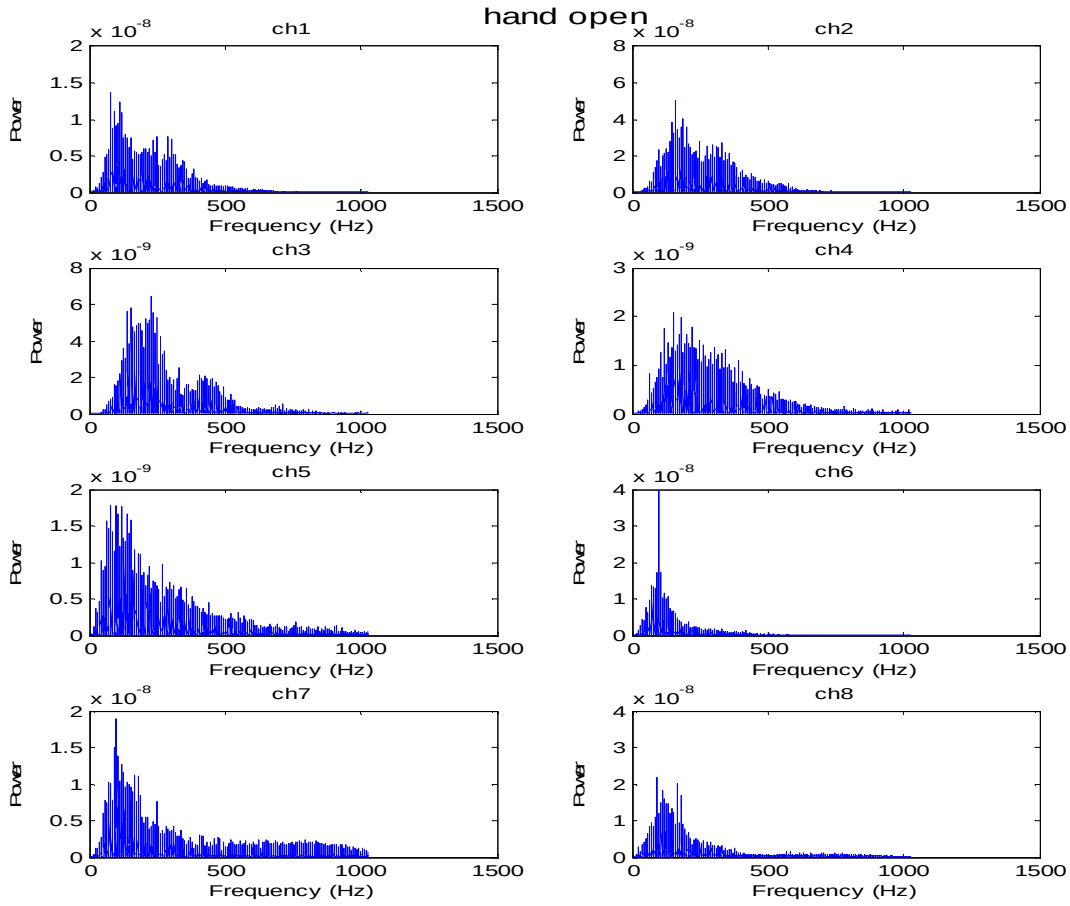

Fig. 36: The power spectra of the sEMG signal from 8 channels for Subject 1.

The classification accuracy for 18 features with seven different sampling rates is shown in Table 6. The classification accuracies are an average values calculated of the data collected from the seven subjects. The classification accuracies achieved with the data from Subject 8 were much lower than the results achieved with the data from the other subjects. Therefore, Subject 8 was excluded when average classification accuracies were calculated in Table 6. The window length was set to 100 samples with an overlap of 50 %.

The results in Table 6 agree the results reported by Li et al.: The sampling rate can be significantly decreased from the commonly used sampling rate of 1000 Hz. However, perhaps somewhat surprisingly, with respect to the most features the average classification accuracy is even slowly increasing up to 400 Hz. After 400 Hz the classification accuracy starts to decrease. Thus, an optimal sampling frequency for most of the features seems to be 400 Hz. These results suggest that using lower sampling frequency than commonly used 1000 Hz may not only improve the real-time properties, but also the classification accuracy. However, this does not apply for the all features. The classification accuracy of AR and CC is best at the frequency of 800 Hz. When the sampling rate is decreased from 800 Hz to 400 Hz, the classification accuracy decreases about

2.67 percentage points for AR and 3.60 percentage points for CC. SSC has the best classification accuracy at 1000 Hz, and at the sampling rate of 400 Hz it has decreased 1.58 percentage points. TM4 and TM5 yield the best accuracy with relatively low sampling rate, at 300 Hz. The error bounds are usually lowest at 400 Hz which means that at this frequency the discrepancy across the subjects is low.

Table 6: The classification accuracy for 18 features with seven different sampling rates

frequency (Hz)	300	400	600	800	1000	1500	2000
MAV	93.13±6.1	94.24±5.3	93.41±6.9	92.98±7.7	92.6±7.9	90.77±8.9	89.49±9.5
MAV1	92.75±6.2	93.75±5.8	93.14±6.9	92.21±8.1	91.92±8.2	90.22±9.2	88.92±9.5
MAV2	79.24±9.9	81.27±9.7	78.73±10	75.74±10	72.51±9.5	66.92±8.6	63.35±8.3
VAR	84.52±8.3	81.97±8.6	80.38±9.0	79.49±9.1	78.58±9.0	76.73±9.2	74.51±9.5
RMS	93.12±6.0	94.30±5.4	93.85±6.5	93.49±7.4	93.10±7.9	91.42±8.7	89.91±9.3
TM3	54.45±6.8	55.85±5.2	54.38±3.2	53.66±4.0	53.07±3.7	50.71±5.3	49.06±4.6
TM4	55.78±5.4	52.78±3.3	51.74±3.6	51.32±3.3	52.26±3.4	48.84±4.2	47.27±4.5
TM5	55.78±5.4	52.78±3.3	51.74±3.6	51.32±3.3	52.26±3.4	48.84±4.2	47.27±4.5
AAC	92.68±6.4	93.59±6.3	92.76±7.0	92.12±8.1	91.53±8.3	88.39±9.2	85.70±9.3
DASDV	93.14±5.8	94.00±5.9	93.51±7.0	92.99±7.7	92.56±8.2	90.50±8.8	88.54±9.2
V-ORDER	92.11±6.7	93.68±6.3	93.24±7.1	92.96±7.6	92.52±8.1	90.76±9.0	89.18±9.6
LOGDET	91.54±7.3	91.95±7.3	91.01±8.5	90.22±9.1	89.89±9.4	87.99±9.9	86.72±10
WAMP	87.83±11	93.27±5.9	93.17±6.4	93.34±7.1	93.65±6.9	93.00±7.1	90.70±8.1
MYOP	86.27±11	91.70±7.8	91.77±7.5	91.08±8.2	91.84±7.8	91.10±8.2	89.48±9.0
ZC	77.10±16	90.40±7.7	89.80±7.8	89.29±8.3	85.55±11	86.00±10	85.48±9.9
SSC	84.92±11	88.50±10	88.76±8.8	89.69±8.2	90.08±7.7	89.41±8.1	88.00±8.4
AR	82.17±8.1	90.36±6.2	92.71±6.2	93.03±7.5	92.49±7.5	92.53±7	91.95±7.7
CC	80.55±7.7	89.54±6.3	92.46±6.6	93.14±6.8	92.55±7.3	92.51±7.1	91.80±7.9

5.3 Preprocessing with FastICA

Fast ICA was tested as a preprocessing technique in order to eliminate muscle crosstalk. The correlation matrix in Table 7 illustrates the amount of crosstalk between channels before ICA. After ICA the correlation coefficients were about zero. However, the classification accuracy was not improved after ICA. This may be because the channels were placed relatively far from each other, and therefore the amount of crosstalk is not significant. The correlation matrix in Table 7 shows that the correlations are in general small (-0.0022–0.3312) between different channels which indicates that the amount of crosstalk is relatively low. The correlation matrix is calculated by using the data from Subject 3, but the correlation coefficients calculated of the data from the other subjects were at the same size range. The two previous studies [31, 91] that have shown ICA to significantly improve the classification accuracy placed the channels much nearer to each other than they were placed in this study. In this study the distances between channels were several centimeters whereas in the study of Sueaseenak et al. the distance between two channels was only 10 mm, and the correlation coefficient between these two measurements was 0.4710 before ICA [91]. Al-Timemy et al. placed sixteen channels near to each other around the upper part of the forearm around the circumference. He has not

reported the exact distance between electrodes, but it was obviously smaller than in this study [31].

Table 7: Correlation matrix of the data from Subject 3.

channel	1	2	3	4	5	6	7	8
1	1							
2	-0.0183	1						
3	0.0079	-0.0906	1					
4	-0.0022	0.0508	-0.0259	1				
5	-0.0304	0.1887	-0.1025	0.1435	1			
6	0.0171	0.0227	-0.0244	0.1284	0.1064	1		
7	0.0528	0.0135	0.0178	-0.0428	0.0139	-0.0514	1	
8	0.3312	-0.0361	-0.0209	-0.0026	-0.0357	0.0151	0.0830	1

5.4 TD Feature Set Comparison

Secondly, we determined an optimal feature subset for each subject by using the sampling rate of 400 Hz, the cut-off frequency of 60 Hz, and the window length of 100 samples with the 50 % overlap. Optimal subsets were formed by using SFS algorithm. The results are presented in Table 8. The classification accuracies were calculated by using 10 fold crossvalidation. The results in Table 8 suggest two to be an optimal number of features in the feature set. The classification accuracy for six of eight subjects was not increased significantly when more features were added. This result is in consistent with the study by Phinyomark et al. [56] where it was found only a slight increase in the classification accuracy when the number of features in Hudgins's had Du's feature sets was greater than two.

Table 8: The results of SFS algorithm for each subject.

subject	feature set
1	RMS, WAMP
2	DASDV, VAR
3	RMS, VAR, CC
4	RMS, VAR, CC, WAMP
5	RMS,VAR,CC
6	DASDV, VAR
7	RMS, WAMP, VAR
8	RMS, WAMP

No any feature set outperformed the others, but instead the feature set that yielded to the highest classification accuracy seemed to be depending on the subject. However, some features seemed to be selected more often than the others. For example, VAR was included in seven, RMS in six and WAMP in four feature sets. Thus, a combination of some of these features may yield relatively high classification accuracy for all subjects.

A good subset may be RMS and WAMP, because they describe different signal properties: RMS is a measure of power and WAMP describes the frequency properties. Additionally, these two features have a different distribution in space, as can be seen in Fig 37. Thus, it can be assumed that both of the features give some new information. Another good alternative would be a combination of VAR and WAMP. RMS, WAMP, and VAR have also been very commonly used in sEMG classification.

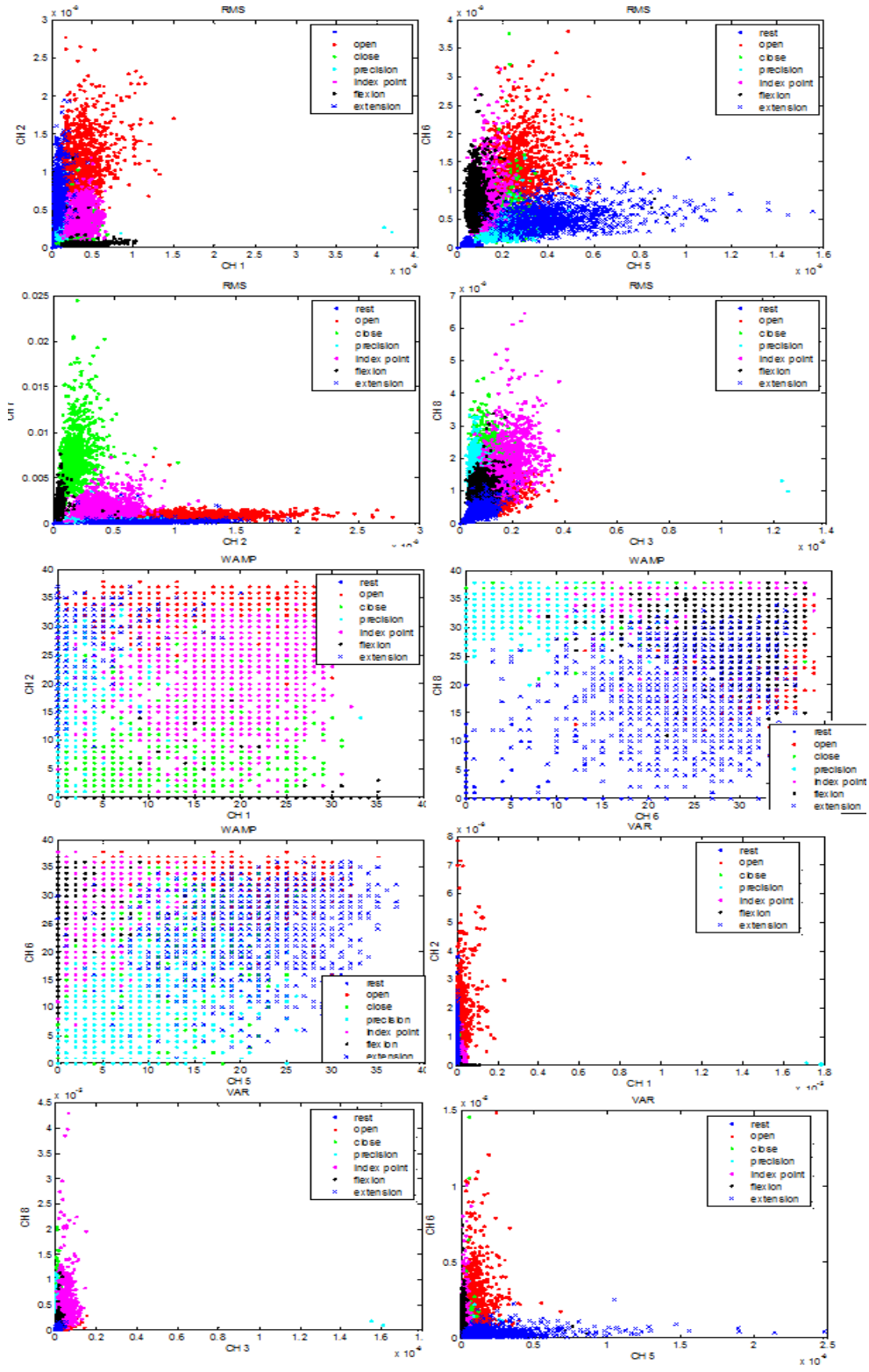

Fig. 37. Scatter plots for 2 channels and 7 movements (i.e. rest, hand open, hand close, precision grasp, index point, flexion, and extension) of Subject 1 by applying RMS, WAPM, and VAR. The classes are linearly separable which suggests that they could be effectively separated by the LDA classifier.

Table 9 compares the classification accuracies achieved by using the following feature sets:

- two feature sets, WAMP-RMS and WAMP-VAR, which are suggested by the results achieved in this study
- Hudgins's TD feature set (MAV-WL-ZC-SSC) and the feature set suggested by Englehart (AR-RMS), both of which are frequently used in the previous studies
- The feature set that SFS algorithm suggested to be an optimal for an individual

In addition, MAV, RMS, DASDV, and V-order were also investigated individually because Table 9 indicates that these features may yield the high classification accuracy. The data is divided into two sets, of which the smaller includes the first seven grasps (test set) of the trial and the other includes the rest grasps (training set). Four types of classification accuracies have been evaluated. The steady state accuracy and the dynamic state accuracy have been evaluated by using separate data for training and testing. The steady state accuracy describes the classification accuracy during constant contractions whereas the dynamic state accuracy describes the classification accuracy during the periods when a subject switches from a hand posture to another. A dynamic period was assumed to begin when the hand of a subject starts to move. The cross-validation accuracy is calculated by applying 10 fold cross-validation on the training data. The error types are described more detail in Chapter 4.6. When separate training and testing sets were used, MV has been used to improve the classification accuracy.

Summary of the comparison of the feature sets and some individual features is presented in Table 9. The more detail table is presented in Appendix 3. As it is apparent from Table 9, there is no significant difference between the performance of the five feature subsets and the single features. This result is in consistent with the observation of Osokei et al. [54] who compared the performance of 14 individual features and four feature sets by using disjoint segments of 200 samples, 1000 Hz sampling rate and SVM classifier. However, Osokei et al. also found that the feature sets provide much lower discrepancy in accuracy during several independent attempts across different subjects. Thus, the range of classification accuracy for feature sets, in several independent observations, is significantly narrower than the range of classification accuracy for single features. Osokei et al. named this as the major advantage of using feature sets instead if single features. In this study, however, the same effect was not observed.

Table 9: Classification accuracies

all subjects included	SFS	WAMP-RMS	WAMP-VAR	MAV-WL-ZC-SSC	AR-RMS	MAV	RMS	DASDV	V-Order
total avg.	88.4	86.6	83.2	81.7	86.1	79.9	85.9	82.3	84.9
total sd.	12.7	13.8	15.5	19.0	16.1	20.8	17.7	18.6	17.9
crossval. avg.	87.7	85.4	82.9	85.3	85.5	83.9	82.6	80.0	81.4
crossval. sd.	13.0	13.8	14.5	15.1	15.7	15.2	15.2	16.0	14.7
subject 8 excluded									
total avg.	92.3	90.1	87.2	87.4	91.4	85.9	91.9	87.5	90.8
total sd.	7.00	10.1	11.5	10.9	6.20	12.9	6.00	12.4	6.40
crossval. avg.	89.8	87.1	84.7	87.6	87.4	86.3	84.4	82.0	83.2
crossval. sd.	12.6	13.9	14.6	14.7	15.9	14.7	15.4	16.1	14.9
subject 5 & 8 excluded									
total avg.	94.6	93.6	90.9	90.6	93.3	89.7	92.8	91.6	91.6
total sd.	3.60	4.90	6.30	7.50	4.10	8.80	6.00	6.8	6.70
crossval. avg.	94.3	91.3	89.2	92.8	93.3	91.6	90.0	86.8	88.5
crossval. sd.	4.00	9.50	9.40	5.20	3.80	4.40	4.60	10.9	5.20

The classification accuracy varies significantly between subjects, as the high standard derivations indicate in Table 9. The large range in the classification accuracies between individuals may be due to the fact that the electrical conductivity varies with tissue type, thickness, physiological changes and temperature, and these conditions can greatly vary between subjects. For Subject 8 the classification accuracy was rather poor: the total classification accuracy was at highest 61.4 %. This classification accuracy was achieved by using the feature set suggested by the SFS algorithm. It seemed that for the other feature sets and single features the classifier was not able to classify the signal. However, the classification accuracy given by cross-validation is much higher, between 65.7 % and 73.3 %. This indicates that something may be wrong in the testing data. For instance, the lower muscle contraction force during testing set than during training set may result poor classification accuracy. For Subject 5 the classification accuracy was at highest 86.6 %, and the classification accuracies for the all other subjects were over 90 %, at least for some of the features or feature sets. The hand postures that were most commonly mislabeled one as another were precision grip, index point and hand close. This would be expected, because these postures are somewhat similar.

5.5 Fast Fourier Transform

The results from FFT based classification are shown in Table 10. PCA was used to reduce the dimensionality of the feature vectors. As it is apparent from Table 10, the classification accuracies are at the same size as the accuracies obtained by TD-feature vectors. This result is agrees with the previous studies. The classification accuracy for Subject 8 was again significantly poorer compared to the classification accuracies for the other subjects. The window lengths were 32 samples. However, for Subjects 5 and Subject 6, the window length of 64 was used because it increased the classification accuracy

significantly (the total accuracy increased from 77.3 % to 94.6 % for Subject 6 and from 68.5 % to 83.6 % for subject 5). Overlap was 50 % of the window length, the window function was Hamming-window, and the data was postprocessed with MV.

Table 10: Results from FFT based classification.

subject	steady state	transient	total	crossv.
1	99.5	86.8	98.0	97.0
2	98.3	81.0	96.6	91.1
3	87.6	81.6	86.9	85.9
4	90.3	97.2	90.9	85.2
5	81.2	100.0	83.6	70.1
6	96.0	87.4	94.6	93.0
7	83.1	52.1	78.4	74.4
8	51.7	31.0	47.5	60.2
avg.	86.0±15.4	77.1±23.6	84.6±16.4	82.1±12.7
avg. *	90.9±7.3	83.7±15.7	89.9±7.2	85.2±9.8

**Subject 8 excluded*

5.6 Discrete Wavelet Transform

The classification accuracies obtained by using third level DWT are summarized in Table 11. We tested several wavelet functions from the following wavelet families: Daubechies (db), Symlets (sym), Coiflets (coif), and BiorSplines (bior). Daubechies 44 is the most similar mother wavelet function across a variety of biological signals. However, the similar wavelet function is not necessarily the proper choice for hand posture classification because wavelet functions in wavelet-based processors also depends on problem's parameters.[92] According to the results obtained in this study the suitable wavelet functions for hand posture classification seemed to be db4, bd7, db10, coif4, sym4, bior4.4 or bior4.5. These wavelet functions have also been suggested in previous studies [76, 92, 93, 94]. We obtained good results also by using db44, but it did not outperform the more simple wavelets. The results in Table 11 are obtained by using db7, that is suggested to be the suitable wavelet function also in previously [76].

Table 11: Results from DWT based classification.

subject	steady	transient	total	crossv.
1	99.3	93.4	98.6	98.3
2	98.6	96.4	98.4	94.5
3	94.6	94.4	94.6	84.8
4	97.4	57.0	92.5	88.0
5	74.8	78.8	75.3	52.6
6	88.3	79.7	87.2	90.8
7	84.1	51.6	79.2	79.6
8	50.0	77.1	54.7	66.1
avg.	85.9±17.0	78.6±17.0	85.1±14.8	81.8±15.6
avg.*	91.0±9.1	78.8±18.2	89.4±9.2	84.1±15.2

**Subject 8 excluded*

5.7 Dimensionality Reduction

PCA was used to reduce the dimensionality of the feature sets. The classification accuracy was not improved after applying PCA to the TD feature sets, instead it was found to decrease. This may be because the dimensionality of TD feature sets is somewhat low (two TD features form 16-dimensional feature vector). However, the classification accuracy was improved dramatically for FFT after PCA. Before PCA the feature vectors were 136-dimensional with window length of 32 samples and 264-dimensional with window length of 64. By using PCA we reduced the dimensionality to 15 or 20, depending on the classification results. The average delay estimate for the window length of 32 samples (80 ms) is 160 ms and the delay range is 40 ms. Corresponding values for the window length of 64 samples (160 ms) are 320 ms and 80 ms. Fig 38 displays the classifier outputs for four different combinations of the feature dimension and the window length.

The dimensionality of DWT is reduced by calculating RMS from the detail coefficients of each three level as well as from approximation coefficients. The dimensionality reduction using PCA was also tested. However, the classification accuracies after PCA dimensionality reduction were poor.

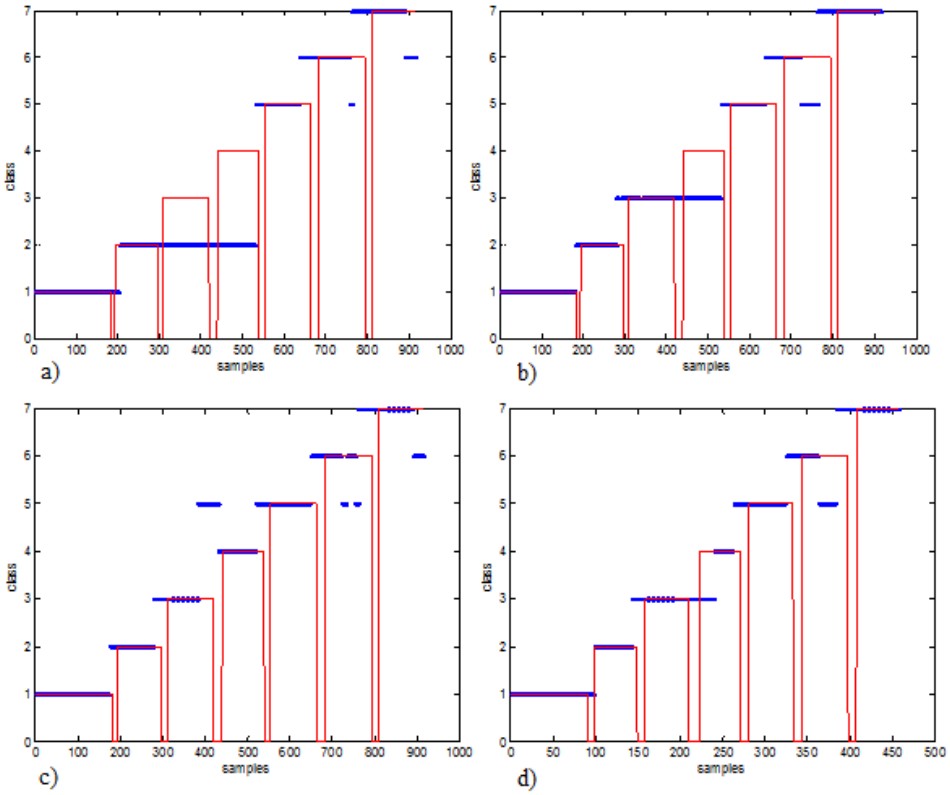

Fig 38. The output of the classifier for Subject 5 by using a) window length of 32 sample and reducing the dimensionality to 15; b) window length of 32 samples and reducing the dimensionality to 20; c) window length of 64 and the dimensionality to 20 d) window length of 64 and reducing the dimensionality to15. The classes describe the hand postures as follows: 1. rest, 2. open hand, 3. close hand, 4. precision grip, 5. index point, 6. wrist flexion, 7. wrist extension

5.8 Majority voting, Window Length and Delay

Fig. 39 shows the effect of MV on the classification accuracy for each subject in the case of TD features presented in Table 8 in Chapter 5.4. MV improved the classification accuracy significantly: The average classification accuracy of all subjects increased 11.3 percentage points (from 76.1 % to 87.4 %). The classification accuracy was increased clearly for each subject. However, there were great differences in the amount of the increase of classification accuracy between individuals. The range of the increase was from 4.6 percentage points to 21.2 percentage points. The increase in classification accuracy was the most significant for the subjects whose unprocessed sEMG signals were poorly classified. For example, for Subject 5 the classification accuracy increased from 57.2 % to 78.4 %. Fig. 40 illustrates the effect of MV on the classification accuracy for Subject 5. The clear improvement in classification accuracy after MV was observed also when using STFT and DWT.

The standard derivations for classification accuracies were high both for the data before and after MV, 18.2 and 14.0 respectively. After applying MV on the data the standard derivation of the total classification accuracy decreased 4.2 percentage points. The detail information of the effect of MV on the classification accuracy can be found in Ap-

pendix 4. This study uses 5 or 6 points in MV decision, depending on the subject. These values give the best classification accuracy with acceptable delay.

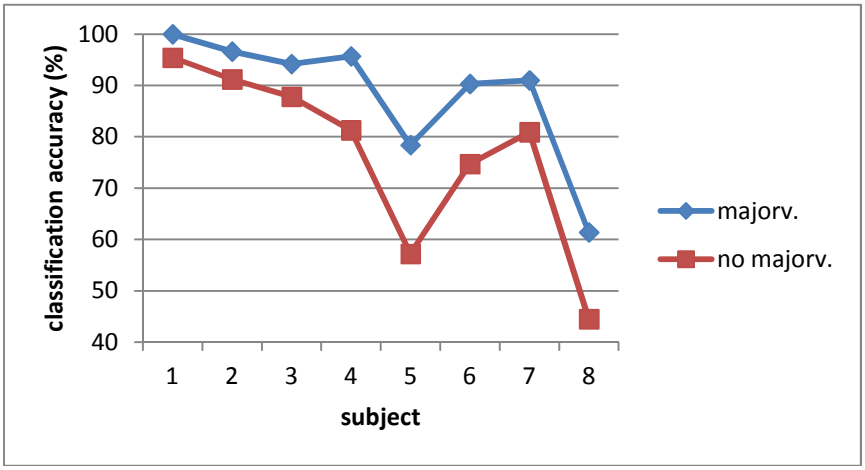

Fig. 39: The effect of majority voting on the classification accuracy using the window length of 40 samples with 50 % overlap, sampling rate of 400 Hz, and the feature vectors presented in Table 8.

The previous studies have also reported on the improvement in the classification accuracy after applying MV on the data [51, 77, 95, 96]. However, the improvement in accuracy in most of the studies has been only at highest two percentage points. This may be because MV is particularly effective for small windows, and most of the previous studies have used the window length of 200 samples or 256 samples, which is much larger than the window length of 40 samples used in this study. Englehart and Hudgins [51] demonstrated the effect of MV on the classification error by using different window lengths between 8 ms (8 samples) and 256 ms (256 samples). For window lengths between 128 ms and 256 ms the increase in classification accuracy was only about one percentage point or less while for the window lengths of 8-64 ms the increase in classification accuracy is much higher, approximately 2-14 percentage points.

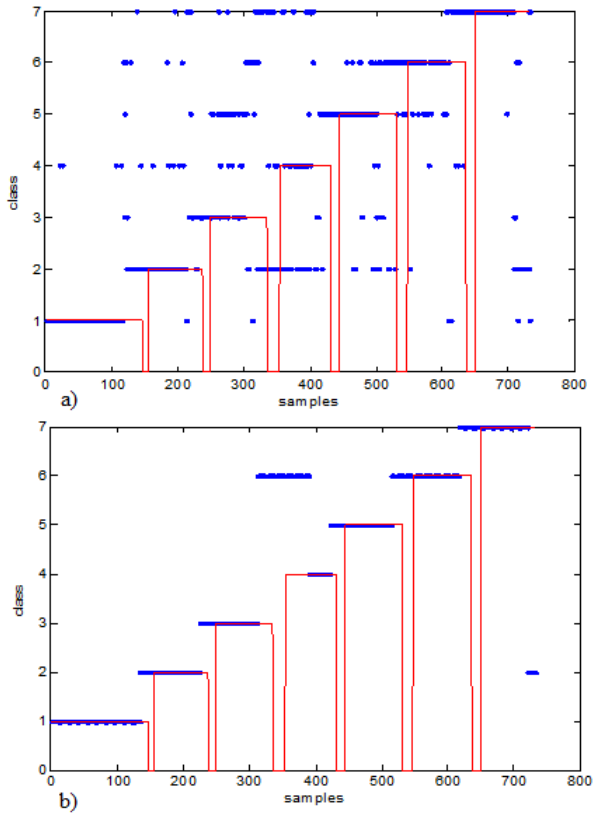

Fig. 40: Output of the continuous LDA classifier for Subject 5 a) without and b) with MV. Output of the classifier is marked with blue, and the actual classes with red. The values for window length and increment are 40 samples and 20 samples, respectively. The number of votes is 5. Clearly, the majority vote processing has eliminated the spurious errors present in the unprocessed decision stream.

MV makes it possible to use the shorter windows without degrading substantially the classification accuracy. Fig. 41 illustrates the rapid degrading of the classification accuracy of the unprocessed data with decreasing analysis window length. If MV averaging is used, this degradation is prevented, due to more decisions available in the shorter windows.

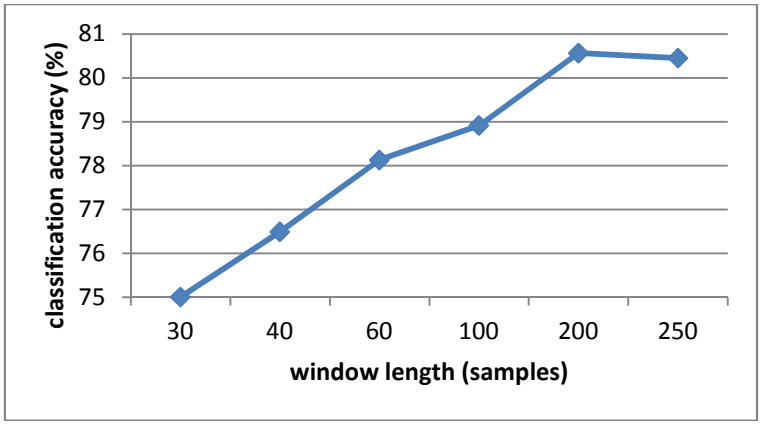

Fig. 41: Effect of analysis window length on the classification accuracy with unprocessed data.

In this study, the window length of 40 samples (100 ms) at 400 Hz sampling rate was found to yield relatively high classification accuracy without compromising the delay

too much. Table 12 compares the theoretical time delay estimates with and without MV. The estimates were calculated by using the equations in Table 4 presented in Chapter 3.6.1.2. By using these values the delay range is also somewhat small. However, it should be noted that because we did not have the real application to use, the processing time in the equations is assumed to be zero.

Table 12: Worst case, best case and average case delays for window lengths of 30, 40 and 60 samples with 50 % overlap. The delays are estimated by using the equations in Table x. The processing time is assumed to be zero.

MV					
win (samp-les)	win (ms)	**worst case delay (ms)**	**average case delay (ms)**	**best case de-lay(ms)**	**delay range (ms)**
30	75	159	131	113	37,5
40	100	200	175	150	50
60	150	300	263	225	75
no MV					
30	75	75	56,3	37,5	37,5
40	100	100	75	50	50
60	150	150	113	150	75

5.9 Further Research

The results achieved in this study indicate that it is possible to classify sEMG signals, measured from able-bodied subjects during they performed seven hand motions, accurately in noise free environment with small subset of TD features. FFT and DWT were also able to classify the sEMG signals accurately, but they did not outperform the classification accuracies achieved by using the simple and computationally efficient TD features. In addition, it was shown that the sampling rate may be significantly reduced from the commonly used 1000 Hz. The optimal size of the feature set seems to be two, and even some individual features yield high classification accuracies. However, many issues and challenges related to prosthetic control need yet to be solved.

This study compares the features only based on classification accuracy. However, in real time applications the computational complexity of the features should also be considered. Previous studies have shown TDS features, and especially simple TD features to be fast to calculate, but the more complicate wavelet transform has dropped dramatically through calculating run time [61]. To ensure the efficient responsibilities, the calculation times of the features should also be investigated, especially in the chase of wavelet transform. The other important property of the feature space that needs further investigation is its sensitivity to noise. The classification accuracies achieved in this study may probably be much lower if noise is present, especially for TD features that are relatively sensitive to noise. Thus, further research is needed to select the feature set that yields high classification accuracy, but is also noise tolerant, and computationally efficient.

Another limitation of this thesis is that, similarly as most investigations of sEMG pattern recognition, this study used subjects with intact limbs instead of those with limb deficiencies. For an amputee several confounding factors introduced by limb deficiency, such as scar tissue, variation in muscle geometry, and possible changes in cortical representation and motor pathways, may affect the classification accuracy. The other issues to consider are the age of operation, the type of amputation and the previous use of myoelectric prosthesis. The examination of previous studies reveals that it is not clear if high classification accuracies achieved for healthy subjects guarantees high classification accuracies for amputees. Castellini et al. [9] investigated the ability of SVM classifier to classify sEMG signals collected from the forearm of three amputees while they performed various grasping postures and forces with their phantom limbs. In agreement with recent neurological studies on cortical plasticity they found that amputees operated decades ago can still produce distinct and stabile signals for each posture and force. The SVM classified the postures up to a precision of 95 % and approximated the force with an error of 7 %. The results were in line with the results Castellini et al. previously obtained by healthy subjects while feed-forward controlling a dexterous hand. Tenore et al [40] showed that it is possible to decode individual flexion and extension movements of each finger with over 90 % accuracy in a transradial amputee. They found no statistically significant difference in decoding accuracy from a transradial amputee and able-bodied subjects. However, some studies have also found the decrease in classification accuracy with amputee subjects. Liu et al. [63] evaluated classification performance of four time-domain features and AR coefficients and their combination in identifying 11 classes of arm and hand movements in both able-bodied subjects and amputees. Their results suggest that the classification accuracy achieved with able-bodied subjects might not apply in amputees: the classification accuracy was about 20 % lower for amputees. In the study of Li et al. [97] five unilateral patients performed 10 wrist and hand motions using both their amputated and intact arms. According to their results, muscles in the residual forearm produce sufficient myoelectric information for real-time wrist control but not for performing multiple hand grasps. Englehart et al. [98] compared the performance of 11 classifiers, including an LDA classifier, with 10 nondisabled subjects and 5 transradial-amputation subjects. They showed that the absolute average performance differs between nondisabled and amputee subjects. The difference in the outcomes between the previous studies indicates that the classification accuracy is depending on the uniqueness of each single stump. This may also challenge the general applicability of the method. As the results from previous studies indicate, the classification accuracies achieved in this thesis may not be directly generalizable to amputees. Probably, the results for amputees may expect to be at least somewhat poorer.

When comparing the performance of 11 classifiers Englehart et al.[98] also made another interesting observation: The relative performance of the classifiers was fairly consistent between amputees and nondisabled population. This result implies an LDA classifier, which is also used in this thesis, is the most suitable for hand movement classification, and may be generalized to amputees. The same result was observed when differ-

ent feature sets are compared: the relative performance of the feature sets is consistent between nondisabled individuals and amputees. According to these results, the features and feature sets that were suggest to yield highest classification accuracy in this thesis would be expected to give the highest classification accuracies also for amputees.

In this study, the sEMG measurements were made with eight channels. However, it has been demonstrated that, using optimal channel subset selection, no significant increase in classification accuracy was achieved by adding more than three channels [6]. Thus, by optimizing the electrode placement, the number of channels may be reduced which makes the computation much faster and improves the responsiveness of the prosthetic.

Major challenges toward clinical robustness include electrode shift, variation in muscle contraction force, and variation in position of limb. Misalignment inevitably occurs during prosthesis donning and doffing, producing a shift in electrode contact locations. The shift may also occur during use because of loading and positioning of the limb. As would be expected, the studies have found electrode shifts perpendicular to muscle fibres to damage the pattern recognition system much more than shifts in a direction perpendicular to the muscle fibers [99, 100]. A shift of 1 cm of four electrodes placed circumferentially about the forearm increases the classification error from roughly 5 % to 20 % if sifted distally and to 40 % if rotated about the forearm. However, the classification accuracy can be improved dramatically by training the classifier with data that represents possible displacements.[99] Increasing the size of the electrode detection surface was also observed to reduce classification accuracy sensitivity to electrode shift [100]. Variability in electrode position may necessitate a daily training session when prosthetic is being donned.

The second issue that may cause problems in practical use is variation in contraction force. Conventional control schemes usually utilize a natural variation in contraction strength by mapping it to velocity or position of a device. Pattern-recognition control, however, aims to identify repeatable patterns of an EMG activity into discernible classes. Thus, contractions performed at different force levels present a challenge to the classifier because they may be very different from one to another. The impact of variation in muscle force has been studied in an experiment where subjects performed nine classes of motion using a contraction force of 20 % to 80 % of the strongest contraction they felt comfortable producing. An LDA classifier was trained and tested using a TD feature set calculated from the data from each force level. The best accuracy was achieved when the classifier was tested and trained at the same force level. When contractions from unseen force levels were added in the test set, the error increased considerably, to the point where the system would be unusable (error of greater than 32 %). As would be expected, the performance further decreased when the classifier was tested only with unseen force levels. To avoid the degradation in performance, exemplars from all force levels should be included in the training set. In this chase the error drops substantially to 17 %, which is not ideal, but approaching a usable system. However, it is not desirable that amputees have to undergo an extensive training session, and therefore

a restricted protocol using only the lowest and highest force levels is investigated. By using this method, the error increased only marginally (to 19 %) from training with all levels. [101]

In this study, the forearm of the subject was resting on the support during the experiment. However, the clinical use of the prosthesis necessitates using the limb in a variety of positions. For transradial and transhumeral amputees, this may impose a loading of the muscles from which sEMG signals are being recorded. As a result, the nature of the sEMG signal may alter due to compression of the muscle, and elicitation of eccentric contraction or mechanical stimulation of the muscle. Different gravitational forces during various positions may also cause electrode shifting. A study by Scheme et al. [102] shows that the EMG classification accuracy is strongly dependent on limb position. EMG data was collected from eight healthy subjects, and processed with TD features and an LDA classifier. As would be expected, the average interposition error was considerably worse than the average intraposition error, 35 % and 6.9 %, respectively. By training the classifier with exemplars from each position, an average error was decreased to 7.4 %. Thus, it may be insufficient to train a classifier with a data collected in a single position and expect it to translate well in multi position-use. The degradation due to variety in limb positions may contribute to the differences seen between the classification accuracies achieved in this thesis and observed clinical performance.

Although, lot of effort in the past has been carried out to make the upper-limb prosthetic devices near to the human hand there is still a huge gap to achieve the target. With its 24 DOFs, 38 muscles, and thousands of sensory organs, the human hand is mechanically incredibly complex. The challenge is to make a prosthesis that is light, but has also many DOFs. Furthermore, with added complexity comes added cost and lower durability. A recent Internet survey of myoelectric prosthetic users concluded that 79 % considered their device to be too heavy. Reducing the number of actuators is one of the basic objectives in the design of prosthetic device [103, 104].

6 Conclusion

The loss of an upper limb is a life-altering accident which makes the everyday life more difficult. A psychological adaption to the new situation is a long and difficult process. Thus, it is easy to see the great need for a low-cost and functional prosthetic arm for these people. However, many amputees do not use their prosthetic hand regularly due to its low functionality, poor cosmetic and unnatural appearance, lack of sensory feedback, and low controllability. This situation calls for the development of versatile prosthetic limbs that will allow amputees to perform tasks that are necessary for activities of daily living.

The non-pattern based control scheme of commercial state-of art prosthesis is rather poor, using one or two electrodes to choose among predefined hand postures. A promising alternative to the conventional control method is the pattern-recognition-based control that identifies different intended hand postures of the prosthesis by utilizing the information of the EMG signals. Thus, the control of the prosthesis becomes natural and easy.

Feature selection is the most important step in the control of the prosthesis because its effect on the classification accuracy is even greater than the effect of the type of the classifier. Most of the previous studies have compared only few combinations of features, or if the larger number of features is compared, the performance of them has been evaluated independently with statistical criteria (for example Mahalonobius distance, Battacharia distance and maximum entropy). However, the feature vector consisting of the best features evaluated separately may not provide the highest classification accuracy since it does not account for the feature dependence. The optimal feature depends also the type of the classifier.

The objective of this thesis was to find the features that yield the highest classification accuracy in the context of the LDA classifier, the most suitable classifier for hand posture classification. The following features were studied: 16 TD features, two TSD features, FFT and DWT. These features were selected to comparison because they have shown to be successful in the hand motion classification in previous studies.

The second objective of this thesis was to investigate whether it is possible to use lower sampling rate than 1 kHz that is commonly used in EMG analysis. The lower sampling rate is desired because it saves the processing time as well as the memory of the controller of the prosthesis. Thus, the time delays of the prosthesis become shorter and the prosthetic device becomes lighter. A preprocessing technique, ICA, was also shortly examined.

sEMG signals were measured with eight channels on the skin surface of the forearm of eight able-bodied subjects during they performed seven hand postures. Bipolar measurements were estimated from the unipolar recordings. PCA was used to reduce the dimensionality of the FFT vectors. The data was postprocessed by MV. The classification was based on the steady state signal. The signal processing, features, and classification were implemented with Matlab.

The results of this study suggest the optimal feature set to be depending on the subject. However, some features, such as RMS, VAR, and WAMP, yielded the high classification accuracy more often than the others. A good method to select an optimal feature set would be to select the features individually from the small number of features of which each describes a different property of the signal and have usually yield the high classification accuracy. The optimal size of feature set turned out to be small: two features or even one feature seems to be enough for reliable classification. The classification accuracy achieved by using FFT and DWT was also high. However, in least in noise free environment, they did not outperform the computationally more efficient TD features.

The effect of sampling rates of the range between 300-2000 Hz was investigated. The sampling rate of 400 Hz seemed to be the most optimal in hand posture classification. Perhaps surprisingly, the classification accuracy even slightly improved when the sampling frequency was decreased from the commonly used 1000 Hz to 400 Hz.

The ICA did not improve the classification accuracy in this study. This may be because the channels were placed somewhat far from each other, and therefore the correlations between them were small. MV improved the classification accuracy dramatically. This corroborates the previous studies that have reported a significant increase in classification accuracy after applying MV on the data.

However, many issues and challenges related to prosthetic control remains still unsolved. The limitation of this study is that the features have been compared only based on classification accuracy. Because low response times and are important in upper-limb prostheses, the computational complexity of the features should also be considered. In this study we have calculated theoretical estimates for time delays. However, these estimates are overoptimistic, because they assume the controller delay to be zero. We did not have a real application to use, and therefore we could not estimate the true processing delay. A tolerance for noise is another property of the feature space that needs yet to be investigated. It should be studied especially in the case of TD features that are relatively sensitive to noise. Thus, further research is needed to select the feature set that yields high classification accuracy, but is also noise tolerant, and computationally efficient.

Another limitation of this study is that subjects with intact limbs have been used instead of those with limb deficiencies. The results from the previous studies indicate, that the

classification accuracies achieved in this thesis may not be straightforward generalized to amputees, but, the results for amputees may expect to be at least somewhat poorer. However, the relative performance of the feature sets has been shown to be consistent between nondisabled individuals and amputees. Thus, it would be expected that the features that have yield the best results in this study would yield the highest classification accuracy also for amputees.

Major unsolved problems toward clinical robustness include electrode shift, variation in muscle contraction force, and variation in position of limb. The optimal number of measurement channels needs also further investigation. In addition, the human hand is mechanically incredibly complex, and making a prosthetic device that is light, but has also many DOFs is a very challenging issue.

7 References

1. MACKENZIE, E., J. Limb Amputation and Limb Deficiency: Epidemiology and Recent Trends in the United States. *Southern Medical Journal*, 2002, vol. 1.

2. ZIEGLER-GRAHAM, Kathryn, et al. Estimating the Prevalence of Limb Loss in the United States: 2005 to 2050. *Arch Phys Med Rehabil*, 2008, vol. 89. pp. 422-429.

3. MICERA, S. Control of Hand Prostheses using Peripheral Information. *Biomedical Engineering, IEEE Reviews in*, 2010. pp. 48. ISSN 1937-3333.

4. DAVIDSON, J. A Survey of the Satisfaction of Upper Limb Amputees with their Prostheses, their Lifestyles, and their Abilities. *Journal of Hand Therapy*, 2002, vol. 15, no. 1. pp. 62-70.

5. HERLE, S.; and MAN, S. Processing Surface Electromyographical Signals for Myoelectric Control. Technical University of Cluj Napoca. Romania.

6. FARRELL, T. R.; and WEIR, R. F. Pilot Comparison of Surface Vs. Implanted EMG for Multifunctional Prosthesis Control. *Proceedings of the 2005 IEEE 9th International Conference on Rehabilitation Robotics*, 2005, vol. 2005. pp. 277-280. ISSN 9780780390034.

7. HARGROVE, Levi J. A Comparison of Surface and Intramuscular Myoelectric Signal Classification. *Masters Abstracts International*, 2005, vol. 46, no. 4.

8. LI, G. Advances in Applied Electromyography. MIZRAHI, Joseph ed., InTech, 2011. *Electromyography Pattern-Recognition-Based Control of Powered Multifunctional Upper-Limb Prostheses*, pp. 99-116. ISBN 978-953-307-382-8,.

9. CASTELLINI, C., et al. Fine Detection of Grasp Force and Posture by Amputees Via Surface Electromyography. 2009.

10. CONNOLLY, C. Prosthetic Hands from Touch Bionics. Industrial Robot: An International Journal. 35/4, 2008. S. 290–293. ISSN 0143-991X. DOI 10.1108/01439910810876364.

11. . Bebionic's Webside: Http://www.Bebionic.Com/. Referred 6.4.2011.

12. BUTTERFASS, J. DLR-Hand II: Next Generation of a Dextrous Robot Hand. *Robotics and Automation, 2001.Proceedings 2001 ICRA.IEEE International Conference on*, 2001. pp. 109. ISSN 0-7803-6576-3; 1050-4729.

13. ORABONA, F. Model Adaptation with Least-Squares SVM for Adaptive Hand Prosthetics. *Robotics and Automation, 2009.ICRA '09.IEEE International Conference on*, 2009. pp. 2897. ISSN 978-1-4244-2788-8; 1050-4729.

14. Ottobock. *SensorHand Speed – Grasping Quickly and with Precision. Referred: 1.7.2012.* , 2012Available from:<http://www.ottobock.com/cps/rde/xchg/ob_com_en/hs.xsl/3652.html>.

15. ZHENG, J., Z.; ROSA, S., D.and DOLLAR, A., M. *An Investigation of Grasp Type and Frequency in Daily Household and Machine Shop Tasks.* Shanghai, China ed. IEEE International Conference on Robotics and Automation: , May 9-1, 2011. ISBN 978-1-61284-380-3/11/$26.00.

16. *The Shadow Robot Company Ltd. Shadow Dexterous Motor Hand. Avaliable:Http://www.Shadowrobot.com/hand/motorhand.Shtml. Referred 15.6.2012.*

.

17. BELTER, J., T.; and DOLLAR, A., M. *Performance Characteristics of Anthropomorphic Prosthetic Hands.* Switzerland ed. IEEE International Conference on Rehabilitation Robotics, June 29 - July 1, 2011. ISBN 978-1-4244-9861-1/11/$26.00.

18. Myo Electric Upper Extremity from Centri and Motion Control. Referred 16.8.2011. Avaliable: Http://www.Centri.se/pdf/catalogmyohands.Pdf.

19. OTTOBOCK. User's Guide. DMC Plus® - System Electric Hand Instructions for use. Avaliable: Http://www.Ottobockus.com/cps/rde/xchg/ob_us_en/hs.xsl/6955.Html?id=teaser2#teaser2. Referred 2.4.2012.

20. TOUCHBIONICS. I-LIMB Ultra. Avaliable:Http://www.Touchbionics.com/products/active-prostheses/i-Limb-Ultra/. Referred: 1.3.2012.

21. TORTORA, Gerard J. *Principles of Anatomy and Physiology. Organization, Support and Movement, and Control Systems of the Human Body 1.* . DERRICKSON, Bryan ed., New York: Wiley, 2008. ISBN 978-0-470-39495-3.

22. KONRAD, P. The ABC of EMG. A Practical Introduction to Kinesiological Electromyography. Version 1.0, 2005.Noraxon INC. USA.

23. ELLIOT, R., B. Feature Extraction Techniques for Grasp Classification. Master Thesis. University of Canterbury. 1998.

24. MERLO, A. A Fast and Reliable Technique for Muscle Activity Detection from Surface EMG Signals, 2003, vol. 50, no. 3. pp. 316-323. ISSN 0018-9294.

25. HAYES, M., H. *Statistical Digital Signal Processing and Modeling. s.82.* John Wiley & Sons, Inc., 1996. ISBN 0-471 59431-8.

26. OSKOEI, M., A.; and HU, H. Myoelectric Control Systems - A Survey. Biomedical Signal Processing and Control 2. 2007. s. 275-294.

27. CLANCY, E. A. Theoretic and Experimental Comparison of Root-Mean-Square and Mean-Absolute-Value Electromyogram Amplitude Detectors. *Engineering in Medicine and Biology Society, 1997.Proceedings of the 19th Annual International Conference of the IEEE,* 1997. pp. 1267. ISSN 0-7803-4262-3; 1094-687X.

28. PEUSCHER, J. H. J. The Measurement of EMG. A Practical Example. TMS-International. Viitattu 3.8.2011. Saatavissa: Http://www.Tmsi.Com/?id=26.

29. Basics of Surface Electromyography. Applied to Psychophysiology. 2008. Thought Technology Ltd.

30. DAS, K.; OSECHINSKIY, S.and NENADIC, Z. A Classwise PCA-Based Recognition of Neural Data for Brain-Computer Interfaces. Proceedings of the 29th Annual International Conference of the IEEE EMBS. Cité Internationale, Lyon, France. , 2007.

31. AL-TIMEMY, A., H., et al. *Reduction in Classification Errors for Myoelectric Control of Hand Movements with Independent Component Analysis.* The 5th International Conference on Information Technology: , 2011.

32. MERLETTI, Roberto. Technology and Instrumentation for Detection and Conditioning of the Surface Electromyographic Signal: State of the Art. *Clinical Biomechanics,* 2009, vol. 24, no. 2. pp. 122-134. ISSN 02680033.

33. ANDREWS, Alex; MORIN, Evleynand MCLEAN, Linda. Optimal Electrode Configurations for Finger Movement Classification using EMG. 31st Annual International Conference of the IEEE EMBS Minneapolis, Minnesota, USA, September 2-6, Pp. 2987-2990, 2009.

34. DE LUCA, C. J. The use of Surface Electromyography in Biomechanics. *Journal of Applied Biomechanics*, 1997, vol. 13, no. 2. pp. 135-163. ISSN 10658483.

35. SCOTT, H., et al. Optimization of Electrode Placement in Electromyographic
Control of Dielectric Elastomers. Electroactive Polymer Actuators and Devices (EAPAD) 2009, Edited by Yoseph Bar-Cohen, Thomas Wallmersperger, Proc. of SPIE Vol. 7287, 728724 · © 2009 SPIE · CCC Code: 0277-786X/09/$18 · Doi: 10.1117/12.815833.

36. WALBRAN, S. H., et al. A Technique for Optimizing Electrode Placement for Electromyographic Control of Prostheses. *Proceedings of the 31st Annual International Conference of the IEEE Engineering in Medicine and Biology Society: Engineering the Future of Biomedicine, EMBC 2009*, 2009. pp. 1331-1334. ISSN 9781424432967.

37. ANDREWS, Alexander James. Finger Movement Classification using Forearm EMG Signals. *ProQuest Dissertations and Theses*, 2005. ISSN 9780494462157.

38. TSENOV, G. Neural Networks for Online Classification of Hand and Finger Movements using Surface EMG Signals. *Neural Network Applications in Electrical Engineering, 2006.NEUREL 2006.8th Seminar on*, 2006. pp. 167. ISSN 1-4244-0433-9.

39. UCHIDA, Noriyoshi. EMG Pattern Recognition by Neural Networks for Multi Fingers Control. *Engineering in Medicine and Biology Society, 1992 14th Annual International Conference of the IEEE*, 1992. pp. 1016. ISSN 0-7803-0785-2.

40. TENORE, F. Towards the Control of Individual Fingers of a Prosthetic Hand using Surface EMG Signals. *Engineering in Medicine and Biology Society, 2007.EMBS 2007.29th Annual International Conference of the IEEE*, 2007. pp. 6145. ISSN 978-1-4244-0787-3; 1557-170X.

41. TOUCHBIONICS. Biosim-Pro. Users Manual. Avaliable:
Http://www.Touchbionics.com/media/48363/biosim-pro_manual_.Pdf .

42. TENORE, F. V. G. Decoding of Individuated Finger Movements using Surface Electromyography, 2009, vol. 56, no. 5. pp. 1427-1434. ISSN 0018-9294.

43. LI, Guanglin. Conditioning and Sampling Issues of EMG Signals in Motion Recognition of Multifunctional Myoelectric Prostheses. *Annals of Biomedical Engineering, 2011, Vol.39(6), Pp.1779-87*, 2011, vol. 39, no. 6. pp. 1779-87. ISSN 15216047.

44. CLANCYA, E., A.; MORINB, E., L.and MERLETTIC, R. Sampling, Noise-Reduction and Amplitudeestimationissues in Surfaceelectromyography. *Journal of Electromyography and Kinesiology*, 2002, vol. 12, no. 1. pp. 1-16.

45. HYVÄRINEN, Aapo; and OJA, Erkki. *Independent Component Analysis: A Tutorial.* Helsinki University of Technology. Laboratory of Computer and Information Science. Espoo, Finland. 19.4.2000, 2000Available from:
<http://cis.legacy.ics.tkk.fi/aapo/papers/IJCNN99_tutorialweb/IJCNN99_tutorial3.html>.

46. GANESH, R., Naik. A Comparison of ICA Algorithms in Surface EMG Signal Processing. *International Journal of Biomedical Engineering and Technology*, 2011, vol. 6, no. 7. pp. 363-374. doi:10.1504/IJBET.2011.041774.

47. HARGROVE, Levi J., et al. Principal Components Analysis Preprocessing for Improved Classification Accuracies in Pattern-Recognition-Based Myoelectric Control. IEEE TRANSACTIONS ON BIOMEDICAL ENGINEERING, 2009, vol. 56, no. 5.

48. DAS, K.; and NENADIC, Z. An Efficient Discriminant-Based Solution for Small Sample Size Problem. *Pattern Recognition*, 2008, vol. 42. pp. 857-866.

49. HARGROVE, L., et al. *Principal Component Analysis Preprocessing to Reduce Controller Delays in Pattern Recognition Based Myoelectric Control.* Cité Internationale, Lyon, France.: , August 23-26, 2007.

50. ENGLEHART, K. A Robust, Real-Time Control Scheme for Multifunction Myoelectric Control, 2003, vol. 50, no. 7. pp. 848-854. ISSN 0018-9294.

51. ENGLEHART, K. A Robust, Real-Time Control Scheme for Multifunction Myoelectric Control, 2003, vol. 50, no. 7. pp. 848-854. ISSN 0018-9294.

52. HERLE, S. Classification of Surface Electromyographic Signals for Control of Upper Limb Virtual Prosthesis using Time-Domain Features. *Automation, Quality and Testing, Robotics, 2008.AQTR 2008.IEEE International Conference on*, 2008. pp. 160. ISSN 978-1-4244-2576-1.

53. CHILDRESS, D., S.; and WEIR, R. F. Atlas of Amputations and Limb Deficiencies: Surgical, Prosthetic, and Rehabilitation
Principles. D. G. Smith, J. W. Michael, and B. J. H. , Eds.3rd ed. , 2004. *Control of Limb Prostheses*, pp. 173-195.

54. OSKOEI, M., A.; and HU, H. Support Vector Machine-Based Classification Scheme for Myoelectric Control Applied to Upper Limb. IEEE TRANSACTIONS ON BIOMEDICAL ENGINEERING, VOL. 55, NO. 8, AUGUST 2008.

55. FARRELL, T. R. Determining Delay Created by Multifunctional Prosthesis Controllers. *J Rehabil Res Dev.*, 2011, vol. 48, no. 6. pp. xxi-xxxviii. ISSN doi: 10.1682/JRRD.2011.03.0055.

56. PHINYOMARK, Angkoon. Feature Reduction and Selection for EMG Signal Classification. *Expert Systems with Applications*, 2012, vol. 39, no. 8. pp. 7420-7420. ISSN 0957-4174.

57. SARIDIS, G. N. EMG Pattern Analysis and Classification for a Prosthetic Arm. *IEEE Transactions on Biomedical Engineering*, 1982, vol. BME-29, no. 6. pp. 403-412. ISSN 0018-9294.

58. TKACH, D.; HUANG, H.and KUIKEN, T., A. Study of Stability of Time-Domain Features for Electromyographic Pattern Recognition. Journal of NeuroEngineering and Rehabilitation 2010, 7:21.

59. KIM, K., S., et al. Comparison of k-Nearest Neighbor, Quadratic Discriminant and Linear Discriminant Analysis in Classification of Electromyogram Signals Based on the Wrist-Motion Directions. *Current Applied Physics*, 2010, vol. 11(3). pp. 740-745. ISSN doi:10.1016/j.cap.2010.11.051.

60. PHINYOMARK, A., et al. Evaluation of EMG Feature Extraction for Hand Movement Recognition Based on Euclidean Distance and Standard Deviation. *ECTI-CON 2010 - the 2010 ECTI International Conference on Electrical Engineering/Electronics, Computer, Telecommunications and Information Technology*, 2010. pp. 856-860. ISSN 9789746724913.

61. BOOSTANI, R.; and MORADI, M. H. Evaluation of the Forearm EMG Signal Features for the Control of a Prosthetic Hand. *Physiological Measurement*, 2003, vol. 24, no. 2. pp. 309-319. ISSN 09673334.

62. KARLIK, B. A Fuzzy Clustering Neural Network Architecture for Multifunction Upper-Limb Prosthesis. *Biomedical Engineering, IEEE Transactions on*, 2003. pp. 1255. ISSN 0018-9294.

63. LIU, Xin. Performance of various EMG Features in Identifying ARM Movements for Control of Multifunctional Prostheses. *Information, Computing and Telecommunication, 2009.YC-ICT '09.IEEE Youth Conference on*, 2009. pp. 287. ISSN 978-1-4244-5074-9.

64. HAN, J.,S., et al. *New EMG Pattern Recognition Based on Soft Computing Techniques and its Application to Control a Rehabilitation Robotic Arm. Proceedings of 6th International Conference on Soft Computing.* , 2000.

65. OSKOEI, M., A.; and HU, H. *GA-Based Feature Subset Selection for Myoelectric Classification. International Conference on Robotics and Biomimetics.* Kuming, China ed. , 2006.

66. LYONS, G., R. *Understanding Digital Signal Processing.* 2nd ed. Prentice Hall, 2004. ISBN 0-13-108989-7.

67. GOYAL, P. Generation of 1D and 2D FFT Function in MATLAB. *International Journal of Science, Technology & Management*, 2010.

68. MERRY, R. J. E. *Wavelet Theory and Applications, A Literature Study.* Eindhoven University of Technology. Department of Mechanical Engineering, 2005.

69. MISITI, M., et al. Wavelet Toolbox: Getting Started Guide. *MathWorks*, 2012.

70. DU, Yi-Chun. Portable Hand Motion Classifier for Multi-Channel Surface Electromyography Recognition using Grey Relational Analysis. *Expert Systems with Applications*, 2010, vol. 37, no. 6. pp. 4283-4283. ISSN 0957-4174.

71. HUANG, Yonghong. A Gaussian Mixture Model Based Classification Scheme for Myoelectric Control of Powered Upper Limb Prostheses. *Biomedical Engineering, IEEE Transactions on*, 2005. pp. 1801. ISSN 0018-9294.

72. CHU, J-U; MOON, I.and MUN, M. S. A Real-Time EMG Pattern Recognition System Based on Linear-Nonlinear Feature Projection for a Multifunction Myoelectric Hand. *IEEE TRANSACTIONS ON BIOMEDICAL ENGINEERING*, 2006, vol. 53, no. 11. pp. 2232-2239. ISSN doi:10.1109/TBME.2006.883695.

73. KARLSSON, S.; and AKAY, J. Enhancement of Spectral Analysis of Myoelectric Signals during Static Contractions using Wavelet Methods. *Trans. Biomed. Eng.*, 1999, vol. 46, no. 6. pp. 670-684.

74. THEODORIDIS, Sergios; and KOUTROUMBAS, Konstantinos. Pattern recognition2nd ed. Elsevier Academic Press, 2003. *5.2.2 Data Normalization*, pp. 165.

75. ENGLEHART, K. Classification of the Myoelectric Signal using Time-Frequency Based Representations. *Medical Engineering & Physics*, 1999, vol. 21, no. 6-7. pp. 431-438. ISSN 13504533.

76. PHINYOMARK, A.; LIMSAKUL, C.and PHUKPATTARANONT, P. Application of Wavelet Analysis in EMG Feature Extraction for Pattern Classification. *MEASUREMENT SCIENCE REVIEW*, 2011, vol. 11, no. 2. ISSN 10.2478/v10048-011-0009-y.

77. ENGLEHART, K.; HUDGINS, B.and CHAN, A. Continuous Multifunction Myoelectric Control using Pattern Recognition. *Technology and Disability*, 2003. pp. 95-103. ISSN 1055-4181/03.

78. AHA, D., W.; and BANKERT, R., L. Learning from Data: Artificial Intelligence and Statistics V (Lecture Notes in Statistics) . FISHER, D.; and LENZ, H-J eds., 1st ed. Springer, 1996. *A Comparative Evaluation of Sequential Feature Selection Algorithms.* ISBN 978-0387947365.

79. HUDGINS, B. A New Strategy for Multifunction Myoelectric Control. *IEEE Transactions on Biomedical Engineering*, 1993, vol. 40, no. 1. pp. 82-94. ISSN 0018-9294.

80. AJIBOYE, A. B. A Heuristic Fuzzy Logic Approach to EMG Pattern Recognition for Multifunctional Prosthesis Control. *IEEE Transactions on Neural Systems and Rehabilitation Engineering*, 2005, vol. 13, no. 3. pp. 280-291. ISSN 1534-4320.

81. SCHEME, E., J.; ENGLEHART, K., B.and HUDGINS, B., S. Selective Classification for Improved Robustness of Myoelectric Control Under Nonideal Conditions. *Transactions on Biomedical Engineering*, 2011, vol. 58, no. 6. pp. 1698-1705. doi:10.1109/TBME.2011.2113182.

82. LI, T. Using Discriminant Analysis for Multi-Class Classification. *Data Mining, 2003.ICDM 2003.Third IEEE International Conference on*, 2003. pp. 589. ISSN 0-7695-1978-4.

83. EVANS, Harry B. Signal Processing for Proportional Myoelectric Control. *Biomedical Engineering, IEEE Transactions on*, 1984, vol. -31. pp. 207. ISSN 0018-9294.

84. PEERDEMAN, B. A Biomechanical Model for the Development of Myoelectric Hand Prosthesis Control Systems. *Engineering in Medicine and Biology Society (EMBC), 2010 Annual International Conference of the IEEE*, 2010. pp. 519. ISSN 978-1-4244-4123-5; 1557-170X.

85. WITTEN, I., H.; FRANK, E.and HALL, M., A. *Data Mining: Practical Machine Learning Tools and Techniques.* 3rd ed. ELSEVIER, 2011.

86. BIOSEMI. ActiveTwo User Manual, 2004. Version: 2.4.

87. . BioSemi Webbage: Http://www.Biosemi.com/index.Htm. Referred: 6.6.2011.

88. SENIAM. Avaliable: Http://www.Seniam.Org/ [12.6.2011].

89. FUKUNAGA, K. Introduction to Statistical Pattern Recognition.2nd ed. Academic Press, 1990. *Backward and Forward Selections.*, pp. 490-491. ISSN 0-12-269851-7.

90. LI, Guanglin. Selection of Sampling Rate for EMG Pattern Recognition Based Prosthesis Control. *Engineering in Medicine and Biology Society (EMBC), 2010 Annual International Conference of the IEEE*, 2010. pp. 5058. ISSN 978-1-4244-4123-5; 1557-170X.

91. SUEASEENAK, D. An Investigation of Robustness in Independent Component Analysis EMG. *Electrical Engineering/Electronics, Computer, Telecommunications and Information Technology, 2009.ECTI-CON 2009.6th International Conference on*, 2009. pp. 1102. ISSN 978-1-4244-3387-2.

92. RAFIEE, J., et al. Biorobotics: Optimized Biosignal Classification using Mother Wavelet Matrix., 2009. ISSN 978-1-4244-4364-2/09/$25.00.

93. PHINYOMARK, A.; LIMSAKUL, C.and PHUKPATTARANONT, P. *Optimal Wavelet Functions in Wavelet Denoising for Multifunction Myoelectric Control.* Japan ed. ECTI Transactions on Electrical Eng., Electronics, and Communications, Vol. 8, No. 1 , 2010.

94. PHINYOMARK, A., et al. Feature Extraction and Reduction of Wavelet Transform Coefficients for EMG Pattern Classification. *ELECTRONICS AND ELECTRICAL ENGINEERING*, 2012, no. 6.

95. CHAN, Adrian D. C. Continuous Myoelectric Control for Powered Prostheses using Hidden Markov Models. *IEEE Transactions on Biomedical Engineering*, 2005, vol. 52, no. 1. pp. 121-124. ISSN 00189294.

96. OSKOEI, M. A. Support Vector Machine-Based Classification Scheme for Myoelectric Control Applied to Upper Limb. *IEEE Transactions on Biomedical Engineering*, 2008, vol. 55, no. 8. ISSN 0018-9294.

97. LI, G.; SCHULTZ, A., E.and KUIKEN, T., A. Surface Electromyography: Use, Design & Technological Overview Quantifying Pattern Recognition—Based Myoelectric Control of Multifunctional Transradial Prostheses. IEEE Trans Neural Syst Rehabil Eng. 2010 April ; 18(2): 185–192. Doi:10.1109/TNSRE.2009.2039619.

98. SCHEME, E.; ENGLEHART, K.and HUDGINS, B. *A One-Versus-One Classifier for Improved Robustness of Myoelectric Control.* Aalborg, Denmark. ed. The 18th Congress of the International Society of Electrophysiology and Kinesiology: , 2010.

99. HARGROVE, L. The Effect of Electrode Displacements on Pattern Recognition Based Myoelectric Control. *Engineering in Medicine and Biology Society, 2006.EMBS '06.28th Annual International Conference of the IEEE*, 2006. pp. 2203. ISSN 1-4244-0032-5; 1557-170X.

100. YOUNG, A. J. The Effects of Electrode Size and Orientation on the Sensitivity of Myoelectric Pattern Recognition Systems to Electrode Shift. *Biomedical Engineering, IEEE Transactions on*, 2011. pp. 2537. ISSN 0018-9294.

101. SCHEME, E.; and ENGLEHART, K. Electromyogram Pattern Recognition for Control of Powered Upper-Limb Prostheses: State of the Art and Challenges for Clinical use. *Journal of Rehabilitation Research & Development*, 2011, vol. 48, no. 6. pp. 643-660. DOI:10.1682/JRRD.2010.09.0177.

102. SCHEME, E. Examining the Adverse Effects of Limb Position on Pattern Recognition Based Myoelectric Control. *Engineering in Medicine and Biology Society (EMBC), 2010 Annual International Conference of the IEEE*, 2010. pp. 6337. ISSN 978-1-4244-4123-5; 1557-170X.

103. MARIAPPAN, M.,; Jan, Sh.,M., M.and IFTIKHAR, M. A Novel Approach for Classification of Underactuated Mechanism in Myoelectric Hand. *American Journal of Biomedical Engineering*, 2011, vol. 1, no. 1. pp. 35-40. doi:10.5923/j.ajbe.20110101.06.

104. CLAWSON, K., A.; and JONES, B. The use of Underactuation in Prosthetic Grasping. *Mechanical Sciences*, 2011, vol. 2. pp. 27-32. doi:10.5194/ms-2-27-2011.

Appendix 1: Effect of the free parameters to the classification accuracy

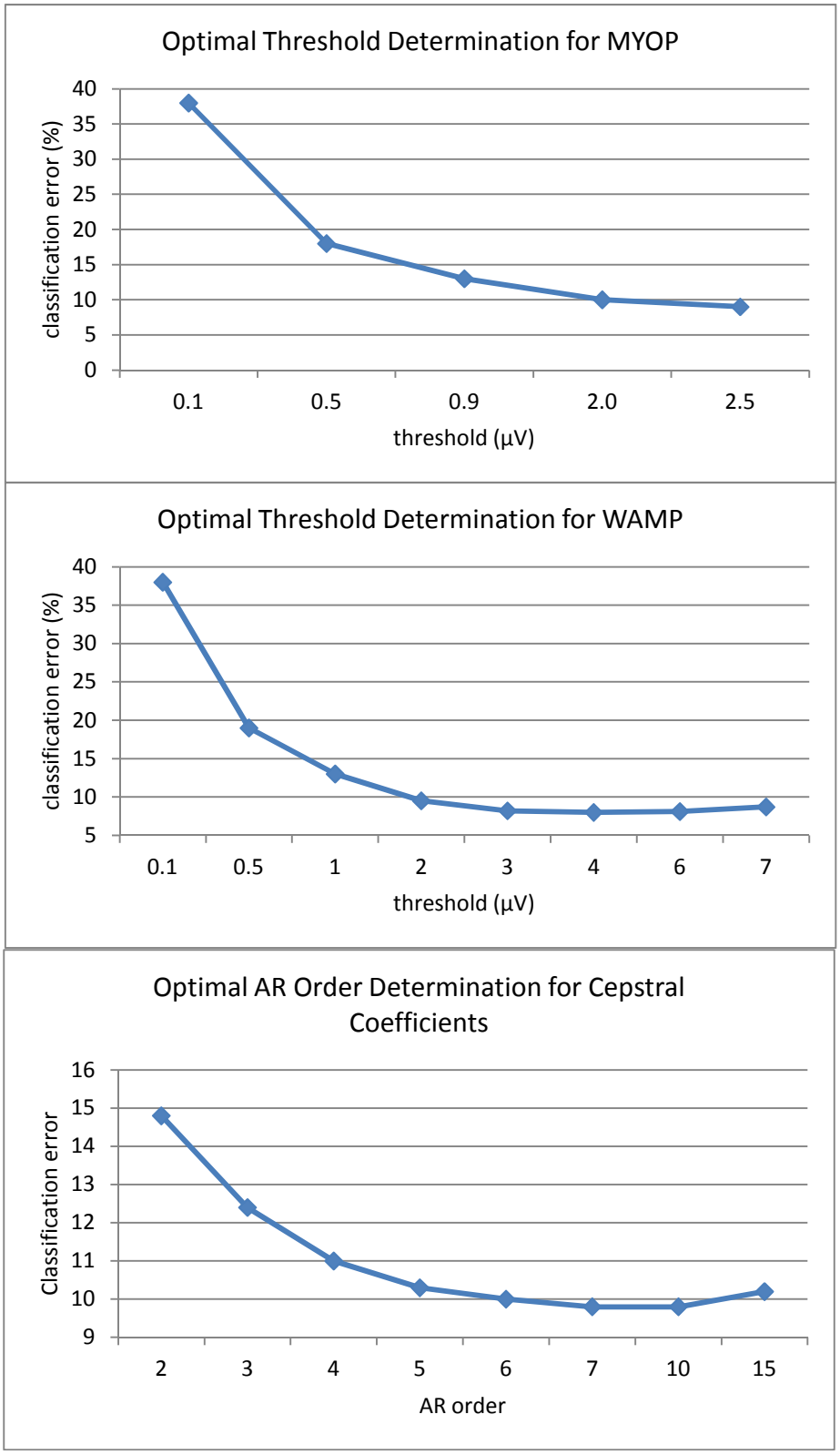

Appendix 2: Power spectra for Subject 2 of seven hand movements

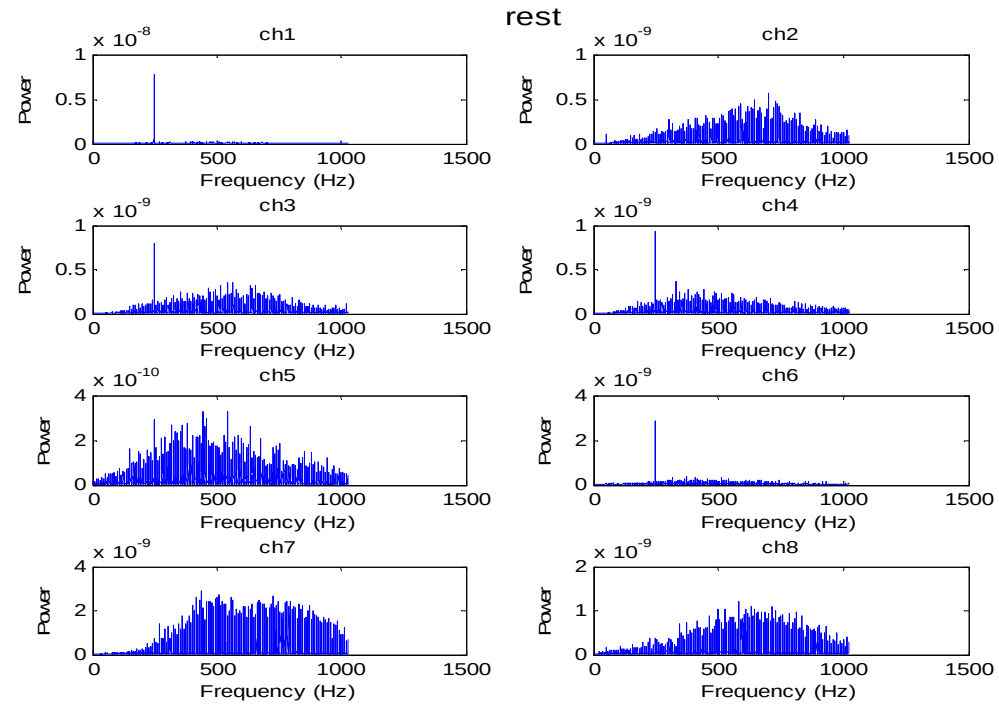

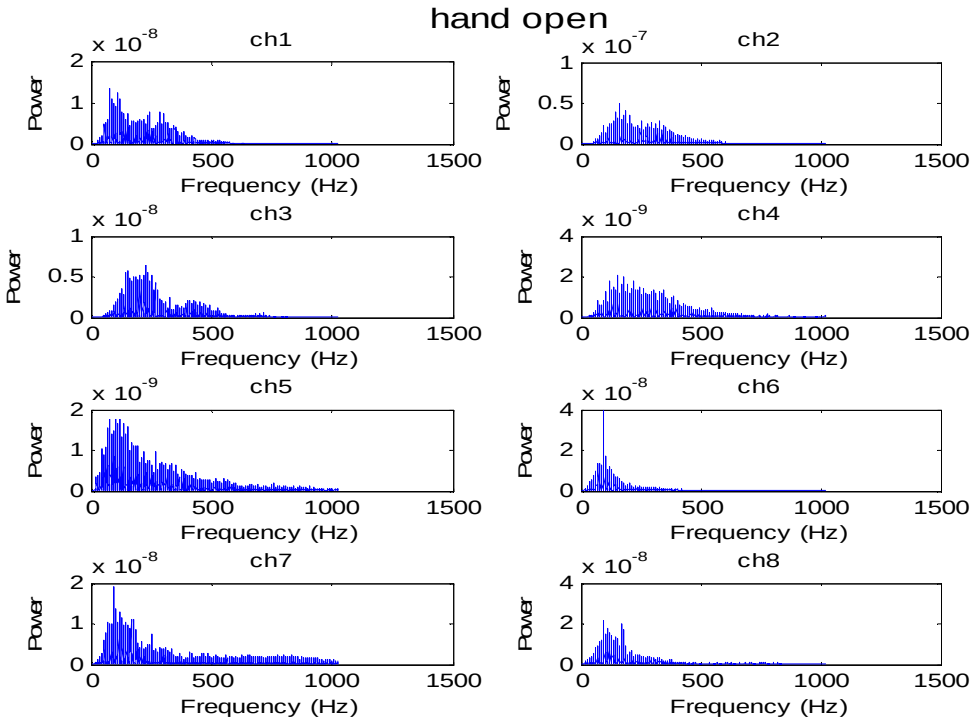

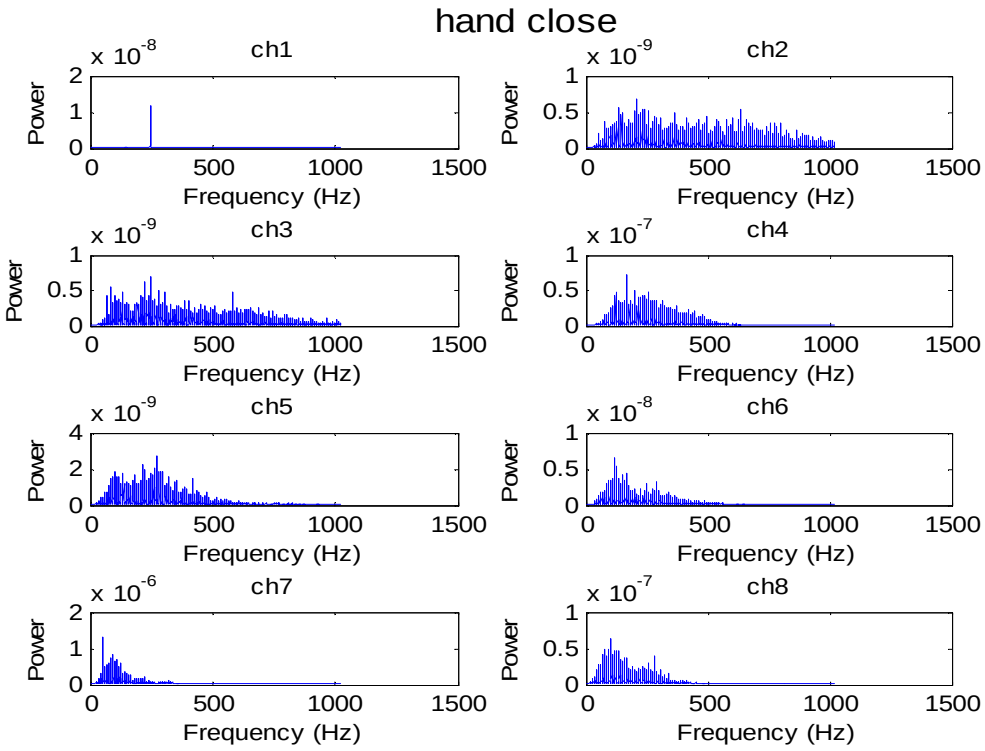
hand close
ch1
ch2
ch3
ch4
ch5
ch6
ch7
ch8
Power
Frequency (Hz)

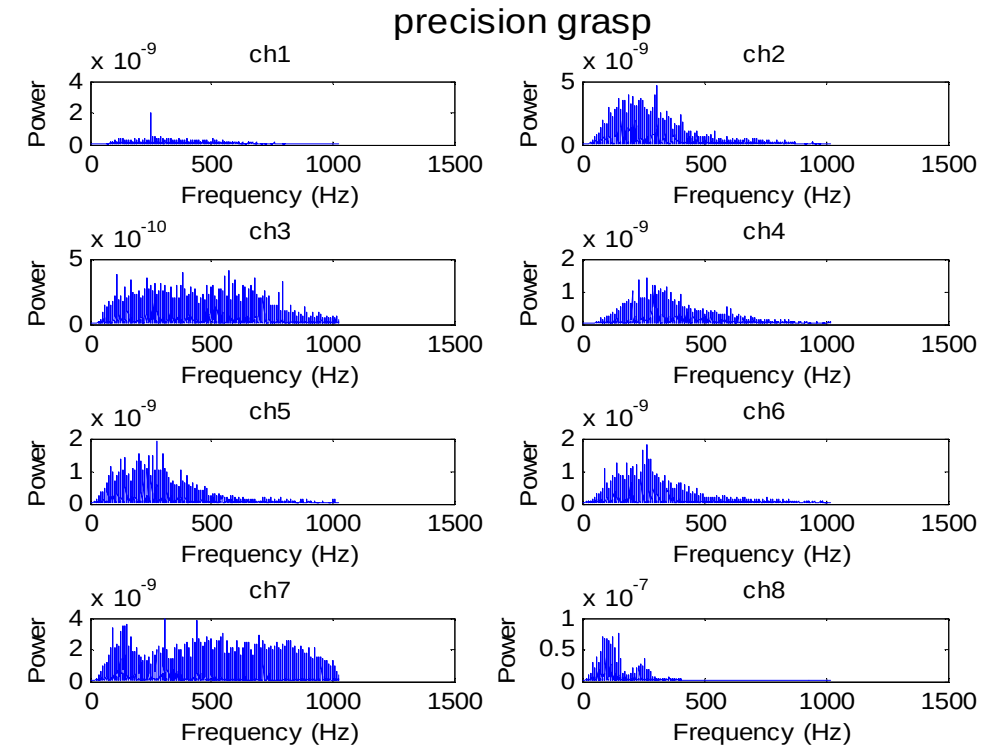
precision grasp
ch1
ch2
ch3
ch4
ch5
ch6
ch7
ch8
Power
Frequency (Hz)

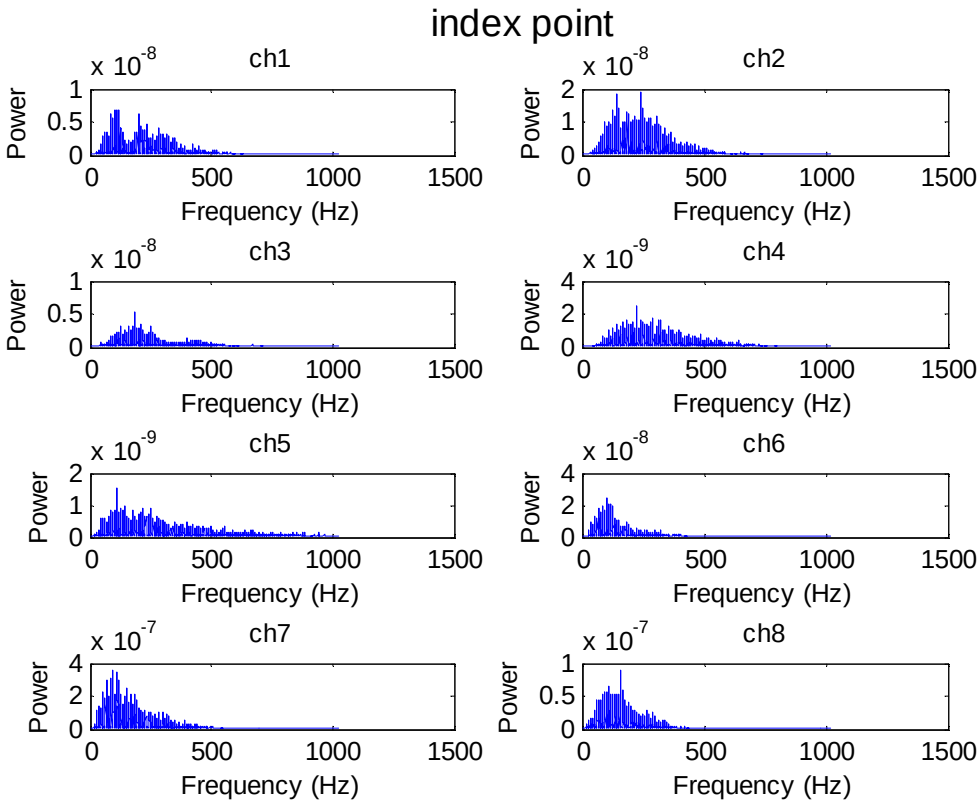
index point
ch1
x 10^-8
ch2
x 10^-8
ch3
x 10^-8
ch4
x 10^-9
ch5
x 10^-9
ch6
x 10^-8
ch7
x 10^-7
ch8
x 10^-7
Power
Frequency (Hz)
0
500
1000
1500

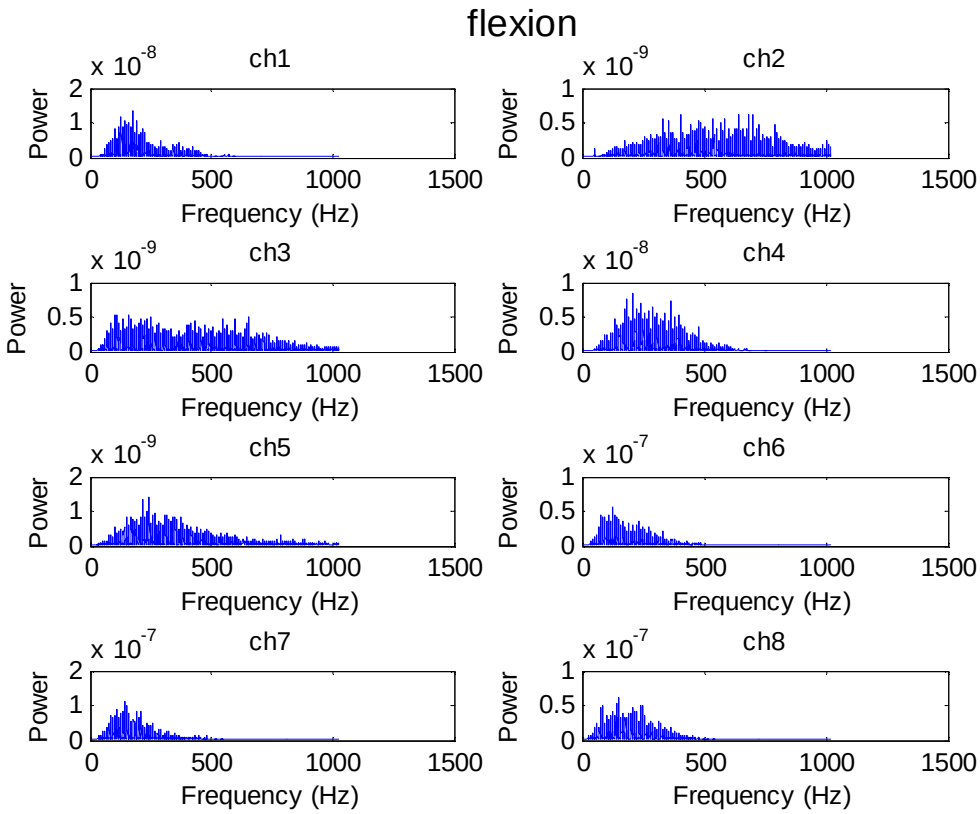
flexion
ch1
x 10^-8
ch2
x 10^-9
ch3
x 10^-9
ch4
x 10^-8
ch5
x 10^-9
ch6
x 10^-7
ch7
x 10^-7
ch8
x 10^-7
Power
Frequency (Hz)
0
500
1000
1500

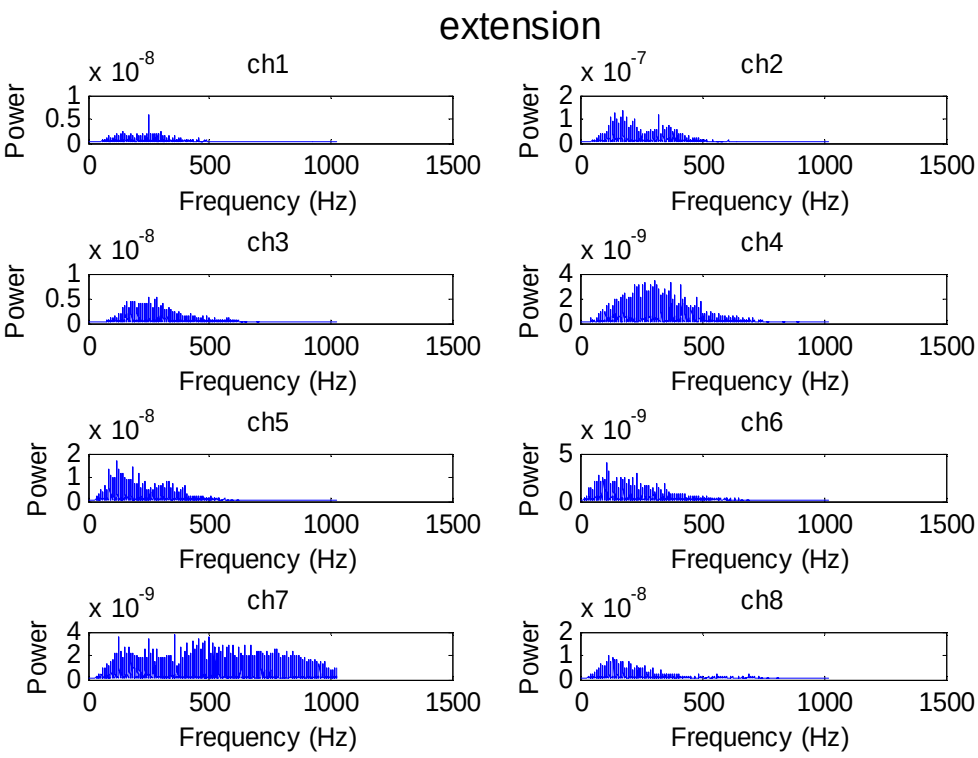
extension
ch1
x 10^-8
Power
1
0.5
0
0
500
1000
1500
Frequency (Hz)
ch2
x 10^-7
Power
2
1
0
0
500
1000
1500
Frequency (Hz)
ch3
x 10^-8
Power
1
0.5
0
0
500
1000
1500
Frequency (Hz)
ch4
x 10^-9
Power
4
2
0
0
500
1000
1500
Frequency (Hz)
ch5
x 10^-8
Power
2
1
0
0
500
1000
1500
Frequency (Hz)
ch6
x 10^-9
Power
5
0
0
500
1000
1500
Frequency (Hz)
ch7
x 10^-9
Power
4
2
0
0
500
1000
1500
Frequency (Hz)
ch8
x 10^-8
Power
2
1
0
0
500
1000
1500
Frequency (Hz)

Appendix 3: Classification accuracies claculated by using the individual feature sets

	SFS	WAMP-RMS	WAMP-VAR	MAV-WL-ZC-SSC	AR-RMS	MAV	RMS	DASDV	V-Order
subject 1									
steady	100	100	99.7	99.7	99.0	99.8	99.8	99.7	99.8
dynamic state	100	100	100	100	100	100	100	100	100
total	100	100	99.8	99.8	99.1	99.8	99.8	99.8	99.8
crossval.	98.9	98.9	98.4	96.3	97.3	96.3	96.3	95.9	96.3
subject 2									
steady state	98.8	98.9	96.3	98.8	98.1	98.5	93.7	98.6	93.05
dynamic state	77.6	77.6	71.6	95.7	76.7	77.6	93.3	76.7	94.4
total	96.6	96.7	93.8	95.7	95.9	96.4	93.7	96.4	93.2
crossval.	97.1	98.0	94.5	96.8	96.1	94.8	84.2	94.2	84.4
subject 3									
steady state	92.8	92.9	95.5	94.7	93.2	92.5	97.2	96.3	96.3
dynamic state	100	93.9	81.6	67.3	92.9	81.6	79.2	81.6	88.8
total	93.8	93.0	93.7	91.1	93.1	91.1	94.9	94.3	95.3
crossval.	96.3	95.1	90.9	90.2	93.3	90.0	91.2	88.8	90.6
subject 4									
steady state	95.2	95.7	83.2	93.8	94	92.7	97.2	90.2	93.1
dynamic state	100	93.3	84.4	93.3	94.4	94.4	79.6	93.3	94.4
total	95.7	95.5	83.4	93.7	94.1	92.9	94.9	90.5	93.2
crossval.	91.1	86.1	85.2	83.4	86.5	83.7	91.2	82.7	84.3
subject 5									
steady state	78.3	68.5	64.5	66.7	80.3	60.8	86.3	61.1	86.3
dynamic state	79.0	79.0	65.4	79.0	79.0	79.0	88.9	79.0	88.9
total	78.4	69.7	64.7	68.3	80.2	62.9	86.6	63.2	86.6
crossval.	62.5	62.4	57.9	56.0	52.2	54.2	50.7	53.4	51.1
subject 6									
steady state	91.1	95.3	96.6	85.1	90.5	83.2	92.6	91.1	92.2
dynamic state	84.9	53.2	55.6	60.3	75.4	63.5	84.9	65.9	57.1
total	90.3	89.4	90.8	81.7	88.4	80.4	91.5	87.6	87.2
crossval.	94.2	95.3	93.9	93.9	92.8	92.6	92.2	92.4	92.0
subject 7									
steady state	91.5	88.7	86.7	85.2	90.1	84.2	86.3	85.8	82.0
dynamic state	87.7	74.0	66.7	57.7	82.9	36.6	52.8	48.8	52.0
total	91.0	86.7	84.0	81.5	89.1	77.8	81.8	80.8	80.6
crossval.	88.3	74.2	72.1	96.3	93.5	92.4	85.1	66.6	83.5
subject 8									
steady state	60.4	60.4	56.1	37.3	45.6	32.4	46.5	42.6	45.2
dynamic state	65.7	65.7	50.0	61.9	62.7	61.9	33.9	61.9	33.9
total	61.4	61.4	55.1	41.8	48.8	37.8	44.3	46.1	43.2
crossval.	73.3	73.3	70.3	69.3	72.0	67.1	70.2	65.7	69.3

Appendix 4: Classification accuracies with and without MV

majority voting	1	2	3	4	5	6	7	8	avg	sd
steady state accuracy	100.0	98.8	97.8	95.2	78.3	91.1	91.5	60.4	87.9	15.0
dynamic state accuracy	100.0	77.6	70.4	100.0	79.0	84.9	87.7	65.7	83.2	12.6
total accuracy	100.0	96.6	94.2	95.7	78.4	90.3	91.0	61.4	87.4	14.0
no mojority voting										
steady state accuracy	97.5	94.4	92.5	84.1	53.9	79.4	84.4	46.1	78.6	19.8
dynamic state accuracy	80.2	63.8	56.1	55.6	82.7	46.0	57.8	36.4	59.1	14.5
total accuracy	95.4	91.2	87.8	81.3	57.2	74.7	80.9	44.5	76.1	18.2
increase in total accuracy	4.6	5.4	6.4	14.4	21.2	15.6	10.1	16.9	11.3	-4.2